CLIMATE ASSESSMENT FOR 1994

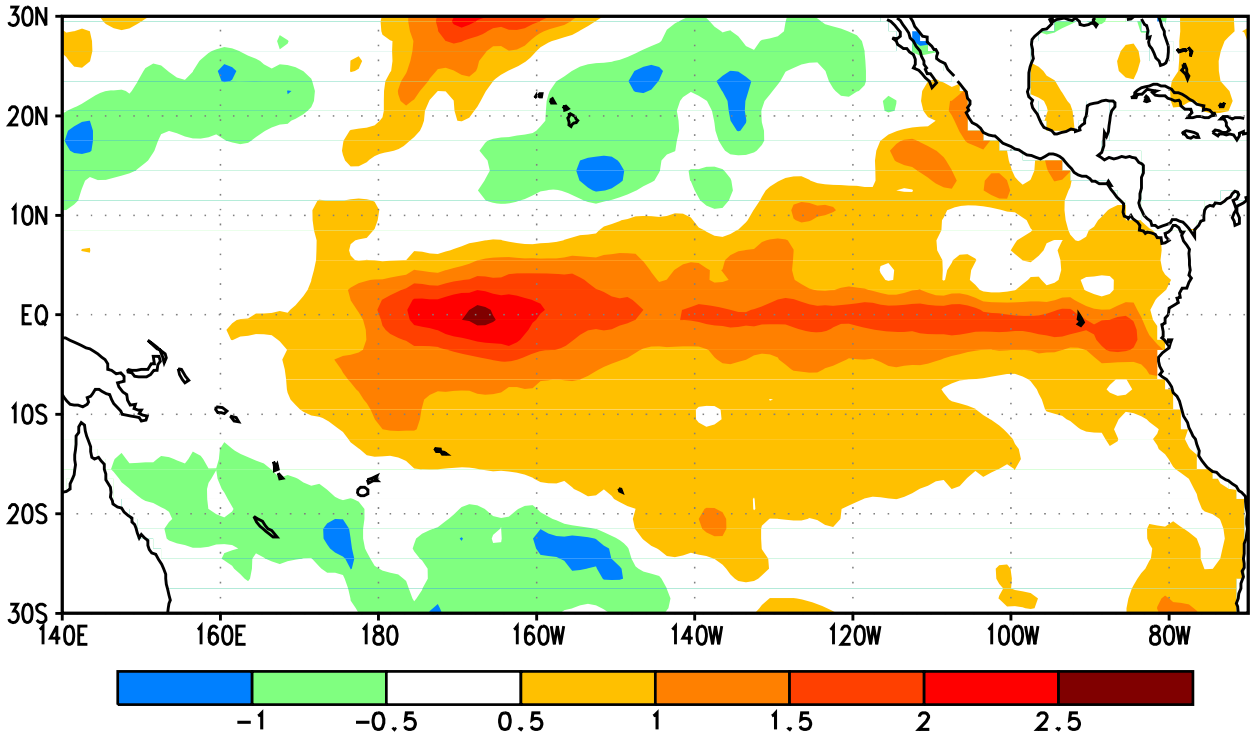

U.S. DEPARTMENT OF COMMERCE
National Weather Service
National Meteorological Center
Climate Analysis Center

COVER: Sea surface temperature anomalies for December 1994. Contour interval is 0.5°C. Anomalies are departures from the adjusted OI climatology (*Reynolds and Smith, 1995*). For information on the warm episode in the tropical Pacific Ocean, see section 2.

Climate Analysis Center
Camp Springs, Md
March 1995

CLIMATE ASSESSMENT FOR 1994

EDITORS: M. S. Halpert, Chief
G. D. Bell
V. E. Kousky
C. F. Ropelewski

U. S. DEPARTMENT OF COMMERCE
NATIONAL OCEANIC AND ATMOSPHERIC ADMINISTRATION
NATIONAL WEATHER SERVICE
NATIONAL METEOROLOGICAL CENTER

TABLE OF CONTENTS

LIST OF FIGURES

PREFACE

The possibility of long-term climate change continues to be a concern and focus for scientific investigations and for the development of government policies and international agreements. However, for commercial interests, especially in agriculture and water resources, seasonal climate anomalies and short-term climatic variability, as well as possible long-term trends, are important.

This report is the best description of recent climatic variations and changes that we can assemble immediately after the end of the past calendar year. Subsequently, the scientific community will examine in greater detail the evidence we have put forward at this time.

Although many components of the global climate system are not fully described, this report intends to assess annual changes in the circulation, structure and constituents of the atmosphere, and changes in surface conditions of temperature, precipitation, snow and ice. It describes the evolution of ENSO during the past year, and identifies major, regional climatic events around the world.

We plan improvements to this report and will expand its scope next year. Your comments and suggestions for improvements are most welcome.

David R. Rodenhuis
Director
Climate Analysis Center
February 28, 1995

Acknowledgments - This assessment was completed with the cooperation and contributions from NOAA scientists as well as from contributors outside of NOAA in other federal laboratories, at universities and at several sites around the world. These scientists are identified on the following page, and we thank them for their timely and useful input. In addition, we would like to thank the reviewers for their comments and quick response: T. Karl, D. Phillips, G. Kiladis, and R. Rosen. The manuscript was also reviewed by J. Kumjian, R. Bermowitz, and E. O'Lenic at the Climate Analysis Center.

CONTRIBUTORS

Air Resources Laboratory/ERL/NOAA

J. Angell

All-Russia Research Institute of Hydrometeorological Information - World Data Centre

R. Reitenbach A. Sterin

Atmospheric and Environmental Research, Inc.

P. Nelson D. Salstein

Australian Bureau of Meteorology, National Climate Centre, Climate Analysis Section

W. Wright

Center for Ocean-Land-Atmosphere Interactions, Univ. of Maryland

B. Doty

Climate Analysis Center/NMC/NWS/NOAA

G. Andrews M. Gelman D. Miskus
A. Basist M. Halpert R. Nagatani
G. Bell J. Harrison C. Ropelewski
R. Churchill J. Janowiak T. Smith
D. Garrett V. Kousky R. Tinker

Climate Monitoring and Diagnostics Laboratory/ERL/NOAA

T. Conway E. Dutton J. Peterson
E. Dlugokencky K. Masarie

Climatic Research Unit, University of East Anglia, (UK)

P. D. Jones

Coupled Model Project/NMC/NWS/NOAA

M. Ji R. Reynolds

Department of Atmospheric Science, Colorado State University

W. Gray

Department of Geography, Rutgers University

D. Robinson

Deutscher Wetterdienst, Hamburg, Germany

G. Rosenhagen

Earth System Science Laboratory, University of Alabama in Huntsville

J. Christy

Hadley Centre for Climate Prediction and Research, (UK)

D. Cullum M. O'Donnell
C. Folland D. Parker

NASA Goddard Institute for Space Studies

J. Hansen

NASA Marshall Space Flight Center

R. Spencer

National Climatic Data Center/NESDIS/NOAA

W. Brown R. Heim Jr.

National Hurricane Center/NMC/NWS/NOAA

L. Avila

Office of Hydrology/NWS/NOAA

S. Kroczynski

EXECUTIVE SUMMARY

Global surface temperature anomalies during 1994 were 0.4°C warmer than normal based on land-only measurements, and slightly greater than 0.3° C warmer than normal based on combined land-sea measurements. This return of relatively large, positive global temperature anomalies after a two-year hiatus coincides with a return to near-normal stratospheric aerosol concentrations as the effects of the June 1991 eruption of Mt. Pinatubo greatly diminished.

A return to warm episode [El Niño/Southern Oscillation (ENSO)] conditions in the tropical Pacific during the second half of the year also contributed to the above-normal global temperatures described above. The recurrence of warm episode conditions for the third time in four years, while not unprecedented, has spurred some climate researchers to reexamine the basic assumptions and presumed mechanisms for generation and maintenance of warm episodes. During 1994, ENSO-related shifts in tropical convection contributed to: (1) extreme drought over much of Australia, (2) significantly below-normal precipitation throughout Indonesia, (3) a delayed start to the rainy season in southern Africa, and (4) abnormal weather patterns across the North Pacific and North America by the end of the year.

Other regional climate anomalies during 1994 included above-normal precipitation in the Sahel and extreme warmth in Europe. During the 1994 Sahel rainy season (May to September), much of western tropical Africa recorded more than 120% of normal precipitation, making this their wettest season in over two decades. In Europe, above-normal temperatures prevailed from July through December, and extreme warmth dominated during July and November. For example, Vienna, Austria recorded its highest annual temperature in over 200 years, while Hamburg, West Germany recorded its warmest July since 1850 and central England reported its warmest November in 336 years.

The year also witnessed near-record low ozone amounts in the Southern Hemisphere stratosphere. The "ozone hole" during October 1994 was comparable in magnitude and spatial extent to the record values observed during 1992 and 1993. In the Northern Hemisphere, the January-February ozone minimum was not as severe as observed in 1993.

1. CLIMATE AND GLOBAL CHANGE ISSUES

a. Surface Temperatures

The estimated global mean temperature anomaly (land only) for 1994, calculated relative to the 1951-1980 base period, increased to +0.4°C. This value is comparable to that observed during 1991, but smaller than the record 1990 anomaly. Thus, 1994 is one of the three warmest years on record (**Fig. 1.1, top**). The global temperature anomalies were estimated from station data received over the Global Telecommunications System (GTS). Most of the warmth during 1994 occurred after February, as global temperatures during the March - December period were the warmest observed during the historical record dating back to 1951 (**Fig. 1.1, bottom**). In addition, individual monthly records for mean global temperatures were set during April, September, and December.

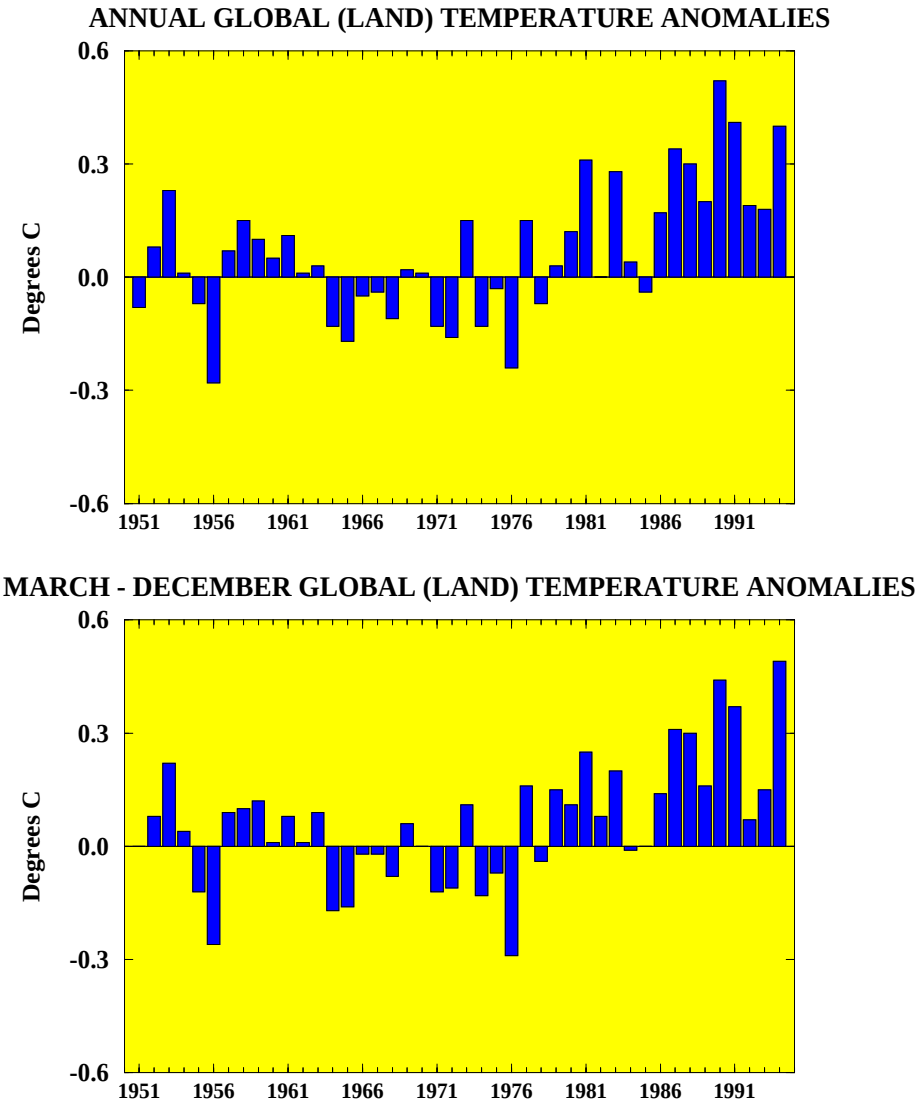

Figure 1.1 Annual (top) and March - December (bottom) global temperature anomalies (land only, °C). Anomalies are departures from the 1951-1980 base period means. (Source: CAC)

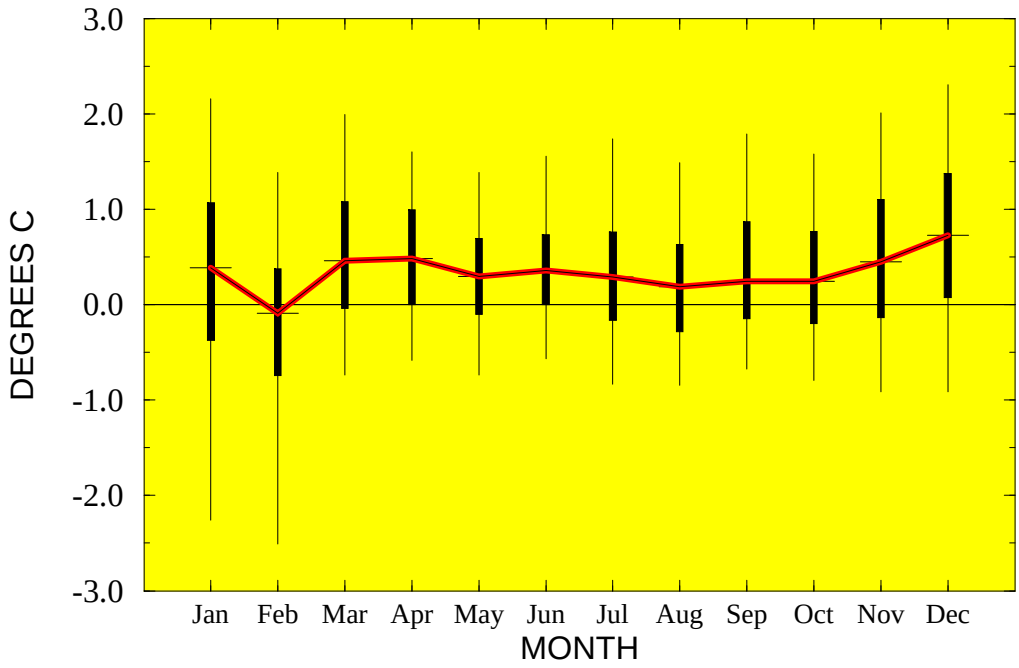

Figure 1.2 Monthly values of the median (land only) temperature anomalies for 1994 (red line). 50% of the 2º latitude by 2º longitude land areas have anomalies above (below) the median. Information about the distribution of monthly temperature anomalies is provided by the solid rectangles, indicating the 30% and 70% levels, and the thin vertical lines, indicating the 10% and 90% levels. The anomalies are departures from the 1961-1990 base period. (Source: CAC)

Median global temperatures (land only) were above normal during every month of 1994 except February (**Fig. 1.2**). In addition, 70% or more of the land area (with data) had above-normal temperatures during April, June, and December. It should be noted, however, that at least 30% of the total land area experienced below-normal temperatures during every month, except for December. This is similar to time series for both 1990 and 1991 (see Climate Assessment 1991, Fig. 1.2), although the median anomalies during those years were warmer than during 1994.

The 1994 estimated global mean surface temperature for land and marine areas was +0.31ºC, calculated relative to the 1951-1980 base period (**Figure 1.3**). The uncertainty in estimates of global temperatures results mainly from data sparsity, especially over the Southern Ocean, parts of the tropics, and Antarctica. As a result, different analysis techniques yield slightly different estimates of the global mean temperature anomaly. All estimates for 1994 rely heavily on land surface air temperature data from the monthly CLIMAT messages and on oceanic surface temperatures obtained from ship and buoy measurements. These data are exchanged over the GTS.

Figure 1.3 shows that 1994 was warmer than 1992 and 1993, was similar to 1988, but was not as warm as 1990 and 1991. The time series also shows that global temperatures have increased approximately 0.5ºC over the past 135 years. Much of this increase has occurred during two periods, a thirty-year period from approximately 1910 to 1940, and over the past 15 years.

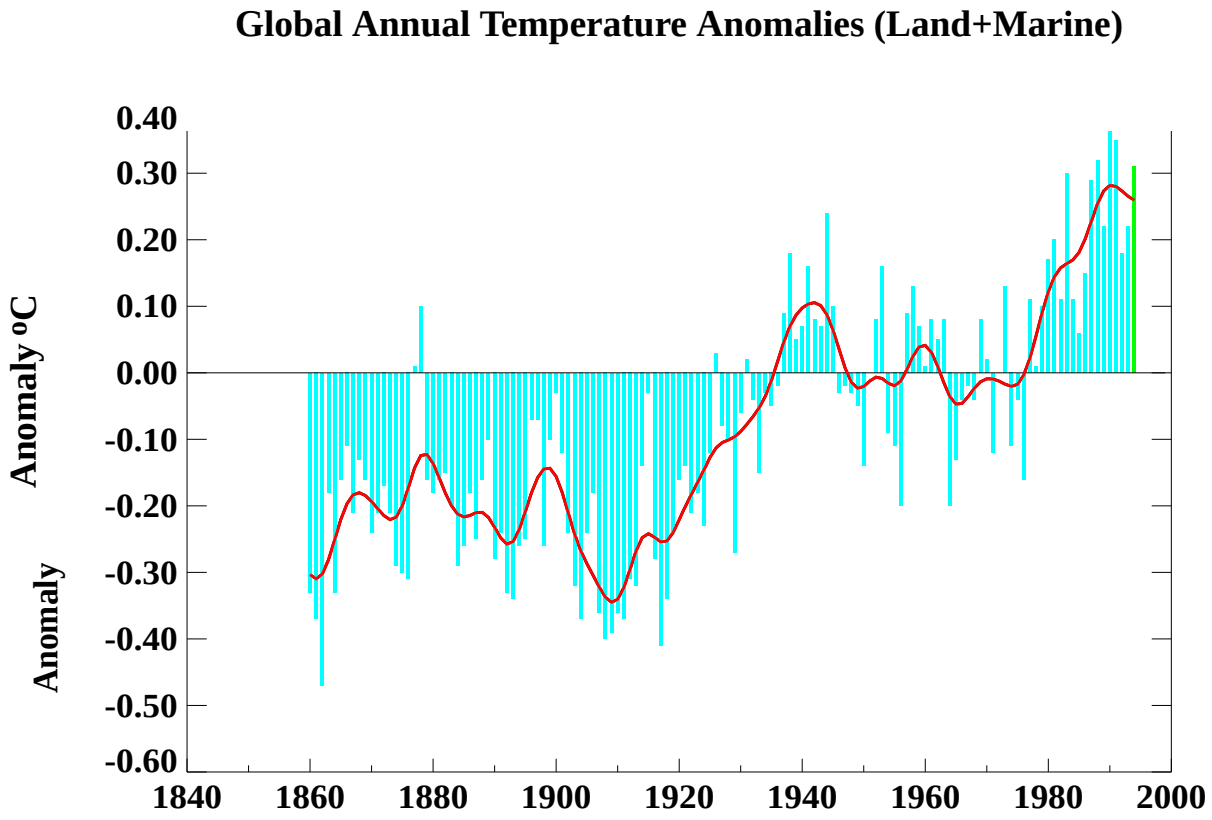

Figure 1.3 Global annual averages of combined land-air and sea surface temperature (SST) anomalies for each year from 1861-1994. Anomalies are computed with respect to the 1951-1980 base period. The red curve is a 13-term Gaussian filter designed to suppress variations on time scales less than 10 years. (Source: Hadley Centre for Climate Prediction and Research, UK)

The abnormally warm conditions during 1994 partly resulted from the redevelopment of El Niño conditions during the second half of the year (see section 2). The El Niño influence is evident in the geographical patterns of ocean temperature anomalies (**Figure 1.4**), which shows warmth in the central equatorial Pacific and along the west coast of North America, warmth in the central Indian Ocean, and cold areas centered north of Hawaii and in the western subtropical South Pacific. Positive land temperature anomalies, exceeding 1°C, were observed over western North America, central and eastern Europe (where the summer was exceptionally hot, see section 4.e) and eastern Asia. Abnormally warm conditions have been observed in northwestern Canada during recent years. The anomalous warmth over Asia is farther south than the persistent pattern that has dominated Siberia during the past 15 years. In contrast, Labrador, southern Greenland, and the northwestern North Atlantic were anomalously cold during 1994, as was observed during 1993 and in many other recent years. The overall distribution of temperature anomalies during 1994 was similar to that observed during the record warm year of 1990.

Volcanic aerosols from the June 1991

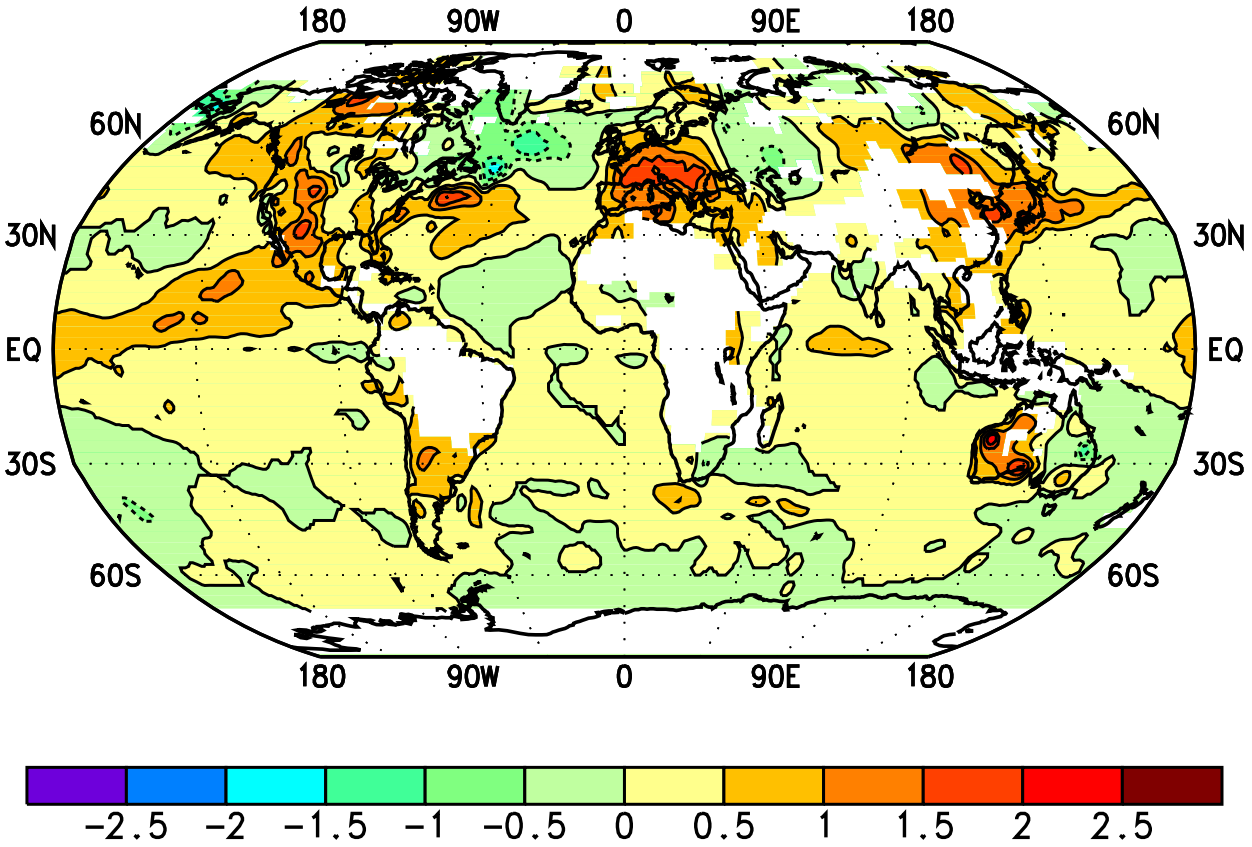

Figure 1.4 Surface temperature anomalies (°C) for January - December 1994. Analysis is based on station data over land and on sea surface temperature (SST) data over the oceans. Anomalies for station data are departures from the 1961-1990 base period means, while SST anomalies are departures from the COADS/ICE climatology (*Reynolds 1988*). White areas are regions with insufficient data for analysis. (Source: CAC)

eruption of Mt. Pinatubo have decreased to near pre-eruption levels, as shown by the "apparent" atmospheric solar transmission, or transmission ratio (*Ellis and Pueschel 1971*) (**Fig. 1.5**). Consequently, the global cooling influence from the aerosols waned (**Fig. 1.6**), as indicated by surface observations and model simulations from the Goddard Institute for Space Studies climate model (*Hansen et al. 1988, 1992*). The model is designed to simulate the global temperature change due to atmospheric aerosols and trace gases and does not incorporate the global temperature response associated with processes such as ENSO. The simulations and observations agree that a maximum surface cooling of approximately 0.5°C occurred by the end of 1992 in association with the eruption of Mt. Pinatubo. The model forecasts suggest that during 1994 global temperatures should have returned to pre-eruption levels. Due to large increases late in the year, observed temperatures had also returned to pre-eruption values by the end of 1994 (**Fig. 1.6**).

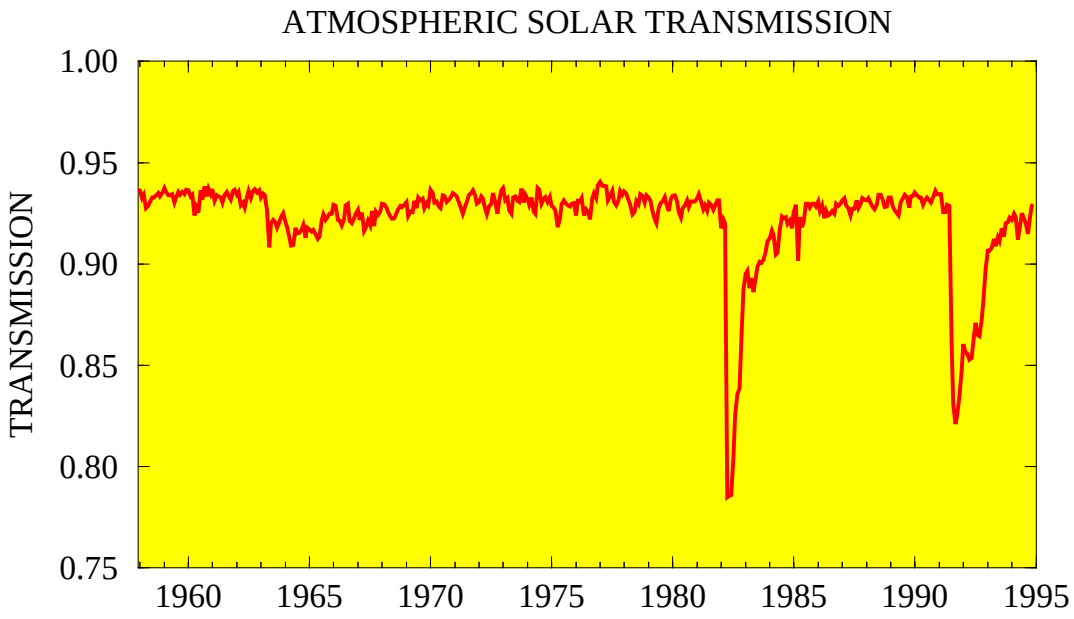

Figure 1.5 "Apparent" atmospheric solar transmission at Mauna Loa Observatory, Hawaii as determined from direct solar radiation measurements. The ratio is derived from broadband (0.3 to 2.8 μ*m)* direct solar irradiance observations and shows the effects of volcanic eruptions of aerosol concentrations over Mauna Loa. (Data provided by the Climate Monitoring and Diagnostics Laboratory.)

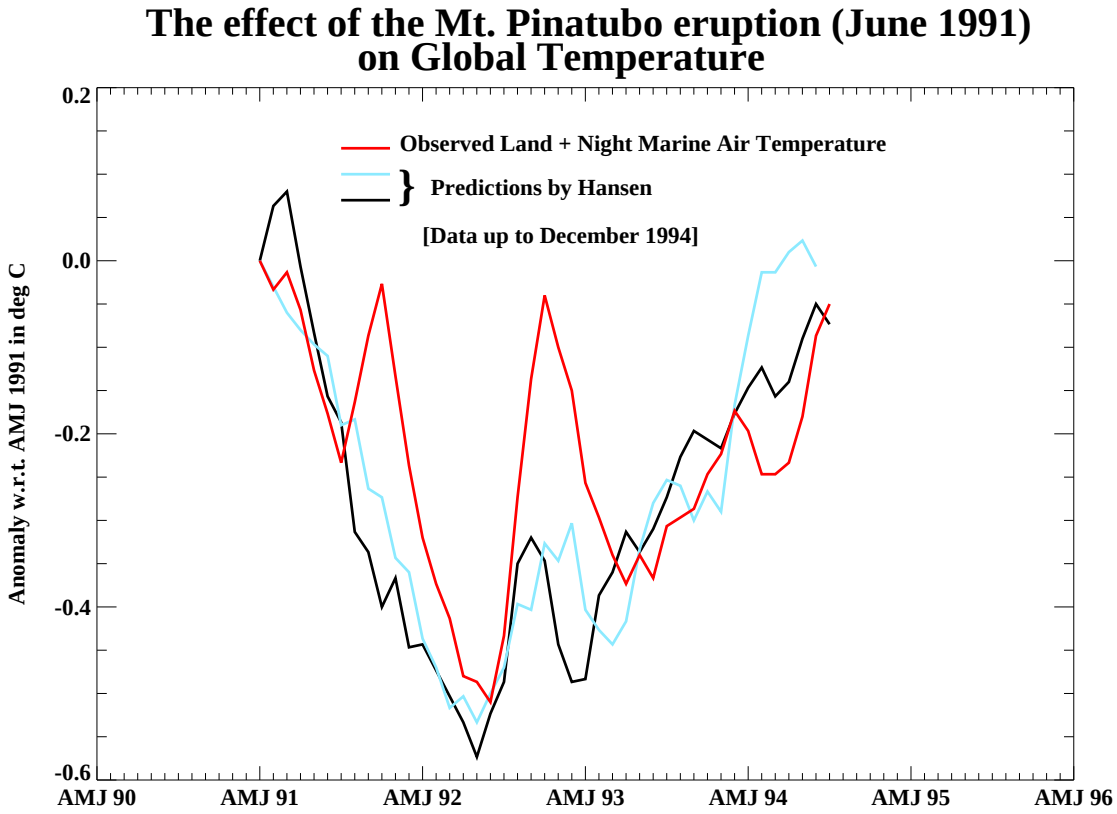

Figure 1.6 Global surface air temperature anomalies (red line) following the June 1991 eruption of Mt. Pinatubo, relative to the global anomaly for the 3-month period April-June 1991. Values are 3-month running mean anomalies ending with October - December 1994. Model results are indicated by blue and black lines. (Source: Hadley Centre for Climate Prediction and Research, UK)

b. Troposphere/Stratosphere Temperatures

1) Troposphere

Since 1979 satellite-derived estimates of lower-troposphere temperature have been obtained from measurements taken by the MSU channel 2R flown aboard the NOAA polar-orbiting satellites (*Spencer et al. 1990*). Interannual variations in global tropospheric temperature primarily reflect the influence of cold and warm episodes in the tropical Pacific and the shading effects resulting from stratospheric aerosols emitted by intense low-latitude volcanic eruptions (**Fig. 1.7**). Global temperature anomalies (**Fig. 1.7a**) reached a maximum in late 1987 following the 1986-

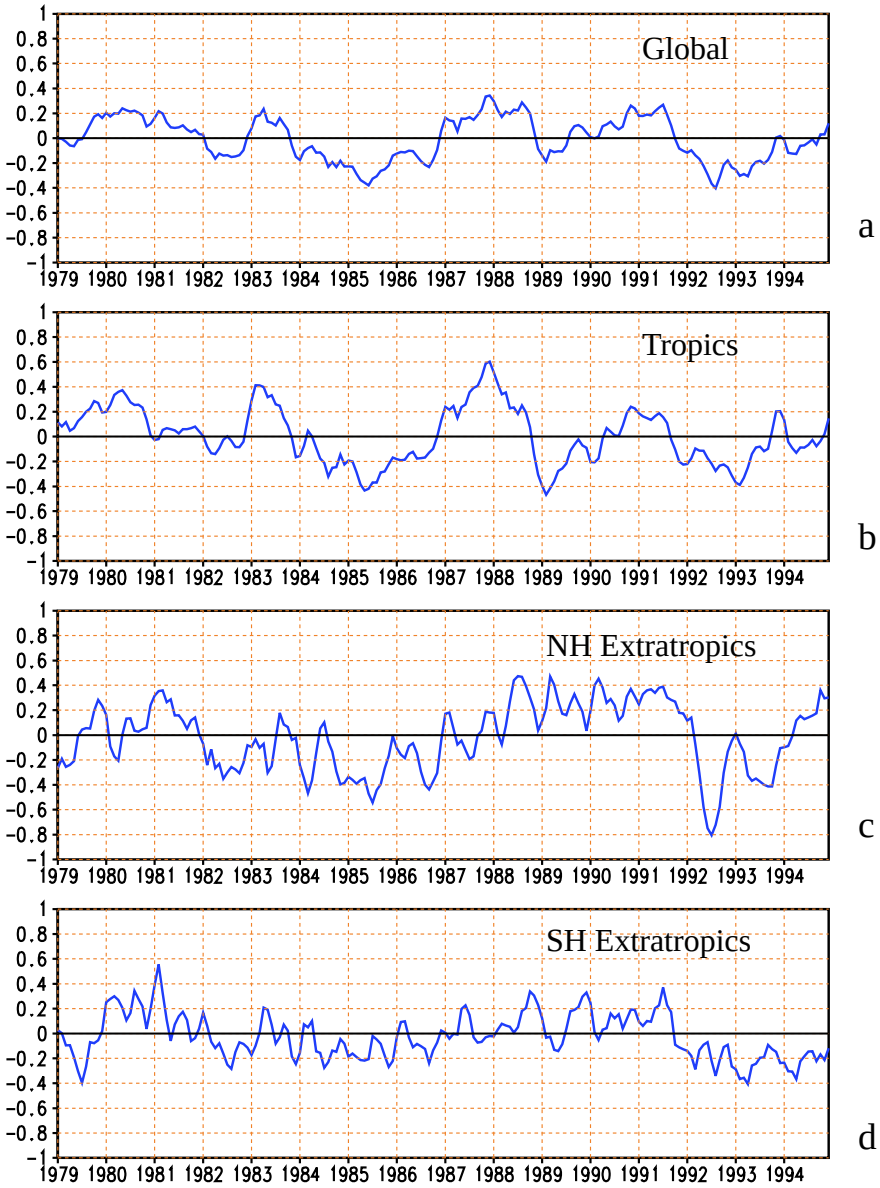

Figure 1.7 Mean tropospheric temperature anomalies (ºC) from the Microwave Sounding Unit (MSU) channel 2R for the a) globe (85ºS-85ºN), b) tropics (30ºN-30ºS), c) Northern Hemisphere extratropics (30ºN-85ºN) and d) Southern Hemisphere extratropics (30ºS-85ºS). Anomalies are computed from the 1982-1991 base period. (Data provided by the University of Alabama at Huntsville.)

1987 warm episode, and then reached a minimum in early 1989 following the peak in the 1988-1989 cold episode. Temperatures then increased until mid-1991 as conditions in the tropical Pacific evolved toward the 1991-1993 warm episode. The cooling effects due to the large increase in stratospheric aerosols, which accompanied the eruption of Mt. Pinatubo, are evident in the tropics and in the extratropics of both hemispheres, particularly during the Northern Hemisphere 1992 and 1993 summer seasons (**Fig. 1.7c**).

During 1994 global temperature anomalies returned to near zero (**Fig. 1.7a**). In part this is due to a return to near-normal concentrations of stratospheric aerosols but may also reflect a warming due to the development of warm episode conditions in the tropical Pacific during the latter half of the year. The upward trend in global tropospheric temperatures during the last two and a half years is also reflected in the radiosonde-based tropospheric temperature anomalies (**Fig. 1.8, top**). For 1994 as a whole, the satellite-estimated global

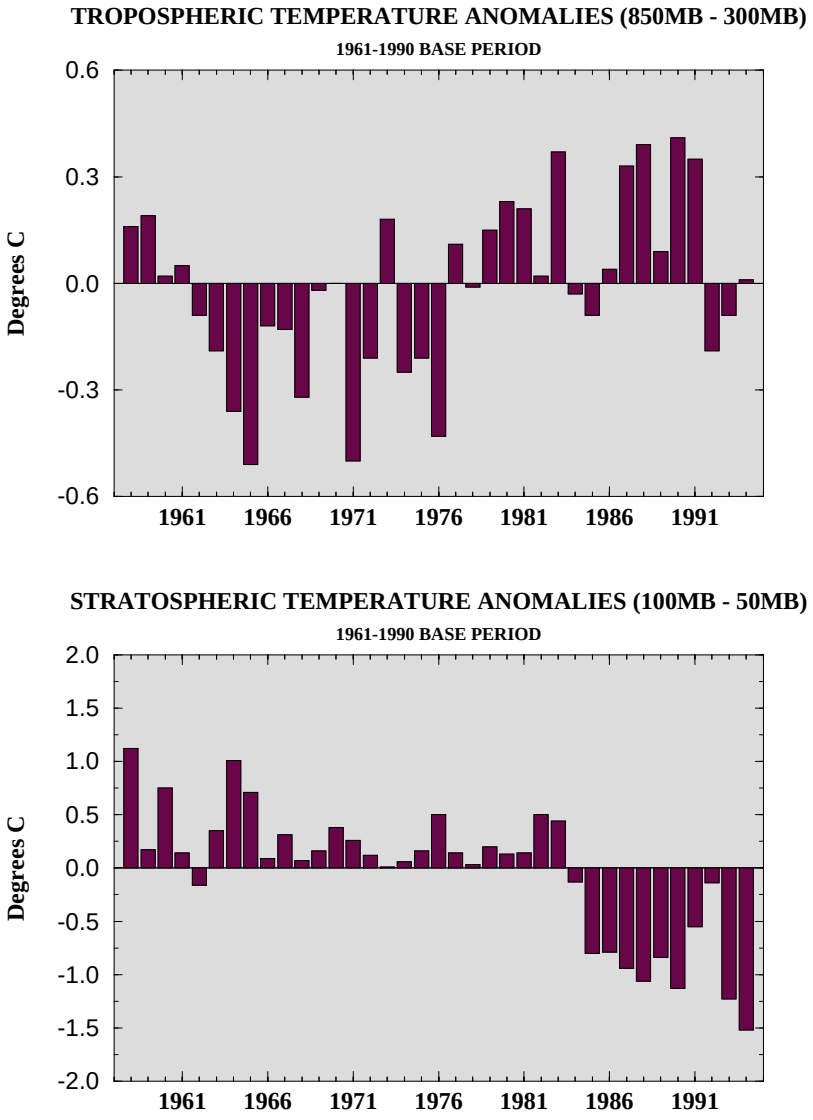

Figure 1.8 Annual global tropospheric (850-300 mb) (top) and stratospheric (100-50 mb) (bottom) temperature anomalies derived from radiosonde data based on a 63-station network. Anomalies are departures from the 1961-1990 base period means (Data provided by the Air Resources Laboratory.)

temperature anomaly was near zero, while the radiosonde-based estimate of tropospheric mean temperature anomaly for the layer from 850 mb to 300 mb was slightly positive. The difference between the estimates is within the uncertainties resulting from the differences in the instruments, networks, methods of calculating the global mean tropospheric temperatures, and differences in base periods used as references for computing the anomalies.

The spatial patterns of tropospheric temperature anomalies based on satellite estimates (**Figs. 1.9 and 1.10**) indicate that positive anomalies prevailed over much of the Pacific Ocean during the last five years. 1992 and 1993 were noticeably cooler than 1990 and 1991 especially for northeastern Siberia, the southwestern United States, northeastern Canada, northern Africa, western Asia, and Antarctica. During 1994, positive temperature anomalies prevailed over Europe, eastern Asia and the western Pacific, extreme northern Canada, and central South America. Negative anomalies continued over many sections of Antarctica, Australia, western Asia, and the northern two-thirds of Africa.

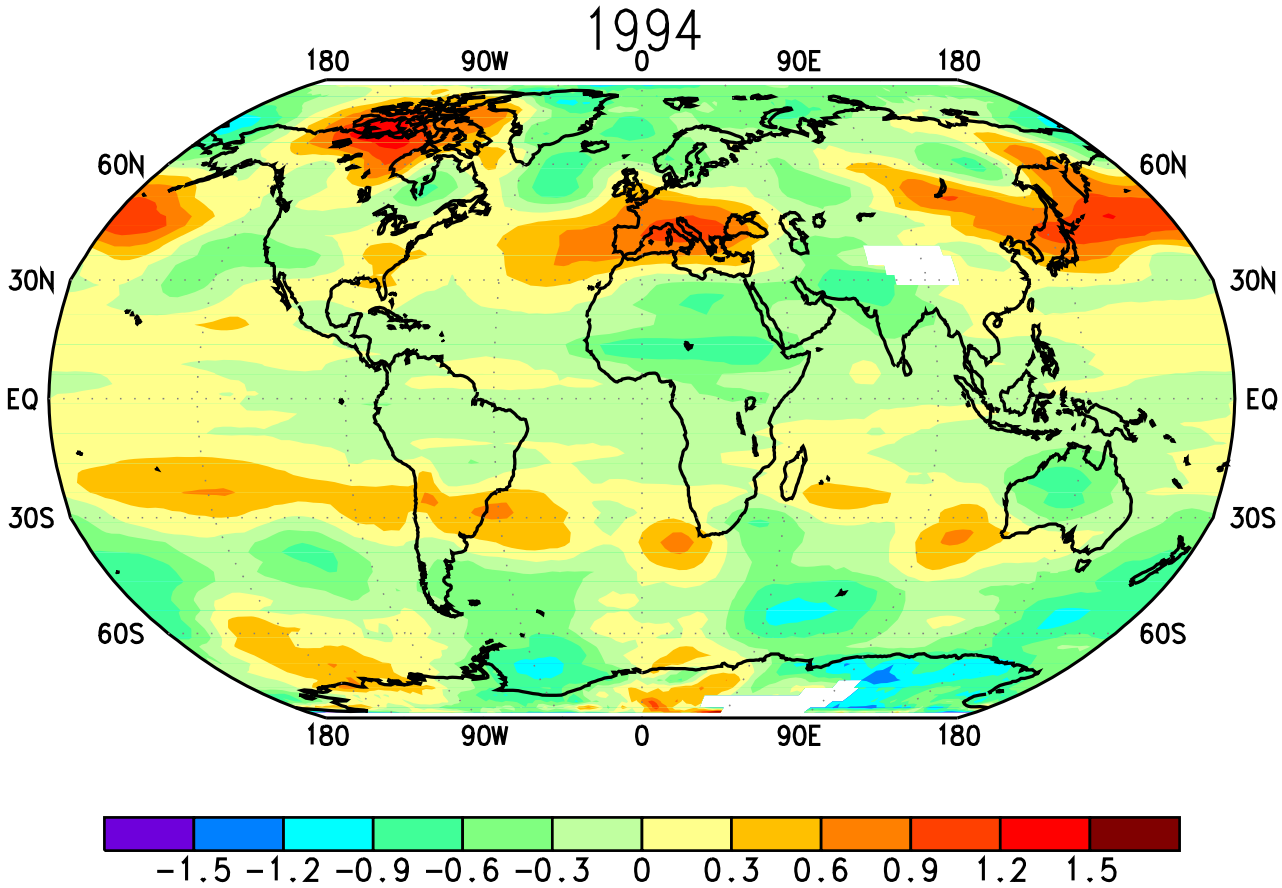

Figure 1.9 Mean annual tropospheric temperature anomalies for 1994 derived from the Microwave Sounding Unit (MSU) channel 2R. Anomalies are departures from the 1982-1991 base period means. (Data provided by the University of Alabama at Huntsville.)

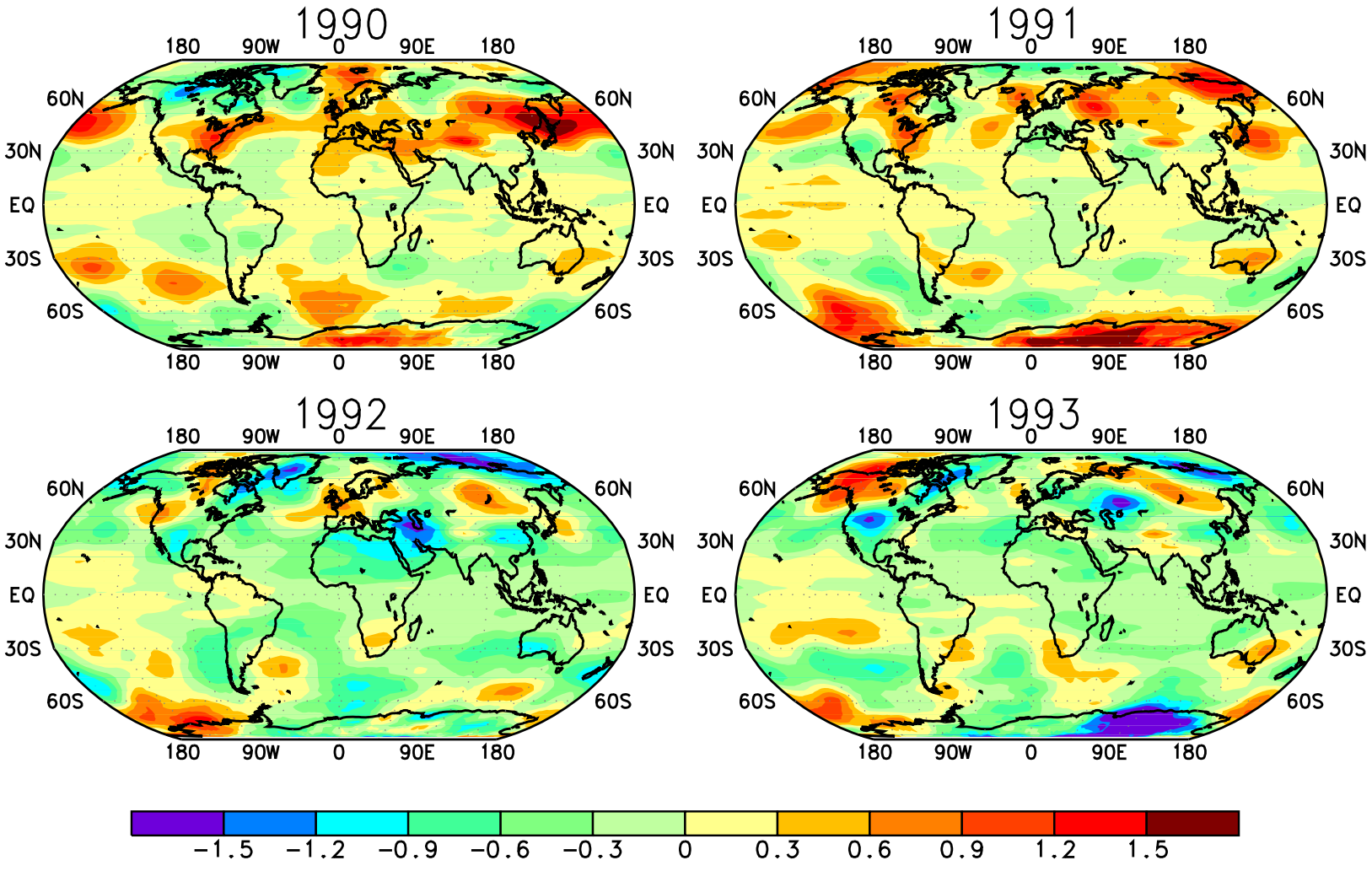

Figure 1.10 Mean annual tropospheric temperature anomalies for 1990, 1991, 1992, and 1993, derived from the Microwave Sounding Unit (MSU) channel 2R. Anomalies are departures from the 1982-1991 base period means. (Data provided by the University of Alabama at Huntsville.)

2) Stratosphere

Stratospheric temperature anomalies at the end of 1994 were the lowest in the 15-year record of satellite data (**Fig. 1.11**) and were also the lowest in the 30-year record of radiosonde-based estimates (**Fig. 1.8, bottom**). The satellite estimates showed almost continuous cooling in the stratosphere throughout the year for all latitude bands, with the exception of the Southern Hemisphere extratropics.

The global patterns of stratospheric temperature anomalies (**Figs. 1.12 and 1.13**), show striking interannual variability. The warming effects of the Mt. Pinatubo eruption are evident in the patterns for 1991 and 1992

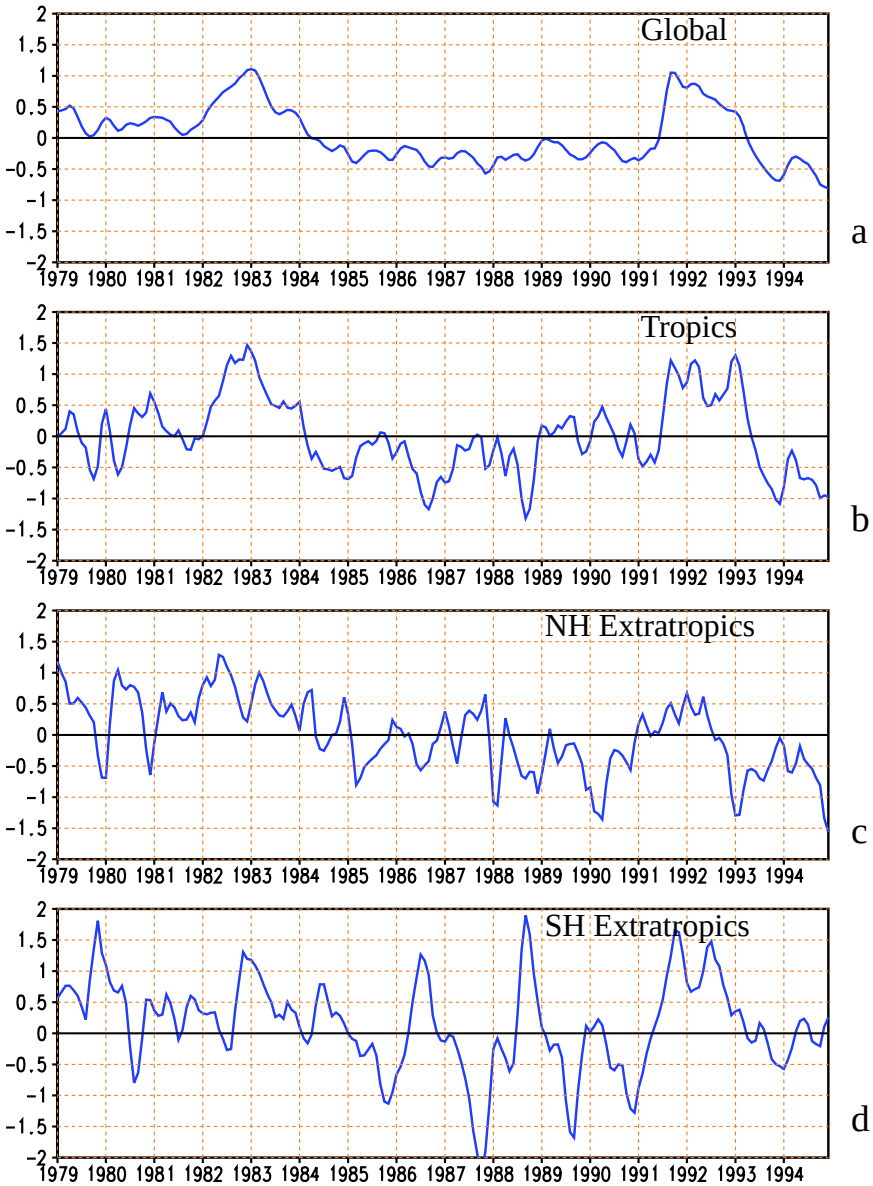

Figure 1.11 Mean stratospheric temperature anomalies (ºC) from the Microwave Sounding Unit (MSU) channel 4 for the a) globe (85ºS-85ºN), b) tropics (30ºN-30ºS), c) Northern Hemisphere extratropics (30ºN-85ºN) and d) Southern Hemisphere extratropics (30ºS-85ºS). Anomalies are departures from the 1982-1991 base period monthly means. (Data provided by the University of Alabama at Huntsville.)

(**Figs. 1.13**). Also evident is a strong global cooling that has occurred thereafter, with most regions experiencing a cooler than normal lower stratosphere during 1994 (**Fig. 1.12**). This cooling continues a trend that began in the early 1980s (**Fig. 1.8, bottom**).

A quasi-biennial oscillation (QBO) of temperatures is also evident in the tropics and subtropics. This QBO featured positive anomalies during 1990 and 1993 throughout the equatorial region (**Fig. 1.13**), and negative anomalies along the equator in 1994 (**Fig. 1.12**). Although the effects of the Mt. Pinatubo eruption dominated the tropics during 1991 and 1992, the QBO can still be noted during that period as a decrease in positive anomalies along the equator from 1990 to 1991.

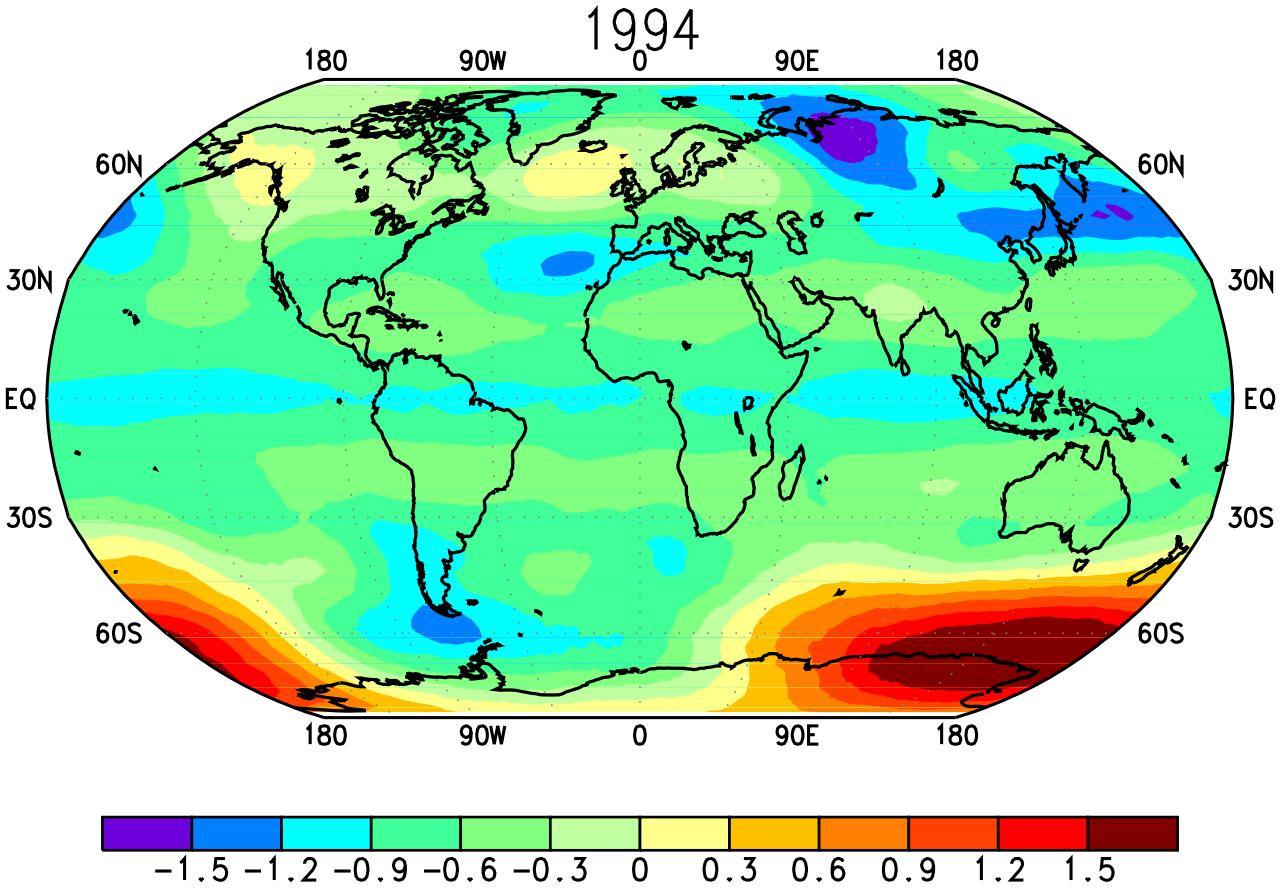

Figure 1.12 Mean annual stratospheric temperature anomalies for 1994 derived from the Microwave Sounding Unit (MSU) channel 4. Anomalies are departures from the 1982-1991 base period means. (Data provided by the University of Alabama at Huntsville.)

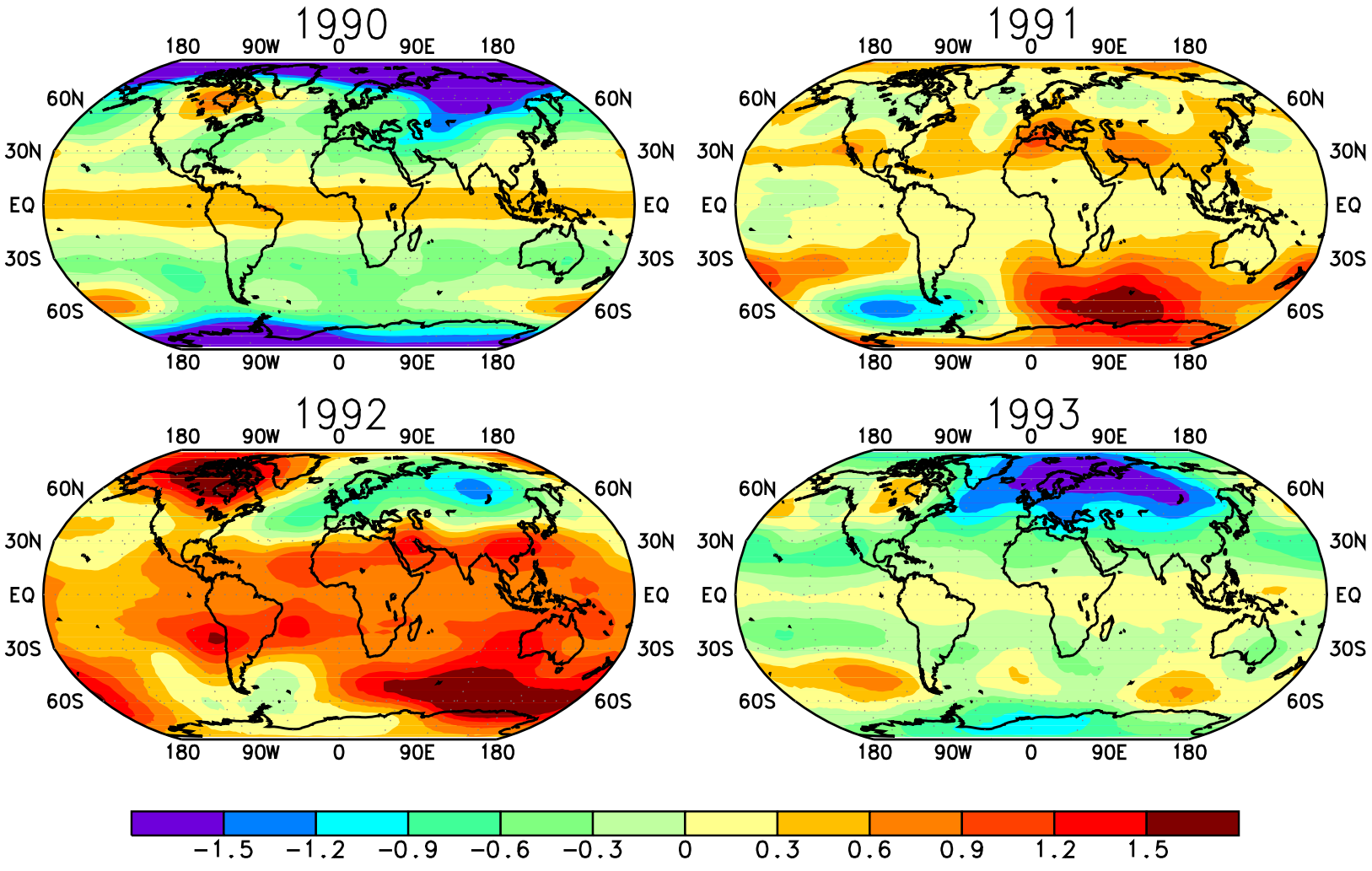

Figure 1.13 Mean annual stratospheric temperature anomalies for 1990, 1991, 1992, and 1993, derived from the Microwave Sounding Unit (MSU) channel 4. Anomalies are departures from the 1982-1991 base period means. (Data provided by the University of Alabama at Huntsville.)

c. Trace Gases

1) Ozone

Gradual destruction of stratospheric ozone, which is attributed to the buildup of man-made compounds that deplete the ozone layer, continued during 1994. According to an executive summary of the 1994 Scientific Assessment of Ozone Depletion released jointly by the World Meteorological Organization and the United Nations Environmental Program, the rate of ozone destruction is expected to peak during the next few years and to begin decreasing early in the twenty-first century. The long-term decrease of total column ozone is presently 4-5 percent per decade at mid-latitudes in both hemispheres. Little negative trend in ozone is observed in the Tropics. [Ozone data are derived from data recorded by the SBUV instrument on the NASA Nimbus-7 satellite from 1979 to mid-1990 and by the SBUV/2 instrument on the NOAA-11 satellite from January 1989 to September 1994.]

In the Northern Hemisphere, ozone concentrations during February have decreased by an average of 3-6% since 1979 (**Fig. 1.14**), with positive (negative) anomalies

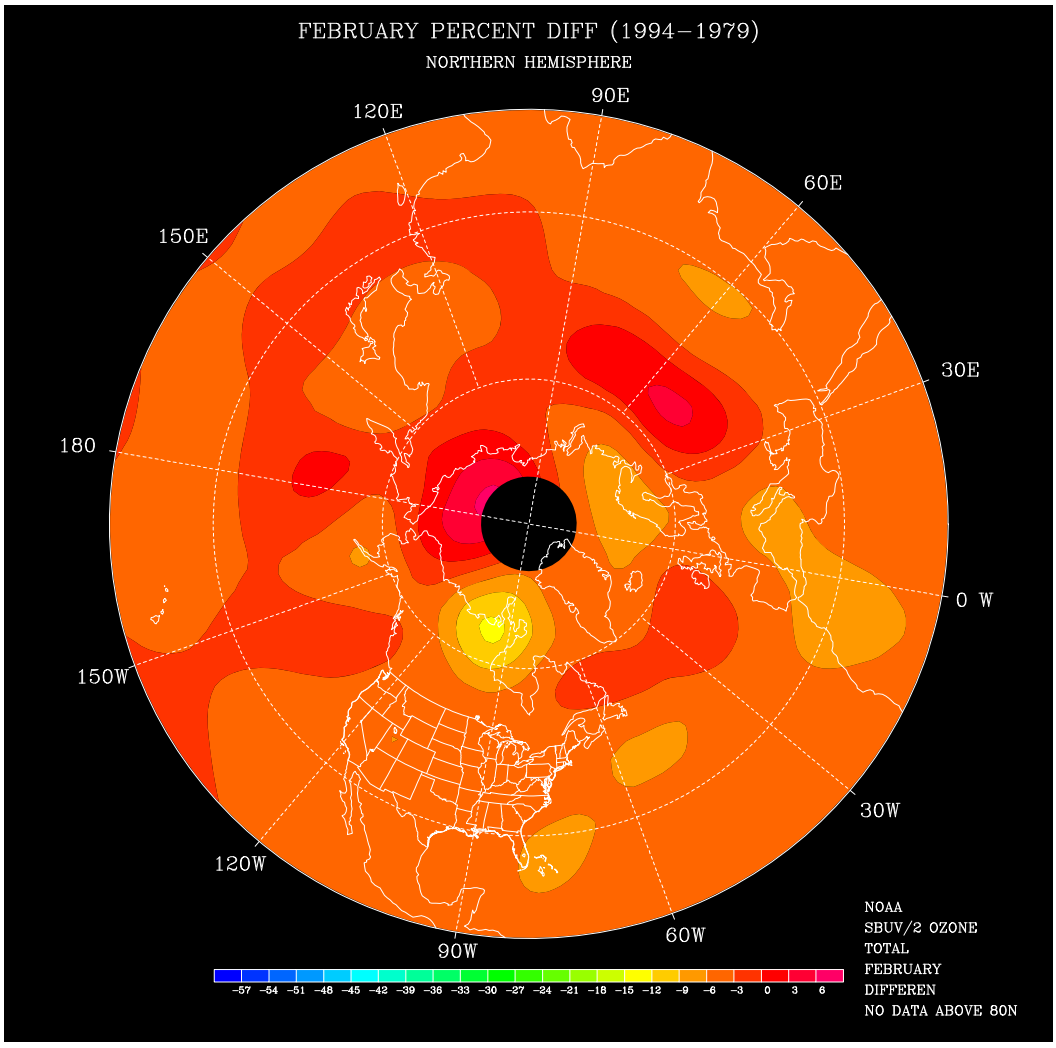

Figure 1.14 Total ozone percent difference between February 1994 and February 1979. Regions of no data are shown in black. (Source: CAC)

dominating the early (late) part of the record (**Fig. 1.15**). Large negative anomalies in the Northern Hemisphere extratropics during 1992-1993 were related to increased stratospheric aerosols that resulted from the Mt. Pinatubo eruption in June 1991. During 1994 negative ozone anomalies decreased in magnitude in the Northern Hemisphere, as volcanic aerosol levels returned to near normal.

In the Southern Hemisphere middle and high latitudes, negative (positive) ozone anomalies also dominated during the latter (early) portion of the record, again indicating a substantial reduction in ozone concentrations

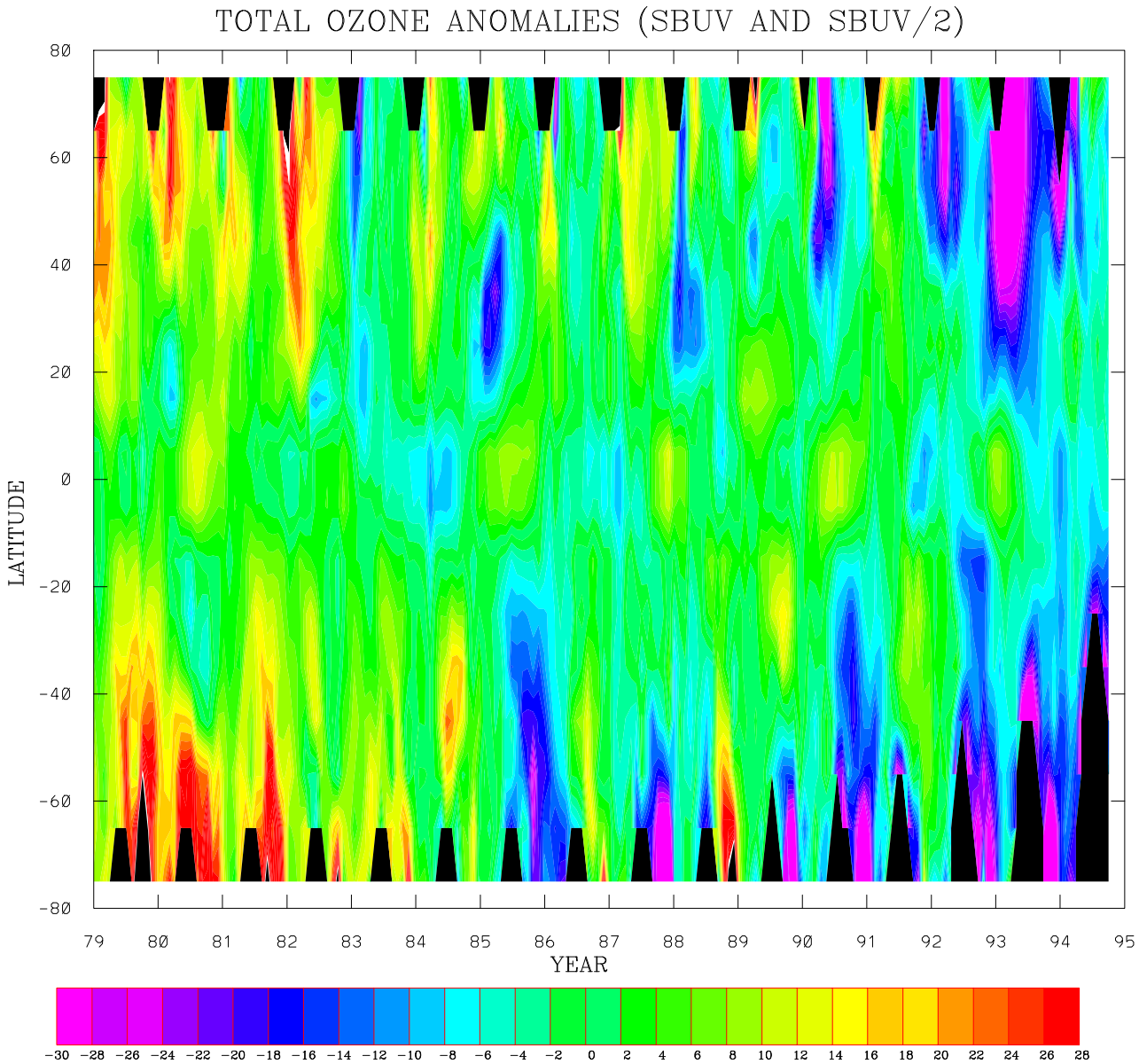

Figure 1.15 Time-latitude section of anomalous monthly average values (Dobson Units) of zonal mean total ozone, derived from Nimbus 7 SBUV from 1979-1988, and from NOAA 11 SBUV/2 from 1989 to 1994. Anomalies are departures from the 1979-1994 base period means. Regions of no data are shown in black. (Source: CAC)

since 1979. For example, October total ozone concentrations have decreased by nearly 100 Dobson Units (DU) over a large portion of Antarctica since 1979, which represents a 50% reduction in ozone in that region (**Fig. 1.16**). During 1994 ozone concentrations continued to decrease in the Southern Hemisphere extratropics and subtropics. The extremely low total column ozone values (near 100 DU) observed over Antarctica during September and October 1994 were similar to the record-setting values observed in 1992 and 1993.

Temperatures in the lower stratosphere are closely coupled to ozone concentrations through dynamics and photochemistry. Over the Antarctic region, extremely low tempera-

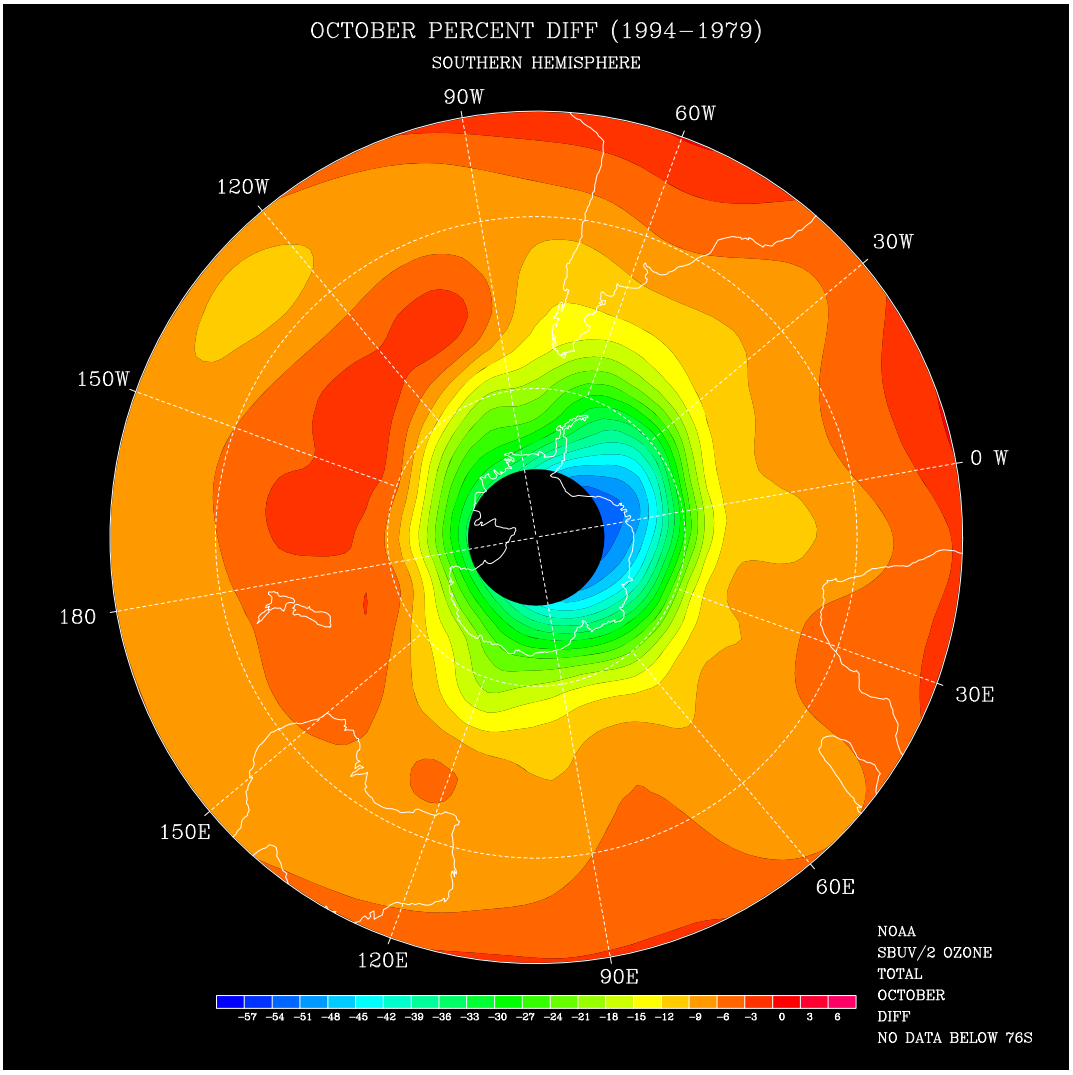

Figure 1.16 Total ozone percent difference between October 1994 and October 1979. Regions of no data are shown in black. (Source: CAC)

tures (lower than -78°C) at the 50-mb level (approximately 19 km) contribute to the formation of polar stratospheric clouds (PSCs). PSCs enhance the production and lifetime of reactive chlorine, leading to ozone depletion. For most of the southern winter and spring of 1994, daily minimum temperatures at 50 mb over the south polar region (65°S to 90°S) were sufficiently low for polar stratospheric clouds to form (**Fig. 1.17**).

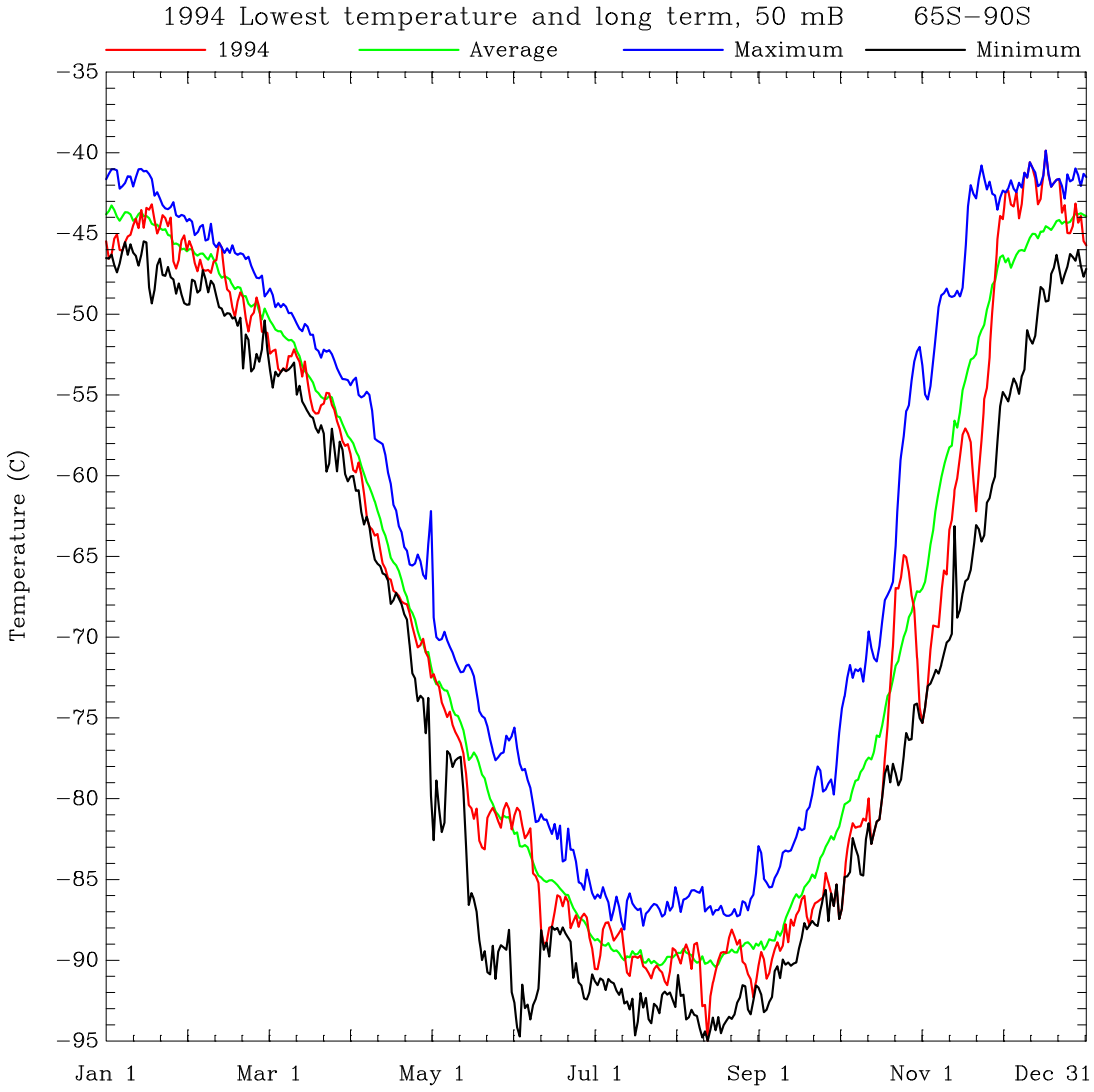

Figure 1.17 Daily minimum temperatures at 50 mb (19 km) in the region 65°S to 90°S for 1994 (red line). Mean daily values for the period 1978-1994 are shown in green, daily extreme minima for any year (black), and daily maxima for any year (blue) are also shown. (Source: CAC)

2) Carbon Dioxide

The atmospheric carbon dioxide (CO_2) measurements made at Mauna Loa Observatory, Hawaii, since 1958 provide unambiguous evidence for human alteration of the environment on a global scale (**Fig. 1.18**). The data through 1973 are from *Keeling et al. (1982*), while data since 1973 are from the NOAA program (*Thoning et al. 1989*).

Because the infrared absorption properties of the greenhouse gases and their role in determining global climate are well understood, it is certain that the CO_2 increase will alter the radiative forcing of the climate system. However, because the earth's climate is very complex and involves the atmosphere, the oceans, ice sheets, and living systems, it is much more difficult to predict how climate change will be manifested. The ongoing measurements will provide a better understanding of the natural carbon cycle and thus assist in the formulation of rational and informed policies concerning climate change and possible mitigation strategies.

3) Methane

Globally-averaged methane mixing ratios are collected approximately weekly from various sites in the NOAA/CMDL cooperative air sampling network (*Dlugokencky et al. 1994*). Air sampling sites are distributed between 90°S and 82°N. The average increase in the globally-averaged methane mixing ratio over the period 1983-1993 is approximately 0.6% per year when referenced to the middle of the sampling record (**Fig. 1.19**). The growth of methane over the past few years has slowed, probably due to a change in the anthropogenic source (*Dlugokencky et al. 1994*). Increased methane affects the Earth's radiation balance and the chemistry of the atmosphere. While the major sources of methane have been identified, their absolute contributions to the global methane budget remain poorly quantified. Until a better understanding of the methane budget is realized, the exact causes of the observed increase will remain uncertain. It is clear, however, that the increase in atmospheric methane is related to increased methane emissions from sources directly influenced by human activity.

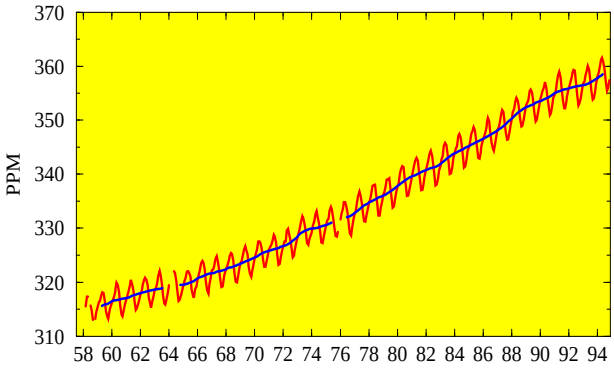

Figure 1.18 Monthly mean (red line) carbon dioxide concentrations (ppm) measured at Mauna Loa, Hawaii, 1958-1994. Blue line is the twelve-month running mean. The data through 1973 are from C. D. Keeling at Scripps Institute of Oceanography. (Data provided by the Climate Monitoring and Diagnostics Laboratory.)

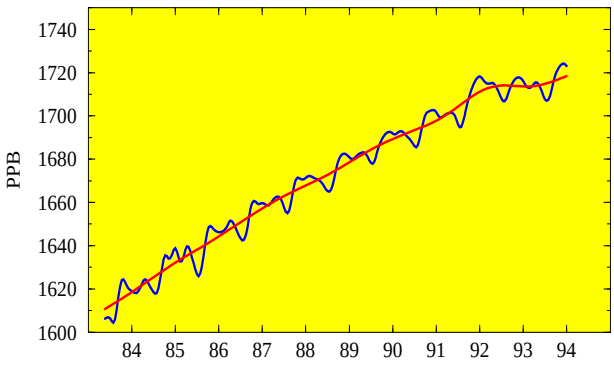

Figure 1.19 Globally-averaged, biweekly methane mixing ratios (ppb) by volume (blue curve) determined from the NOAA/CMDL Carbon Cycle Group cooperative air sampling network. Solid red line shows the growth with the seasonal cycle removed. (Data provided by the Climate Monitoring and Diagnostics Laboratory.)

d. Cryosphere

1) Snow Cover

The annual average areal extent of snow cover in the Northern Hemisphere is approximately 25×10^6 km^2, with a minimum of 3.6×10^6 km^2 in August and a maximum of 45.6×10^6 km^2 in January. Individual monthly departures from normal of 3.0×10^6 km^2 are not uncommon, and areal anomalies greater than 5.0×10^6 km^2 have occasionally been observed in the 23 years of consistently observed satellite estimates of hemispheric snow cover (**Fig. 1.20**). The late 1980's to the present represents the longest interval of below-normal snow cover extent since the beginning of this record in 1972. However, longer term station-based snow cover observations suggest that the late 1970's may have been the snowiest period since the turn of the century (*Robinson 1992*).

For the eight-year period ending December 1994, hemispheric areal snow cover was above normal in only thirteen months. For the 16-month period ending in December 1994 hemispheric areal snow cover was above normal in only 5 months.

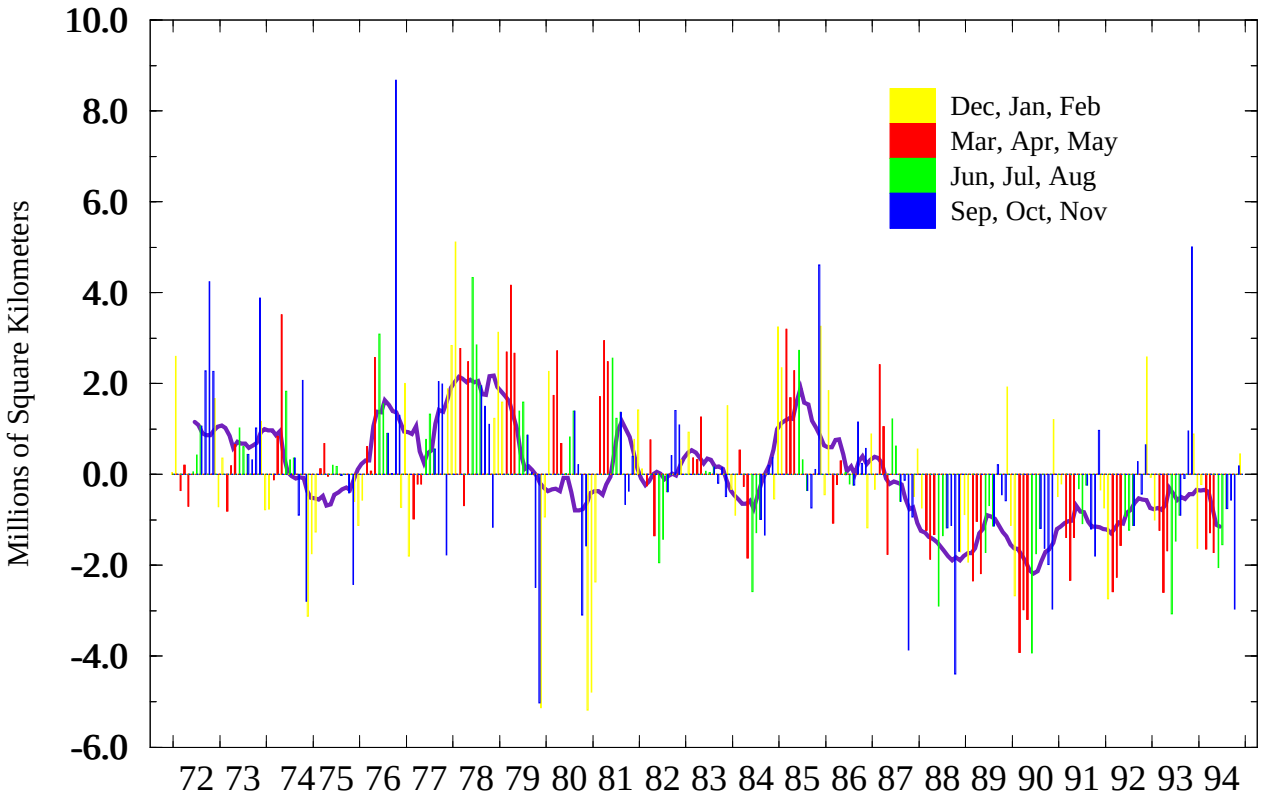

Figure 1.20 Anomalies of monthly snow cover extent over the Northern Hemisphere (including Greenland) between January 1972 and December 1994. Smoothed curve is a twelve-month running mean. Anomalies are departures from the 1972-1994 base period means. (Data provided by Rutgers University.)

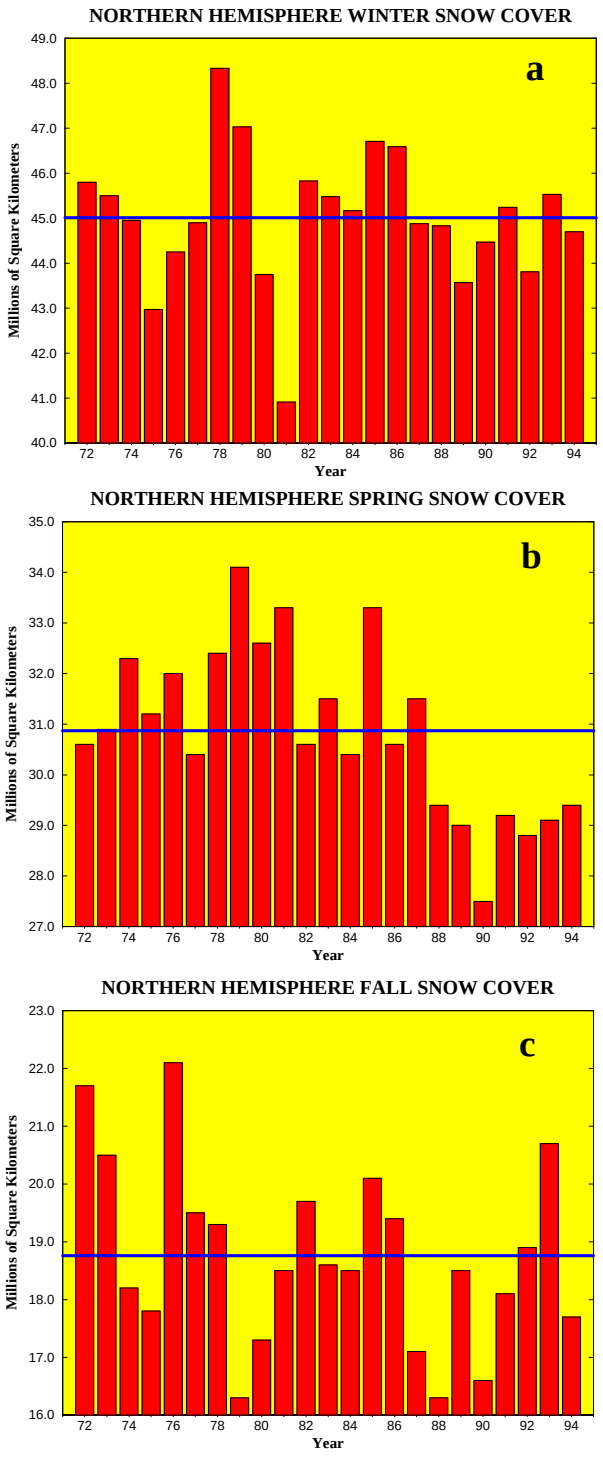

Figure 1.21 Time series of Northern Hemisphere snow-cover area (10^6 km^2) for a) winter (December through February), b) spring (March - May), and c) fall (September - November) estimated from visual satellite imagery. The solid black line depicts normal seasonal snow cover area. (Data provided by NOAA/NESDIS and Rutgers University.)

During the past decade the December - February (DJF) areal snow cover exhibited relatively little interannual variability (**Fig. 1.21a**) compared to the transition seasons (**Figs. 1.21b, c**). While the total hemispheric areal snow cover for DJF 1993/94 was only slightly below normal (**Fig. 1.21a**), above-normal areal snow cover was observed over the northern Plains of the United States, large portions of Manchuria, and east of the Caspian Sea (**Fig. 1.22**). These areas also experienced colder-than-normal surface temperatures during the winter season (see section 3). In contrast, below-normal areal snow cover extent was observed in the western United States, northern Europe, and portions of the Tibetan Plateau, areas where above-normal winter surface temperatures were observed.

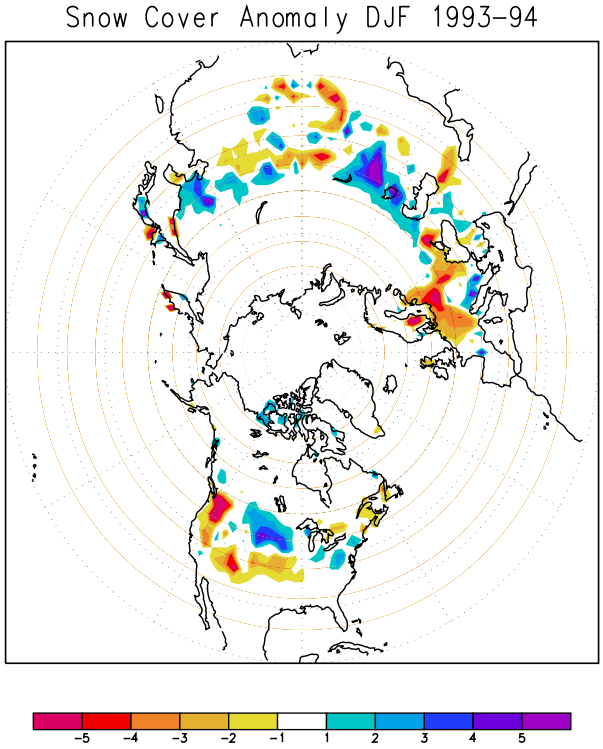

Figure 1.22 Winter (December 1993 - February 1994) snow-cover anomaly in weeks, derived from subjective analysis of visual satellite imagery by NOAA/NESDIS. Anomalies are departures from the 1973-1993 base period. (Source: CAC)

Total Northern Hemisphere areal snow cover during March-May (MAM) was approximately 1.5×10^6 km^2 below normal, making this the seventh consecutive MAM with below-average areal snow cover (**Fig. 1.21b**). The reduced extent of snow cover was most prevalent over the northwestern United States, western Canada, and Alaska, as well as large portions of northern Europe, northern Scandinavia, and southern Russia (**Fig 1.23**). Only isolated areas experienced a greater-than-normal frequency of snow cover during the season, i.e., portions of western Russia and portions of the eastern Tibetan Plateau.

Large interannual variability of total Northern Hemisphere snow cover area has been observed during September-November (SON) for the entire satellite-based record (**Fig. 1.21c**). During SON 1994, total snow coverage was approximately 17.7×10^6 km^2, 1.1×10^6 km^2 below normal, and nearly 3×10^6 km^2 less coverage than observed in 1993. A reduced areal extent of snow cover was observed over much of eastern Canada, central Alaska, and large portions of central and western Siberia (**Fig. 1.24**). Above-normal snow cover areal extent was confined to the western United States during the season, and to scattered portions of southern Russia and western China.

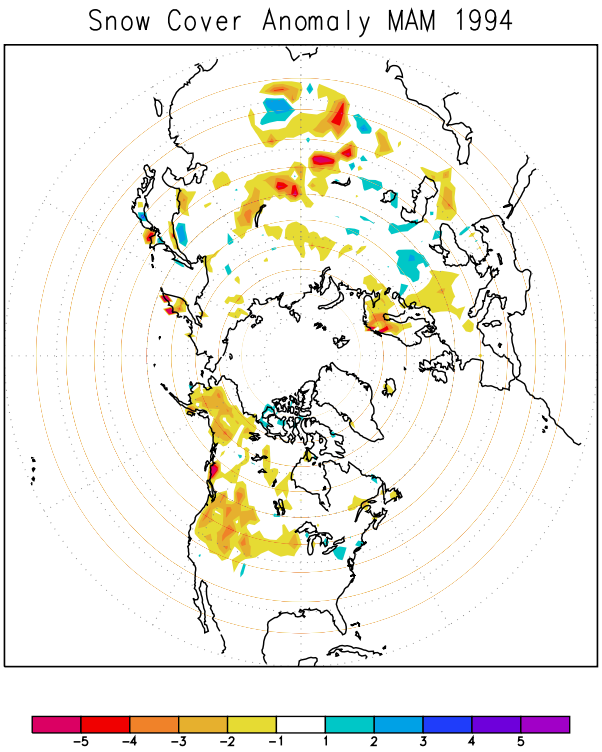

Figure 1.23 Spring (March - May) 1994 snow-cover anomaly in weeks, derived from subjective analysis of visual satellite imagery by NOAA/NESDIS. Anomalies are departures from the 1973-1993 base period. (Source: CAC)

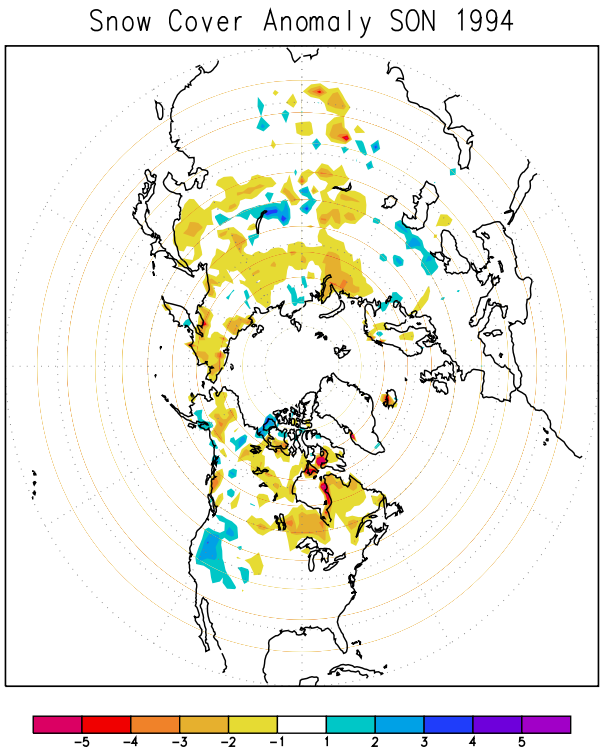

Figure 1.24 Fall (September - November) 1994 snow-cover anomaly in weeks, derived from subjective analysis of visual satellite imagery by NOAA/NESDIS. Anomalies are departures from the 1973-1993 base period. (Source: CAC)

2) Sea Ice

Total Arctic sea ice extent (**Fig. 1.25d**) exhibits relatively large year-to-year variability. A relatively steady increase in the total Arctic sea-ice extent has been observed since July 1993. Over the 18 month period from July 1993 to December 1994, ice cover increased slightly in the Barents and Okhotsk Seas (**Figs. 1.25a, b**), and increased more dramatically in the Beaufort Sea (**Fig. 1.25c**).

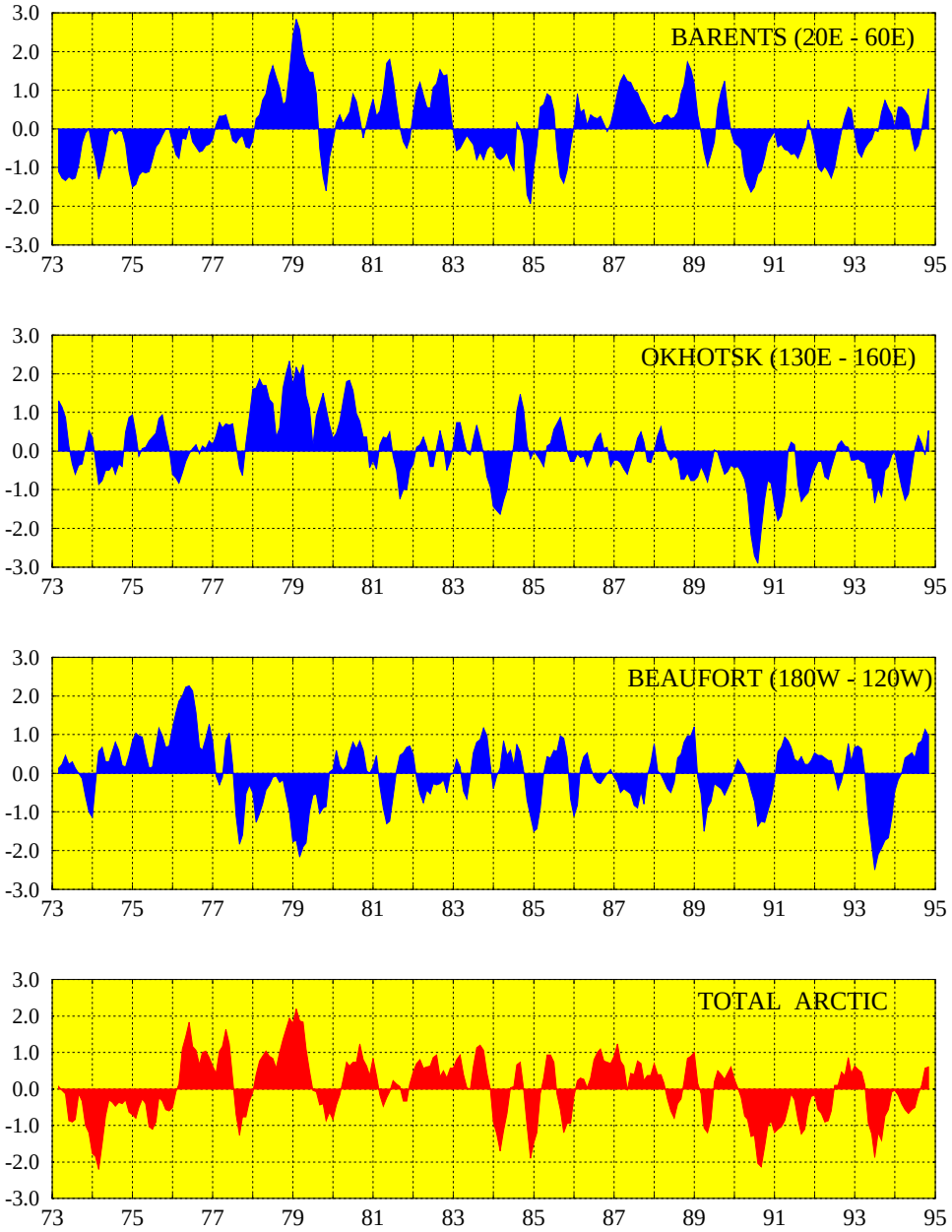

Figure 1.25 Standardized sea-ice area anomalies for the a) Barents Sea, b) Okhotsk Sea, c) Beaufort Sea, and d) Total Arctic. Values are standardized by the standard deviation for the 1973-1994 period. (Source: CAC)

In contrast with the Arctic, total sea-ice cover in the Antarctic has shown little variability since 1989 (**Fig. 1.26d**), suggesting a relatively stable sub-ocean circulation and heat transport in high southern latitudes. These conditions differ from the large anomalies in total sea-ice observed early in the record, which have been linked to slow variations in the subsurface oceanic heat and salinity fluxes.

During the past several years, selected sub-regions around the Antarctic have experienced substantial changes in sea-ice extent (**Figs. 1.26a-c**). However, these changes have tended to be out of phase from one region to the next, resulting in little net change in total ice cover during the period.

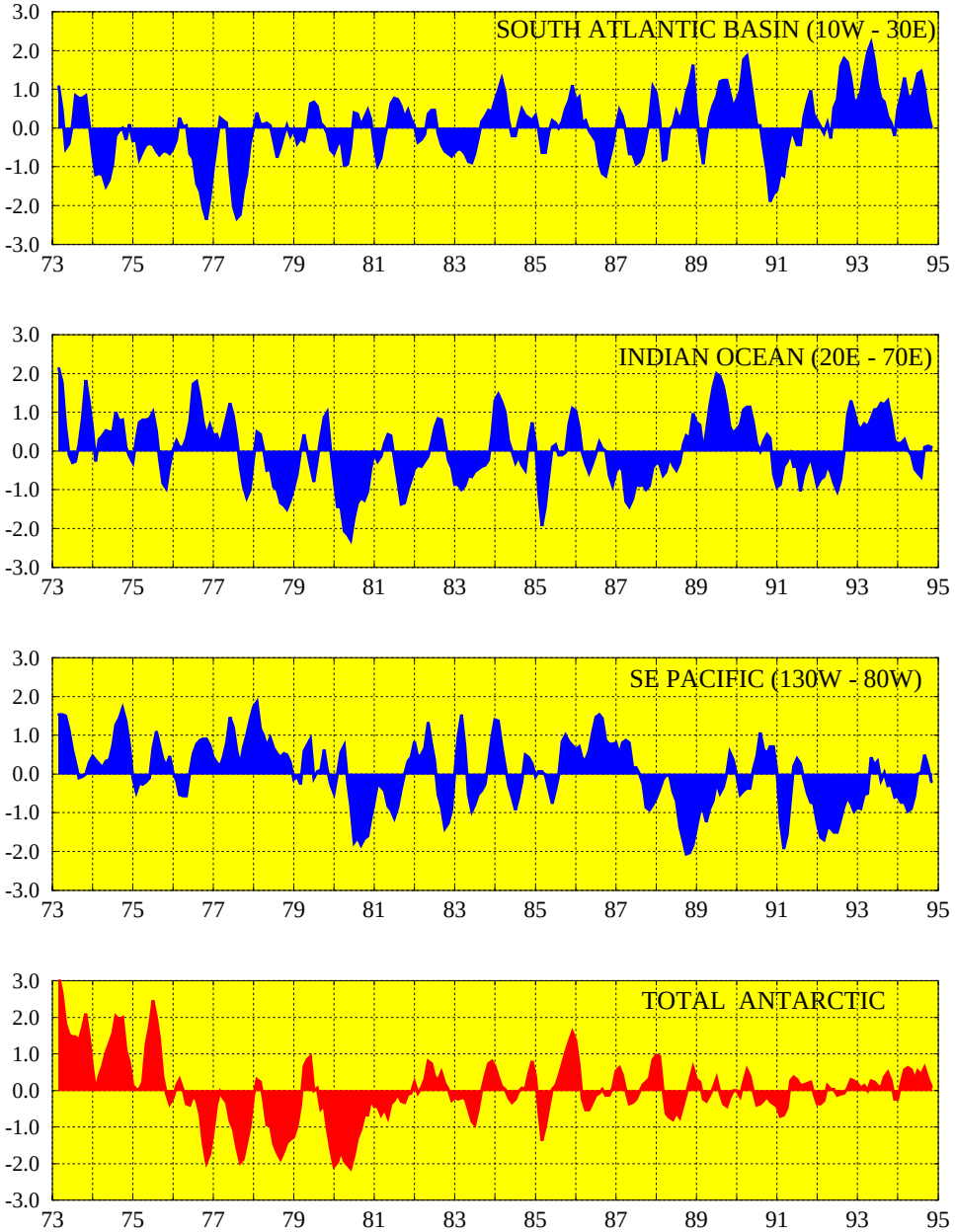

Figure 1.26 Standardized sea-ice area anomalies for the a) South Atlantic Basin, b) Indian Ocean, c) Southeast Pacific, and d) Total Antarctic. Values are standardized by the standard deviation for the 1973-1994 period. (Source: CAC)

e. Atmospheric Angular Momentum

The relative atmospheric angular momentum (AAM) about the Earth's axis is a convenient global index of the intensity of the zonal circulation that can be monitored for climate purposes. It is a function of the zonal winds integrated through the depth of the atmosphere with higher weights given in the low latitudes due to the large radius arm there. Each year, the AAM undergoes a strong annual cycle, related in large part to the strong seasonal variability in the Northern Hemisphere subtropical jets. Superimposed on the seasonal signal are high-frequency fluctuations, often related to the tropical intraseasonal oscillation (*Madden and Julian 1994*). Higher variance tends to occur during the broad maximum during the Northern Hemisphere winter period. On the interannual scale, AAM variations are influenced by El Niño/Southern Oscillation (ENSO) signals. The AAM is also of interest to geodetic science because of its relation to changes in the Earth's rotation, and it is one of several quantities monitored by a specialized data center in this connection (*Salstein et al. 1993*).

A fifteen-year time series of AAM integrated between 50 and 1000 mb (**Fig. 1.27**) reveals the signals on the time scales described

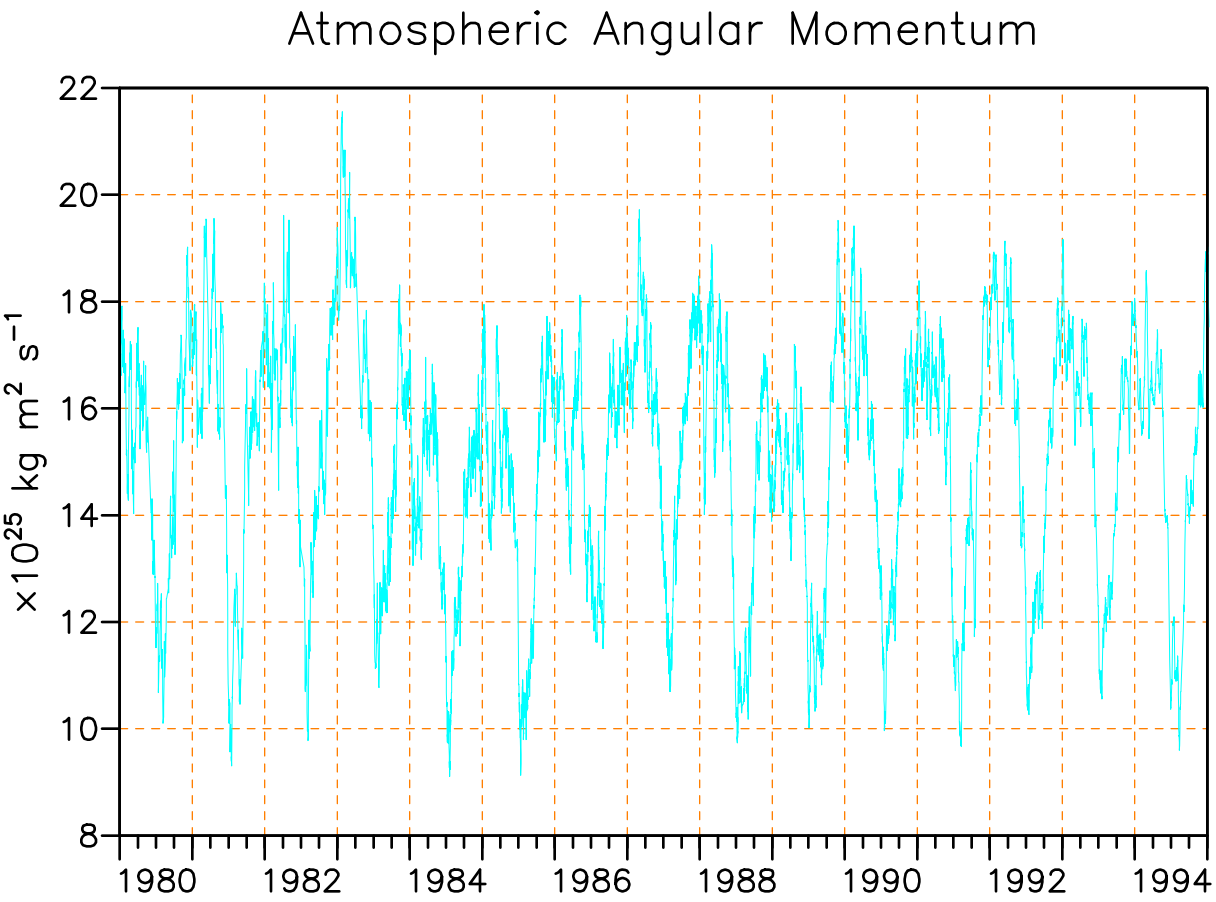

Figure 1.27 Global relative angular momentum of the atmosphere about the Earth's rotation axis during the period 1980-1994, as determined from the National Meteorological Center's daily zonal wind analyses between 50 and 1000 mb. (Source: Atmospheric and Environmental Research, Inc.)

above. Of particular note are the strong peaks during the maximum phases of warm episodes, particularly in 1983, and to a lesser extent in 1987. Minima in AAM occurred in the cold episode years, such as 1988. During 1994, less variance occurred in AAM during the early part of the year compared with many earlier years. However, the last month of the year saw a dramatic increase in AAM, possibly related to the development of mature warm episode conditions in the tropical Pacific (see section 2.b). These signals are revealed in the anomaly plot of **Fig. 1.28**, representing the difference between the 1994 signal and the 15-year mean. The rapid mid-December rise is quite evident, as are other peaks in late February and mid-September. The minimum of AAM usually arrives during July, but in 1994 this low value did not occur until August, when it dropped to its lowest value since 1985.

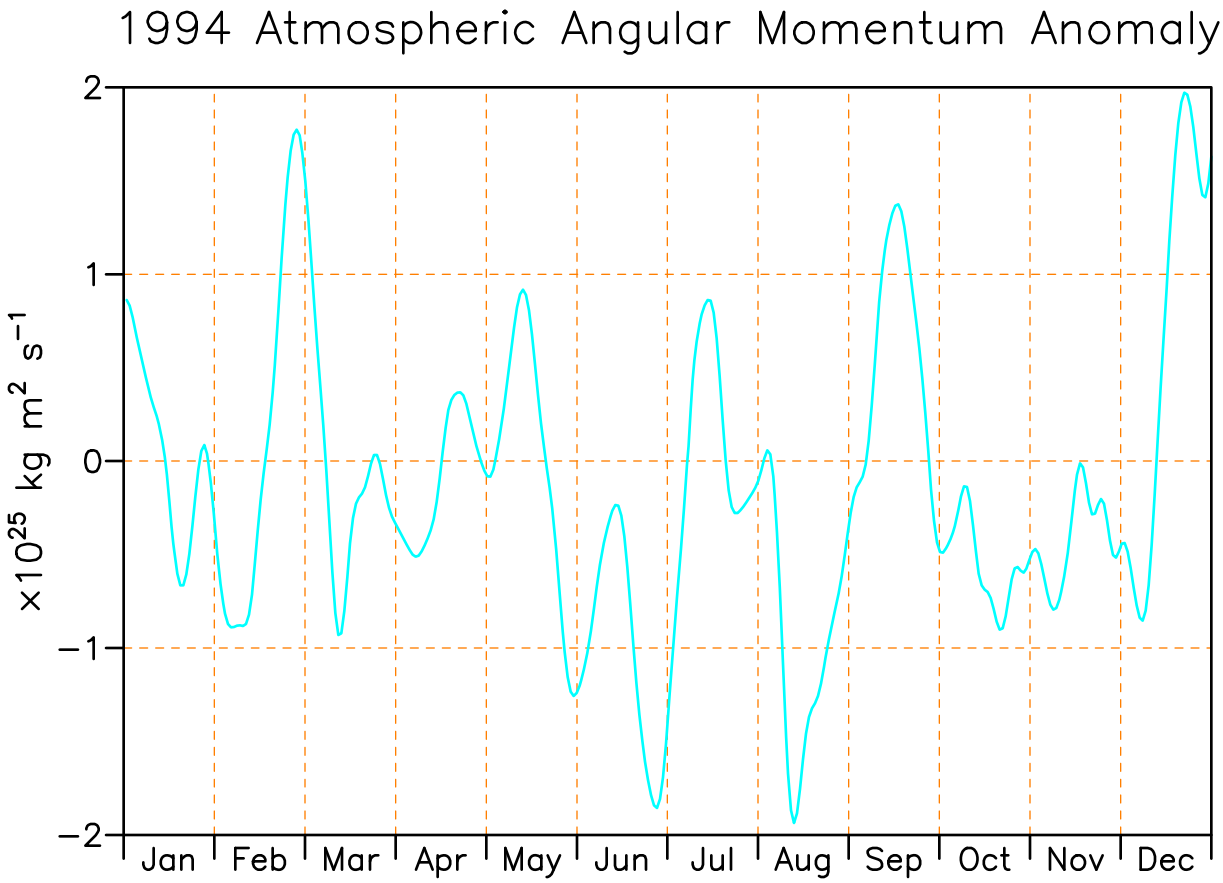

Figure 1.28 Departure of the 1994 daily atmospheric momentum values from the 15-year calendar mean. Values have been smoothed by a filter to damp fluctuations on periods shorter than about 8 days. (Source: Atmospheric and Environmental Research, Inc.)

2. OCEANIC AND ATMOSPHERIC ANOMALIES RELATED TO ENSO

a. Large-scale conditions in the tropics: 1990-1994

During the 1990-1994 period above-normal pressure dominated the Atlantic Ocean, Indonesia, and the western Pacific Ocean, and below-normal pressure covered the eastern tropical and subtropical Pacific (**Figs. 2.1 and 2.2**). In the Pacific, this anomalous pressure pattern reflects a sustained negative phase of the Southern Oscillation (**Fig. 2.3**), as defined by the Southern Oscillation Index (SOI). Accompanying this pattern, positive sea surface temperature anomalies have been prominent in the central and east-central equatorial Pacific (**Fig. 2.4**) and weaker than normal low-level easterlies have dominated the equatorial Pacific (**Fig. 2.5**). Since 1991, ma-

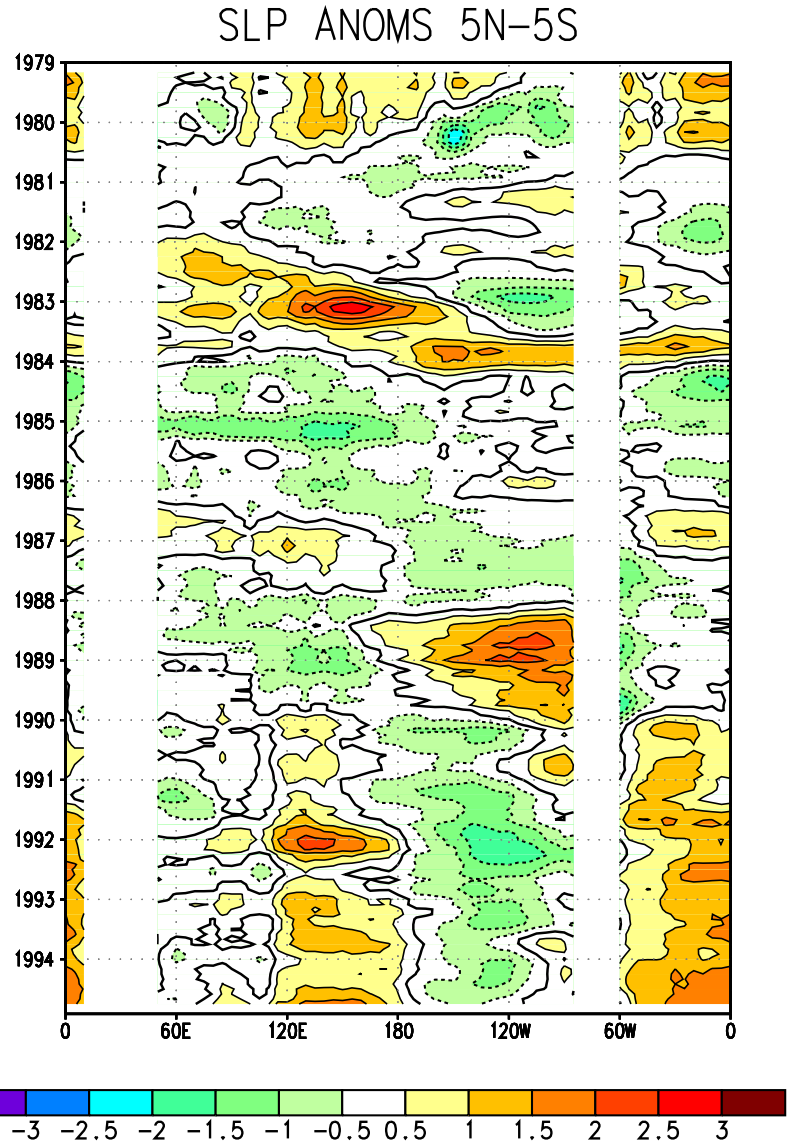

Figure 2.1 Time-longitude section of monthly sea level pressure anomalies averaged for 5ºN-5ºS. Contour interval is 0.5 mb. Anomalies are departures from the 1979-1988 base period means. Elevated regions are masked out. (Source: CAC)

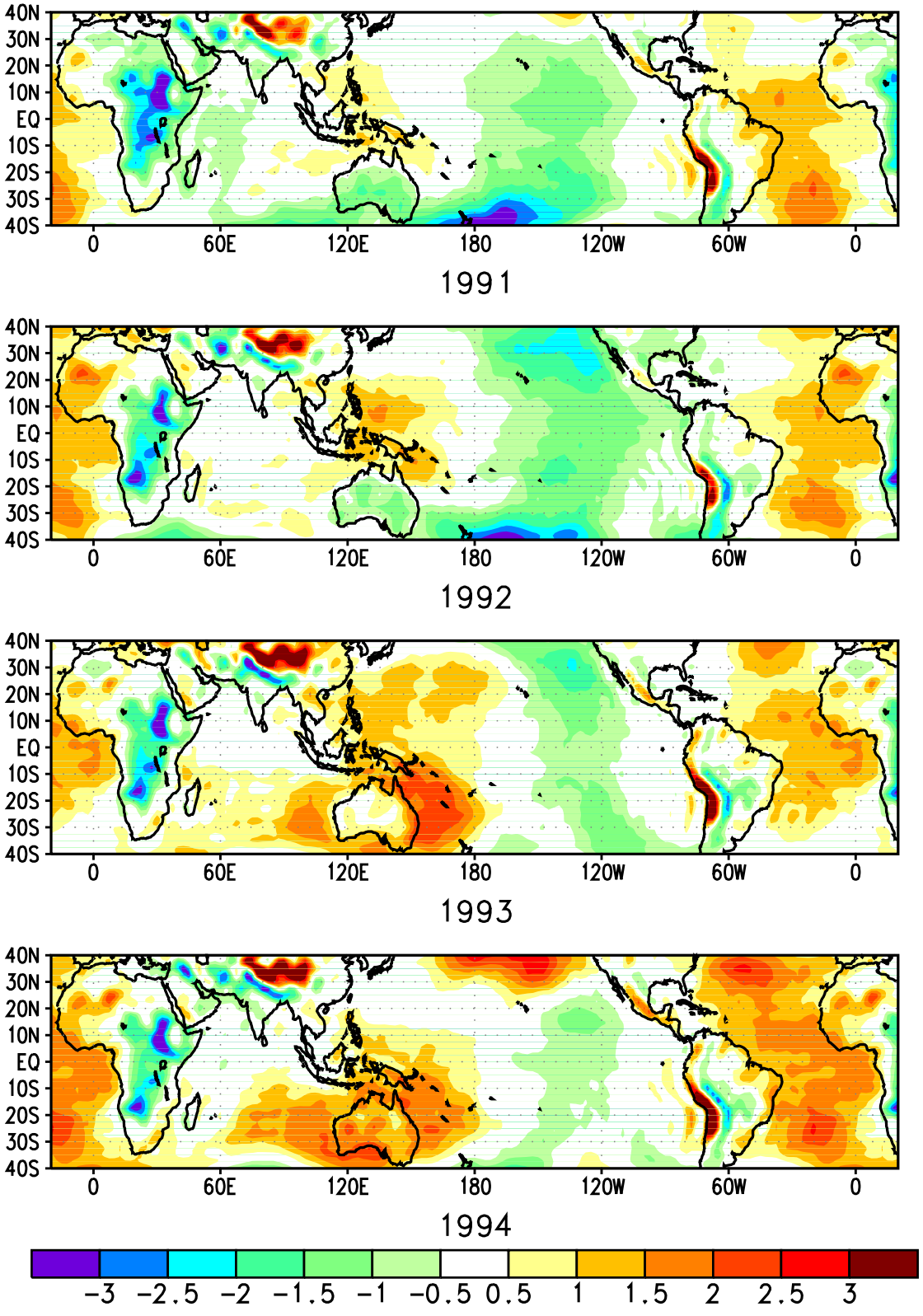

Figure 2.2 Annual sea level pressure anomalies for 1991, 1992, 1993, and 1994. Contour interval is 0.5 mb. Anomalies are departures from the 1979-1988 base period means. The analysis should be treated with caution in regions of high terrain. (Source: CAC)

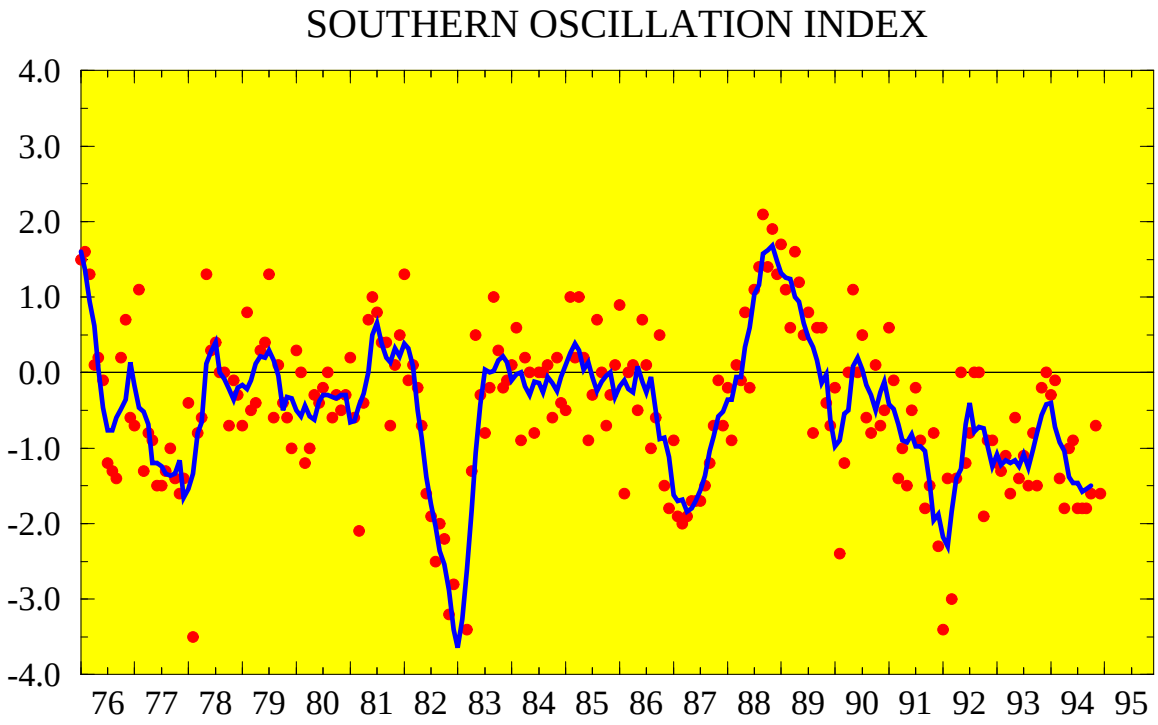

Figure 2.3 Five-month running mean of the Southern Oscillation Index (SOI). The SOI is computed as the standardized difference between the standardized pressure anomalies at Tahiti and Darwin (Tahiti minus Darwin). Individual monthly values are indicated by red dots. (Source: CAC)

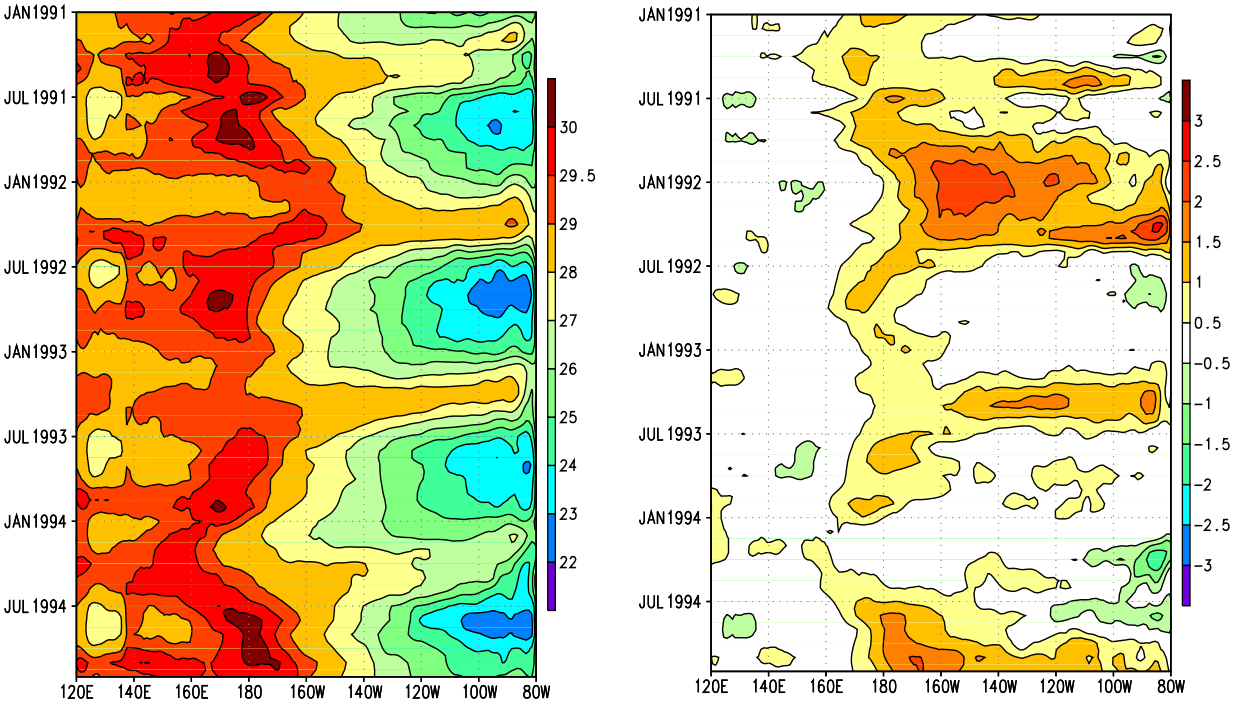

Figure 2.4 Time-longitude section of mean (left) and anomalous (right) sea surface temperature (SST) (°C) averaged from 5°N-5°S. Anomalies are departures from the adjusted OI climatology (*Reynolds and Smith 1995*). (Data provided by the NMC Coupled Model Project.)

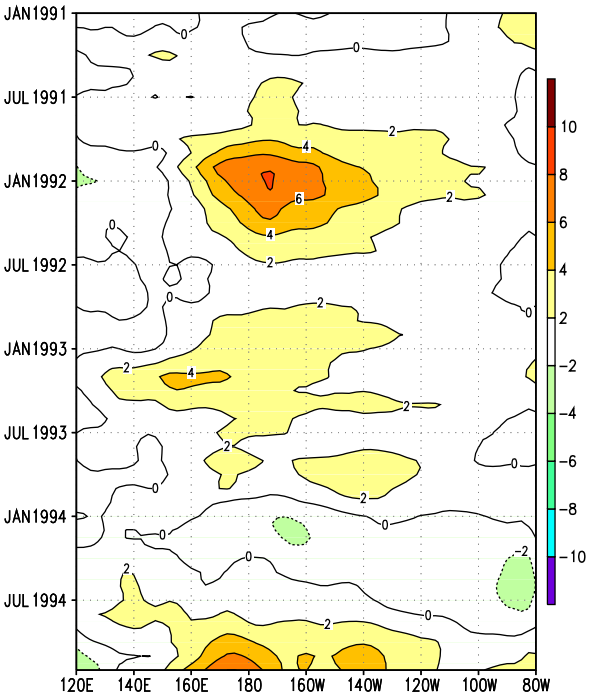

Figure 2.5 Time-longitude section of anomalous 850-mb zonal wind (ms^{-1})averaged from 5°N-5°S. Anomalies are departures from the 1979-1988 base period means. (Source: CAC)

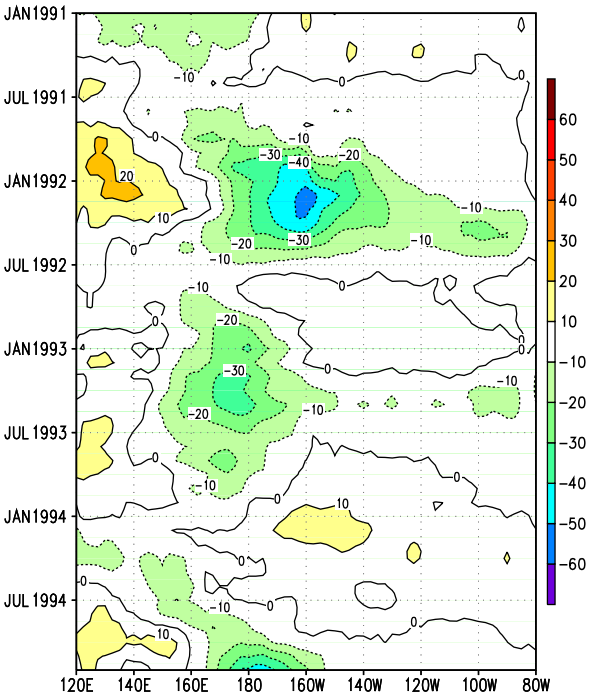

Figure 2.6 Time-longitude section of anomalous outgoing longwave radiation (OLR) Wm^{-2} averaged from 5°N-5°S. Anomalies are departures from the 1979-1988 base period means. (Source: CAC)

ture warm episode conditions have been observed during November 1991-May 1992, January - June 1993, and beginning in November 1994. During these periods, atmospheric convection (as indicated by negative outgoing longwave radiation (OLR) anomalies) was greatly enhanced over the central equatorial Pacific (**Fig. 2.6**). In addition, the South Pacific Convergence Zone was shifted northeastward, and the Intertropical Convergence Zone in the Northern Hemisphere was shifted equatorward. These conditions were accompanied by abnormally warm ocean waters from the date line to the South American coast and by a substantial reduction in the strength of the equatorial easterlies in the area east of the date line.

The redevelopment of mature warm episode conditions in the tropical Pacific during late 1994 for a third time in four years is unprecedented in the last 50 years. However, there is at least one other period during this century, and possibly a few others in the latter half of the 19th century, that featured similar prolonged warm episode conditions. The period 1911-1915 appears to be most similar to the present, at least as indicated by the Darwin SLP anomalies (**Fig. 2.7**). During that period, 1911, 1912, and 1914 are considered El Niño years.

Also since 1990, above-normal sea level pressure has dominated the tropical and subtropical latitudes of the Atlantic, along with large portions of both the North and South Atlantic (**Figs. 2.1 and 2.2**). In the tropics, these positive anomalies have been stronger and more persistent than those observed over Indonesia during the period. These conditions have likely contributed to reduced hurricane activity over the Atlantic Ocean, the Caribbean Sea, and the Gulf of Mexico throughout the period.

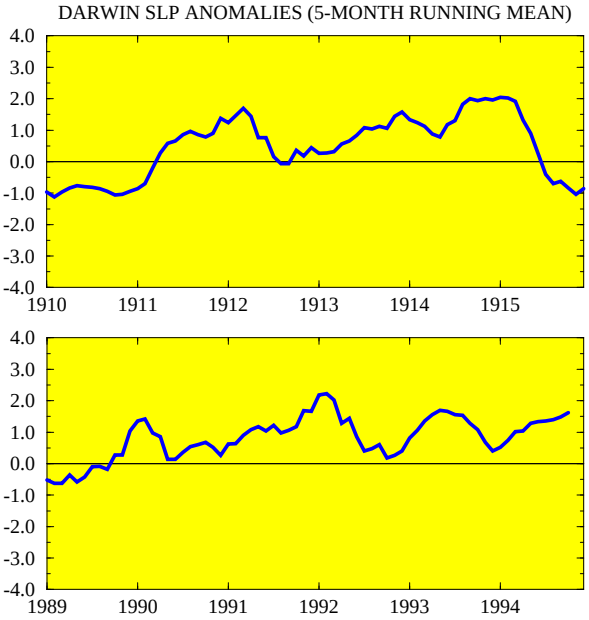

Figure 2.7 Five-month running mean of SLP anomalies (mb) at Darwin, Australia for 1910-1915 (top) and 1989-1994 (bottom). Anomalies are departures from the 1951-1980 base period monthly means. (Source: CAC)

b. The 1994 Pacific warm episode

By late 1993 the low-level equatorial easterlies had become slightly stronger than normal (**Fig. 2.5**), positive SST anomalies in the vicinity of the date line had decreased (**Fig. 2.4, right**), and convective activity in the central tropical Pacific was slightly weaker than normal (**Fig. 2.6**). During the next three months (December-February 1993/94), SSTs finally returned to near-normal throughout the entire equatorial Pacific (**Fig. 2.8a**). This evolution was accompanied by the development of above-normal convection over western Indonesia and the eastern Indian Ocean, and by a continuation of weaker than normal convection over the central equatorial Pacific (**Figs. 2.9 and 2.10**). These conditions, along with a further strengthening of the equatorial easterlies throughout the Pacific (**Fig. 2.5**), supported coupled model and statistical predictions of the possible evolution toward cold episode conditions during the next year.

However, two important features remained unchanged during December-February, indicating that warm episode conditions had not completely disappeared. First, large areas of positive SST anomalies remained in the subtropics of both hemispheres east of the date line (**Fig. 2.8a**). Second, the previously described pattern of anomalous SLP persisted throughout the global tropics during the season (**Figs. 2.1 and 2.2**), despite a return to near-zero values of the SOI (**Fig. 2.3**).

During the March-May season, sea level pressure anomalies at Darwin increased (**Fig. 2.7, bottom**), the SOI decreased to -1.5 (**Fig. 2.3**), and the equatorial easterlies once again weakened (**Fig. 2.5**). During May, positive SST anomalies reappeared along the equator near the date line (**Fig. 2.4, left**), consistent with a further weakening of the equatorial easterlies over the central and east-central Pacific (**Fig. 2.5**). Overall, these conditions indicated a trend away from possible cold episode conditions during the upcoming year. However, they remained inconclusive as far as indicating a return toward mature ENSO conditions in the upcoming 1994/95 boreal winter season.

During June-August, positive SST anomalies continued to increase and spread eastward across the central equatorial Pacific (**Figs. 2.4, right and 2.8**). This evolution was consistent with a gradual eastward shift of the warmest equatorial water (greater than 30°C) to the vicinity of the date line (**Fig. 2.4, left**) and with a deepening of the oceanic thermocline and an increase in subsurface ocean temperature anomalies in the east-central equatorial Pacific (**Fig. 2.11**). By August, SST anomalies averaged 1.0-1.5°C above normal along the equator between 170°E and 160°W. This increase was accompanied by weaker than normal easterlies throughout the central and east-central equatorial Pacific (**Fig. 2.5**) and by sustained negative values of the SOI, which again averaged -1.5 during the season (**Fig. 2.3**).

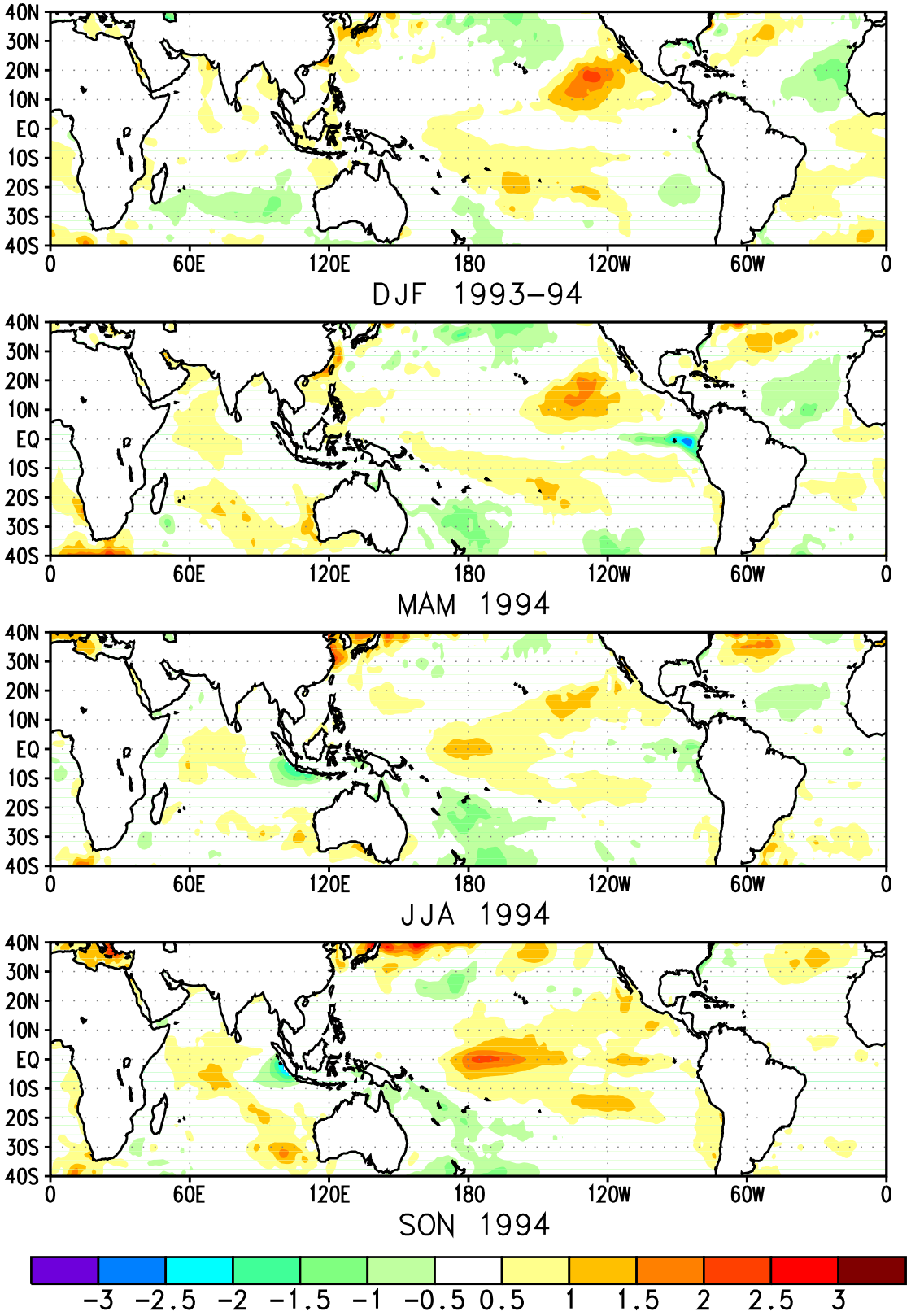

Figure 2.8 Seasonal sea surface temperature (SST) anomalies (°C) computed as departures from the adjusted OI climatology (*Reynolds and Smith 1995*). (Data provided by the NMC Coupled Model Project.)

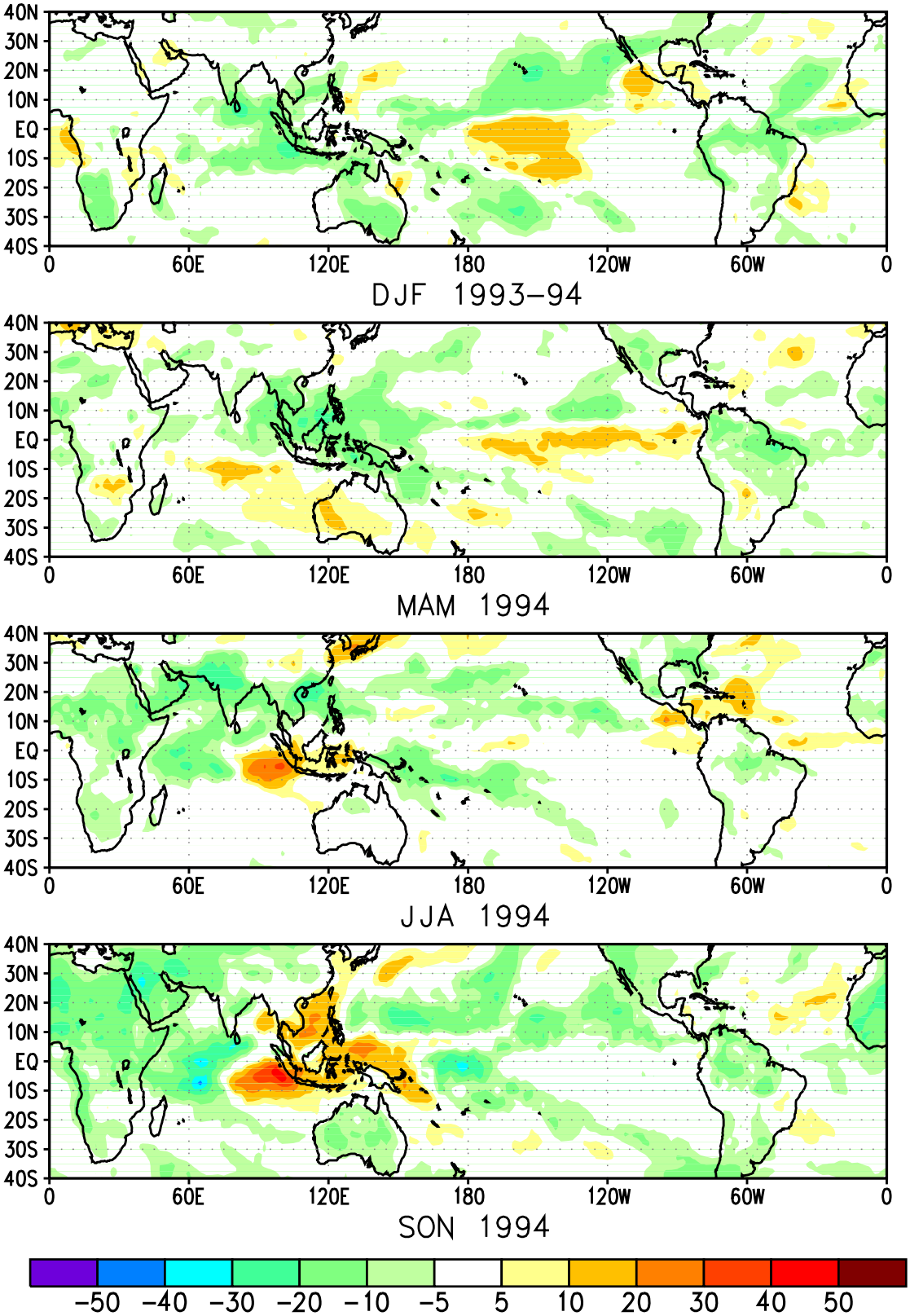

Figure 2.9 Seasonal outgoing longwave radiation (OLR) anomalies (Wm^{-2}) computed as departures from the 1979-1988 base period means. (Source: CAC)

In the past, these features have collectively been good indicators of developing warm episodes. In fact, by August, coupled ocean-atmosphere and statistical model guidance indicated continued warmer than normal conditions through early 1995. These indications, together with atmospheric and oceanic trends, suggested that warm episode conditions would intensify and that a mature warm episode would develop by early 1995.

During September-November, a rapid intensification and eastward spread of positive SST anomalies was indeed observed between the date line and 160°W (**Figs. 2.4 and 2.8**), where anomalies averaged 2-2.5°C above normal. This increase was accompanied by a further weakening of the low-level equatorial easterlies over the central equatorial Pacific (**Fig. 2.12**), particularly during late September and most of October. At times the 850-mb

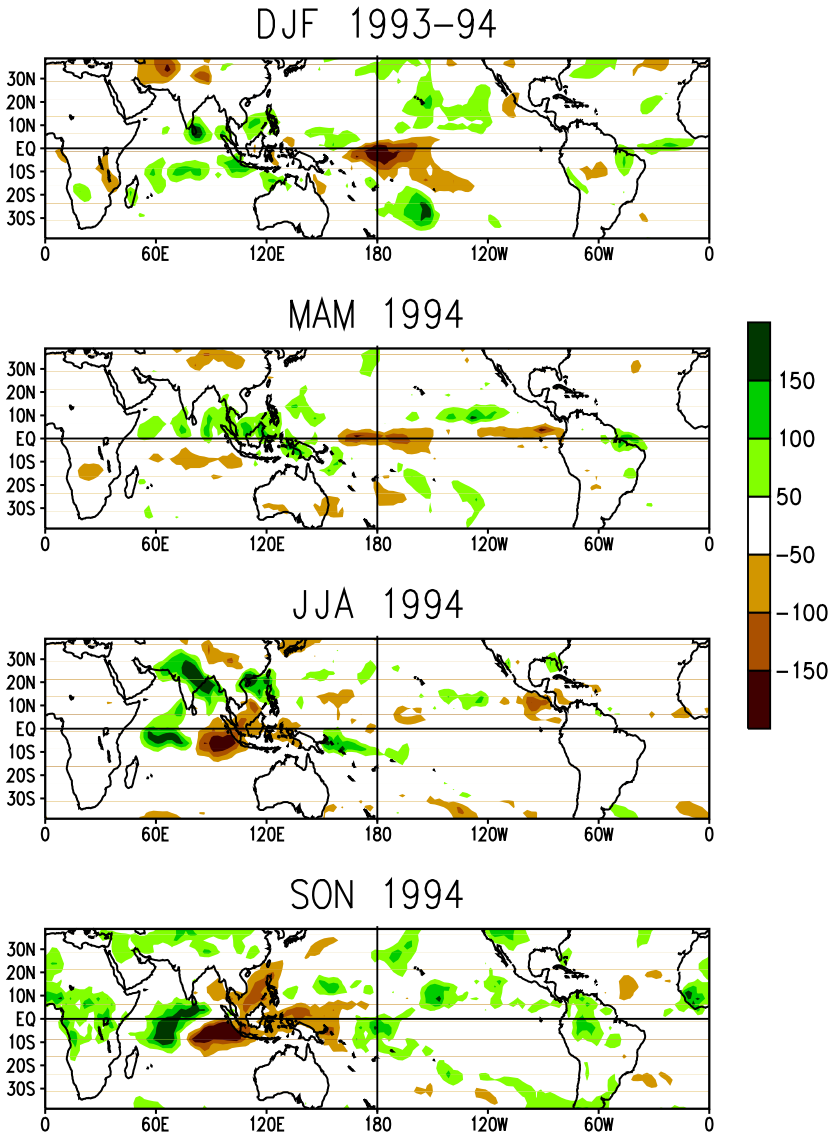

Figure 2.10 Satellite-derived rainfall anomaly estimates in mm per month. Anomalies are departures from the 1986-1993 base period means. (Source: CAC)

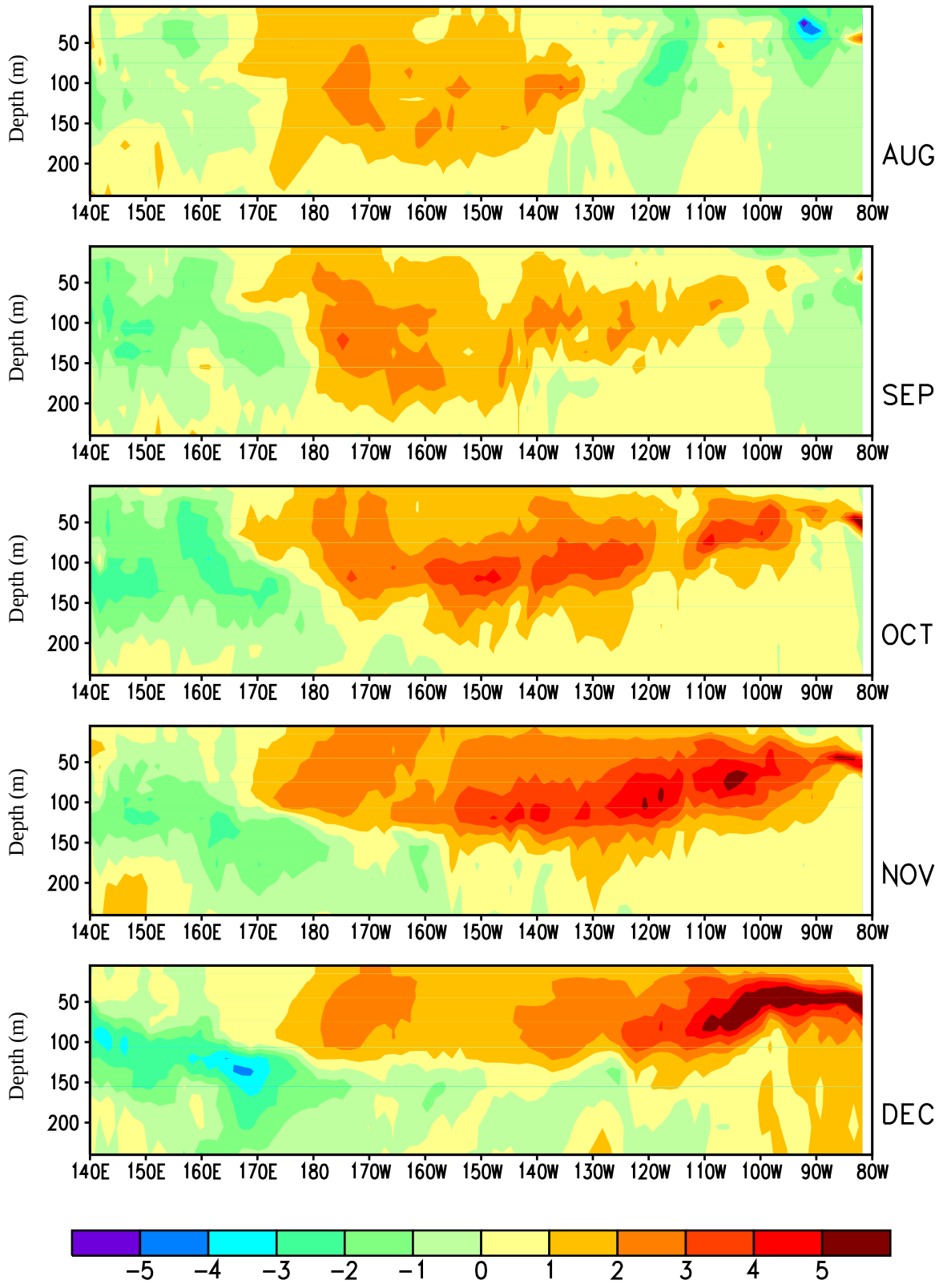

Figure 2.11 Equatorial depth-longitude section of monthly mean ocean temperature anomalies for August through December 1994. Data are derived from an analysis system that assimilates oceanic observations into an oceanic GCM (*Leetmaa and Ji 1989*). Contour interval is 1°C. Anomalies are departures from the 1983-1992 base period means. (Data provided by the NMC Coupled Model Project.)

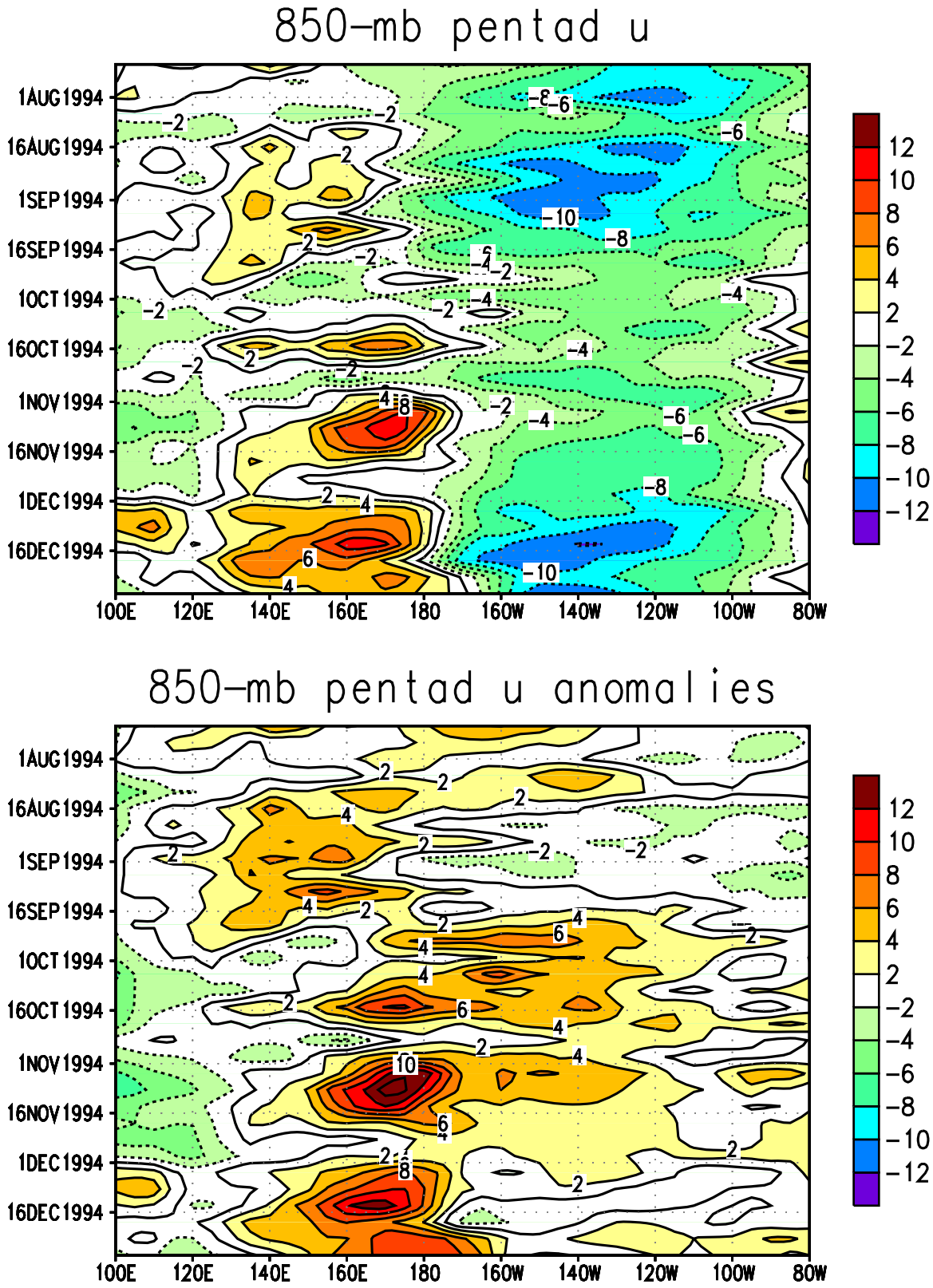

Figure 2.12 Time-longitude section of pentad mean (top) and anomalous (bottom) 850-mb zonal wind averaged for 5ºN-5ºS. Contour interval is 2 ms^{-1}. Anomalies are departures from the 1979-1988 base period pentad means. (Source: CAC)

winds were nearly calm or even westerly (westerly wind bursts, **Fig. 2.12, top**), especially in the central Pacific near the date line. This pattern favored reduced upwelling in the upper ocean in the eastern equatorial Pacific, resulting in a deepening of the equatorial oceanic thermocline, an increase in subsurface temperature anomalies (**Fig. 2.11**), and an increase in SST anomalies everywhere east of the date line (**Figs. 2.4, right and 2.8**). These conditions were accompanied by the development of enhanced convection in the vicinity of the date line and the equator (**Fig. 2.9**) and by a continuation of below-normal convective activity and drought throughout Indonesia (**Fig. 2.10**) and large portions of Australia (see section 4.b).

Although these changes indicated an accelerated evolution toward mature warm episode conditions, convective activity in the central equatorial Pacific was quite variable during September and October in association with intraseasonal (30-60 day) oscillations (**Fig. 2.13**). Finally, during November and December persistent and enhanced convective activity, indicating the onset of mature ENSO conditions, became established in the vicinity of the date line. Thus, 1994 ended with a dramatic return to mature ENSO conditions for the third time in four years.

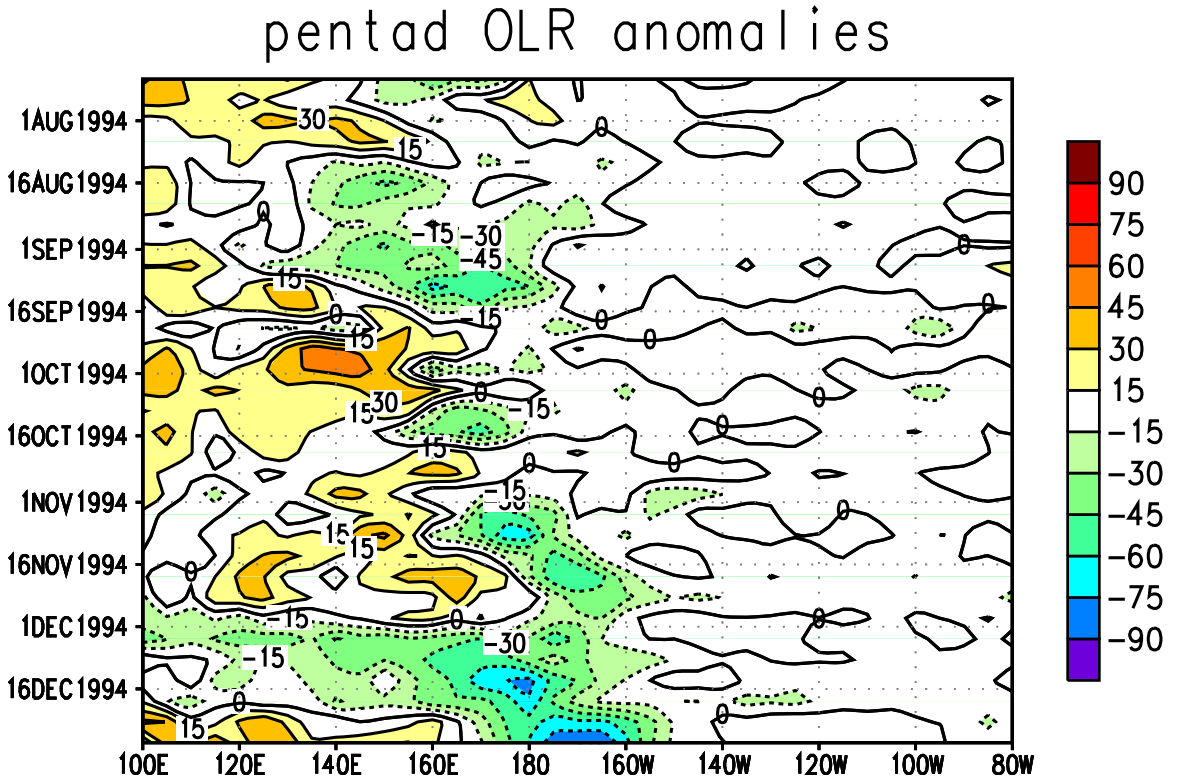

Figure 2.13 Time-longitude section of pentad anomalous outgoing longwave radiation (OLR) averaged for 5ºN-5ºS. Contour interval is 15 Wm^{-2}. Anomalies are departures from the 1979-1988 base period pentad means. (Source: CAC)

3. SEASONAL SUMMARIES

a. December-February

Northern Hemisphere

In the Northern Hemisphere large circulation, surface temperature, and precipitation anomalies were evident during December-February 1993/94 (DJF). Over the Pacific/North America sector, a pattern of above-normal heights at 500 mb was observed over the central North Pacific and the Bering Sea (**Fig. 3.1, top**). This pattern was associated with warmer than normal conditions (2-4°C above normal) over much of Alaska and western North America and with drier than normal conditions over much of southern Alaska and the Pacific Northwest (**Fig. 3.2**).

Farther east large negative height anomalies and much colder-than-normal conditions covered central and eastern Canada, the northern Plains states, the upper Midwest, and the northeastern United States. Additionally, above-normal precipitation was observed in a broad band extending from the lower Mississippi Valley northeastward to southern New England. Accompanying this precipitation, many areas in Pennsylvania, New York and southern/central New England experienced their snowiest winter on record. These anomalously cold and wet conditions were particularly prominent over eastern North America between 23 December-22 January (**Fig. 3.3, top**). During this 30-day period, *temperatures averaged 6-8°C below normal over much of Canada east of the Rockies, and 4-6°C below normal throughout the Northern Plains, the Midwest, and the Northeast*. Minimum temperatures during this period dropped to -40°C over large portions of Minnesota and eastern North Dakota, and to -25 to -35°C across the north-central and northeastern United States (**Fig. 3.3, bottom**). Additionally, minimum temperatures reached -10 to -15°C from northern New Mexico eastward to northern Georgia and the Carolinas, and freezing temperatures

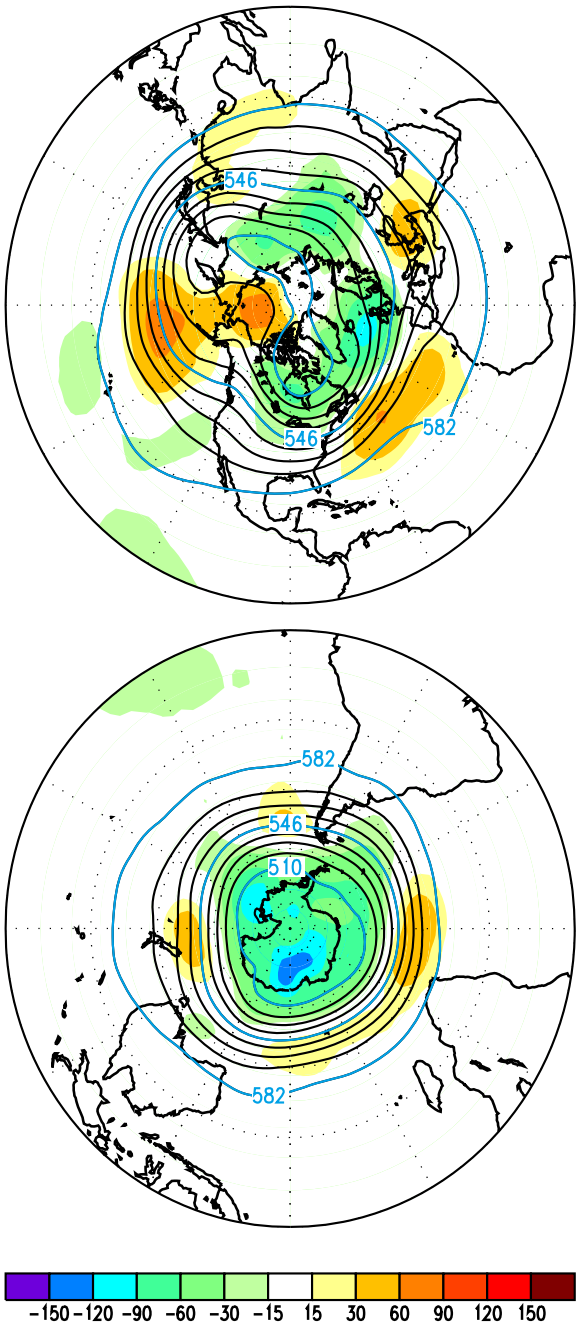

Figure 3.1 Northern Hemisphere (top) and Southern Hemisphere (bottom) 500-mb geopotential height (contours, interval is 9 dm) and anomalies (shading, in m) for December 1993 - February 1994. Anomalies are departures from the 1979-1988 base period. (Source: CAC)

extended southward to central Florida.

Over the North Atlantic Ocean and Eurasia, negative 500-mb height anomalies were observed at high latitudes, with positive anomalies observed in the middle latitudes. This circulation pattern reflected a pronounced positive phase of the North Atlantic Oscillation. Accompanying this circulation, below-normal temperatures were observed over Scandinavia, while abnormally warm and wet conditions dominated much of Europe. Surface temperatures averaged 2-4°C above normal throughout western and central Europe during the season, and averaged more than 4°C above normal over eastern Europe.

Precipitation totals during December and January averaged 50-150 mm above normal throughout northern and western Europe

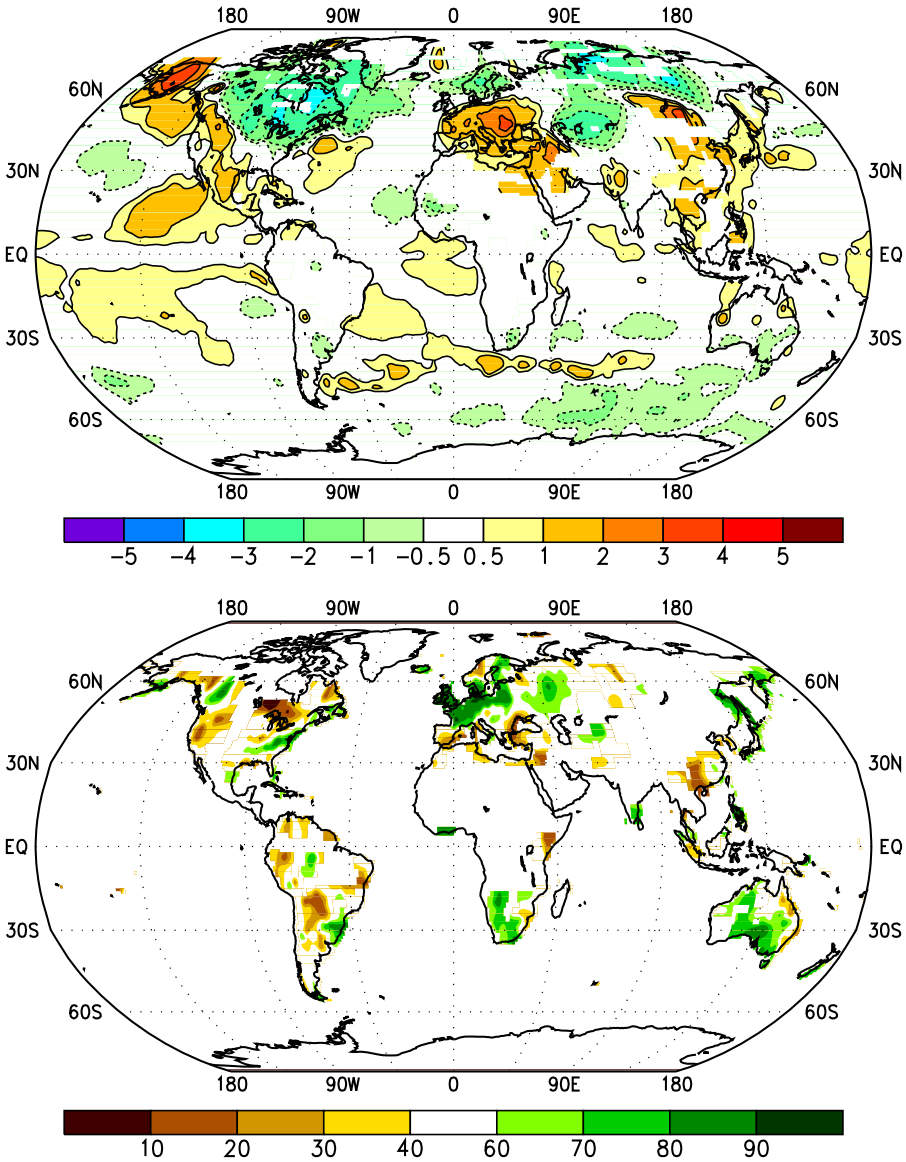

Figure 3.2 Surface temperature anomalies (°C) (top) and precipitation percentiles based on a gamma distribution fit to the 1961-1990 base period (bottom) for December 1993 - February 1994. Temperature anomalies are based on station data over land (1961-1990 base period) and sea surface temperature data (SST) over water (COADS/ ICE climatology). Analysis omitted in data-sparse regions. (Source: CAC)

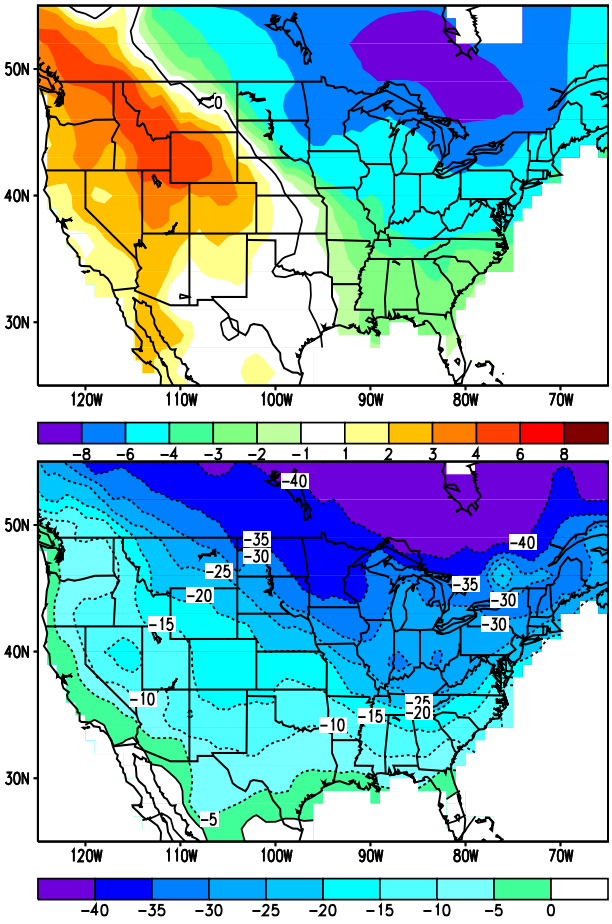

Figure 3.3 Temperature anomalies (top) and extreme minimum temperature (bottom) in ºC for the period 23 December 1993-22 January 1994. (Source: CAC)

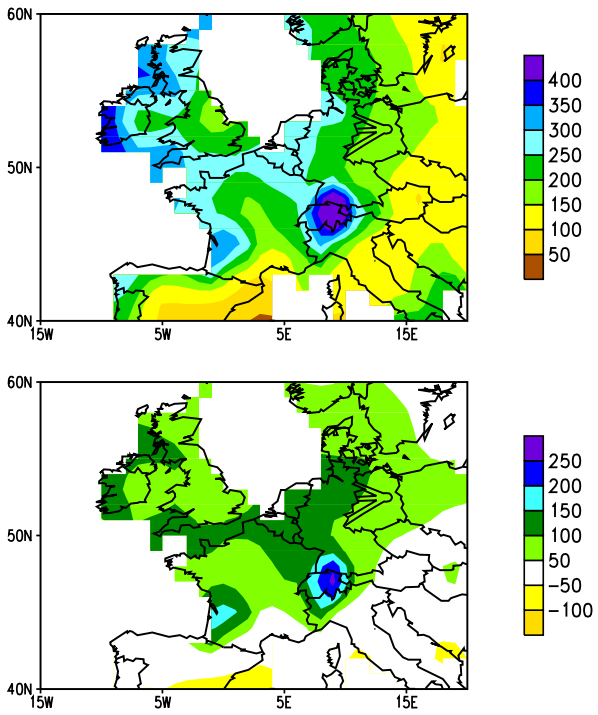

Figure 3.4 Total precipitation (mm, top) and anomalies (mm, bottom) across Europe during December 1993-January 1994. Anomalies are computed with respect to the 1961-1990 base period. (Source: CAC).

(**Fig. 3.4, bottom**), with much of the region experiencing near-record precipitation totals. *In excess of 250 mm of precipitation was recorded throughout western and northern France, the Benelux countries, England, Scotland, and Ireland during the season, and totals exceeding 400 mm were observed over eastern Austria and southwestern Germany* (**Fig. 3.4, top**). During one extreme rainfall event in early January, parts of northern Italy, Switzerland, and southern France received daily amounts exceeding 150 mm, *with 243 mm falling in St. Leger de Ventoux in southern France on 6 January.*

Over Asia, below-normal heights at 500 mb were observed over much of central Siberia and central Russia, while above-normal heights were observed over eastern China and southeastern Asia. These features were associated with below-normal and above-normal surface temperatures in these regions, respectively, during the season (**Fig. 3.2**).

Southern Hemisphere

The Southern Hemisphere circulation was characterized by below-normal heights at 500 mb throughout the polar region, and by above-normal heights in the high latitude extratropics (**Fig. 3.1, bottom**). These conditions reflected a pronounced amplification of the Antarctic circumpolar vortex and an overall poleward shift of the midlatitude jet stream.

In South Africa, much above-normal precipitation was observed in the south and west during DJF for the first time in more than two years (**Fig. 3.2, bottom**). East of Africa, Madagascar was hit by two hurricanes and one

tropical cyclone during the season (landfall dates of 13 January, 1 February and 17 February). The worst of these events was hurricane Geraldo (1 February), which had sustained winds of 57 ms^{-1} and which took nearly 200 lives. In Australia, significantly above-normal precipitation totals were observed over large portions of the southern and central sectors during DJF (**Fig. 3.2, bottom**). This season was followed by below-normal precipitation and severe drought over large portions of Australia during the rest of 1994 (see section 4.b).

b. March-May

Northern Hemisphere

In the Northern Hemisphere, the circulation during March-May 1994 (MAM) was characterized by negative height anomalies at 500 mb over the central latitudes of the North Pacific, eastern Canada, and the high latitudes of the North Atlantic, and by positive height anomalies over much of the United States, the central North Atlantic, and Europe (**Fig. 3.5. top**). Major surface features included abnormally warm and dry conditions over large portions of western North America, southern Europe, and China, and abnormally wet conditions over the eastern United States, northern Europe, and Southeast Asia (**Fig. 3.6**).

Over North America, above-normal heights and temperatures, and below-normal precipitation, dominated large portions of the western United States and western Canada. Temperatures averaged 1-3°C above normal throughout this region, with the largest anomalies observed in western Canada. Overall, the abnormally dry conditions throughout the West during MAM typified the entire western U.S. rainy season (October through April) (see section 4.f).

Below-normal precipitation was also observed over large portions of the central United States during MAM, with parts of the central Plains and Midwest recording one of their driest MAM seasons in the historical record. *In the Midwest, MAM 1994 marked the first season since the great Midwest floods (June-August 1993) in which below-normal precipitation was observed.*

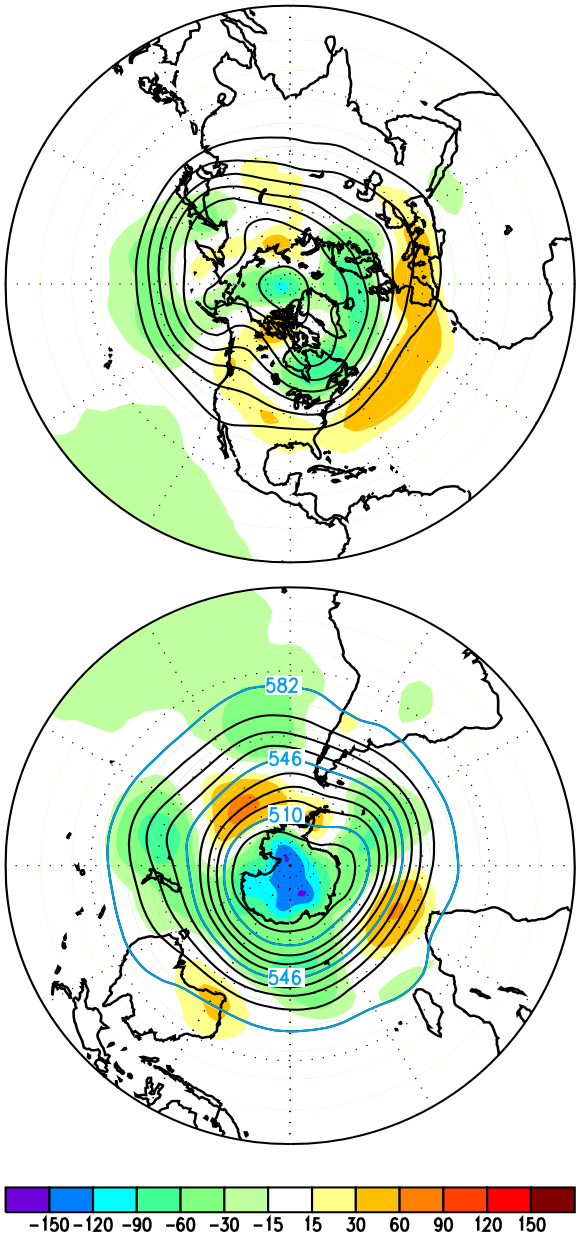

Figure 3.5 Northern Hemisphere (top) and Southern Hemisphere (bottom) 500-mb geopotential height (contours, interval is 9 dm) and anomalies (shading, in m) for March - May 1994. Anomalies are departures from the 1979-1988 base period means. (Source: CAC)

The circulation over the North Atlantic

and Europe during MAM was again characterized by negative height anomalies at high latitudes and by positive height anomalies throughout the central latitudes. These conditions reflected a continuation from the winter season of the positive phase of the North Atlantic Oscillation and were again associated with anomalously warm surface temperatures throughout central and southern Europe and the Middle East, and with excessive precipitation throughout northern and western Europe and portions of western Russia. In contrast, precipitation deficits over southern Europe accumulated during the season, as much of this region received its second consecutive season of significantly below-normal precipitation.

During MAM, much of China experienced a continuation of above-normal (1-2°C)

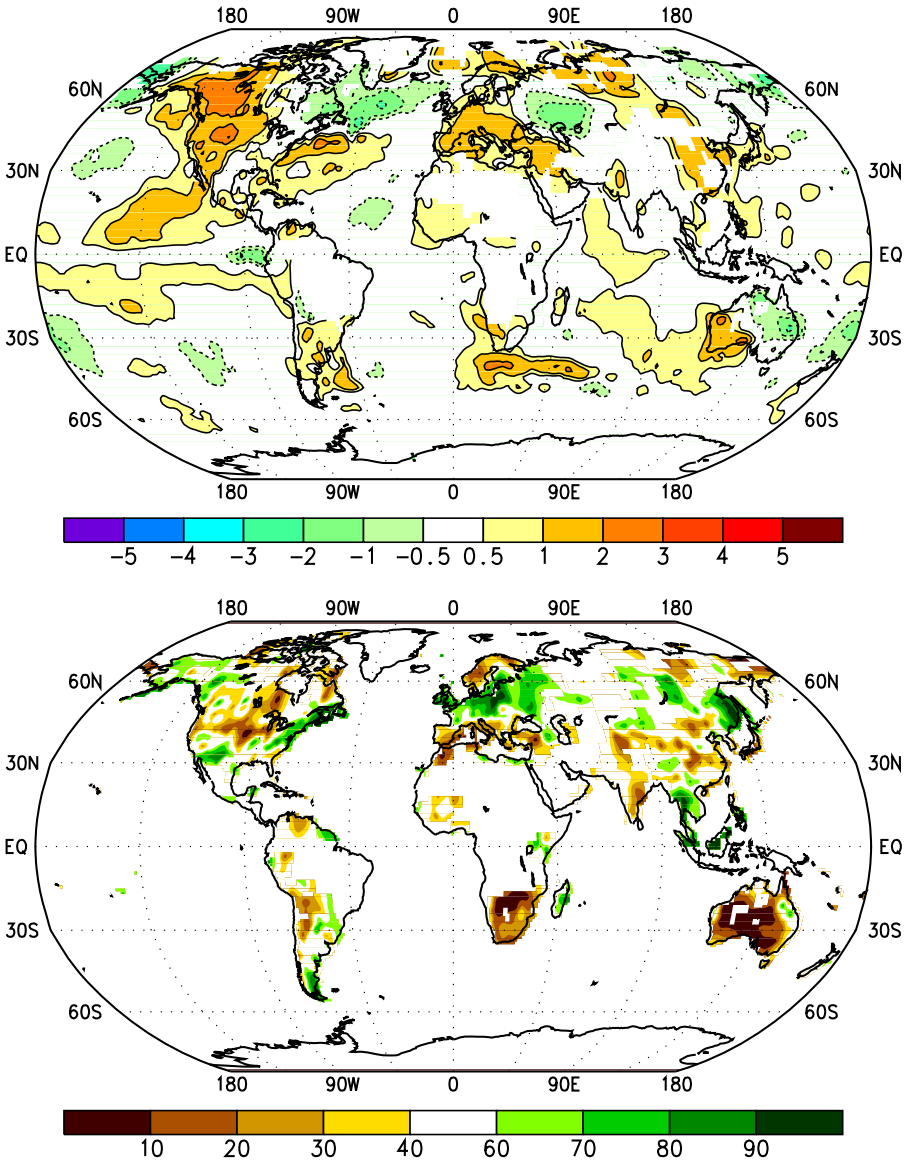

Figure 3.6 Surface temperature anomalies (°C) (top) and precipitation percentiles based on a gamma distribution fit to the 1961-1990 base period (bottom) for March - May 1994. Temperature anomalies are based on station data over land (1961-1990 base period) and sea surface temperature data (SST) over water (COADS/ICE climatology). Analysis omitted in data-sparse regions. (Source: CAC)

temperatures that developed during DJF. Large portions of interior China also recorded below-normal rainfall for the second consecutive season. In contrast, eastern Manchuria and eastern Siberia experienced a continuation of above-normal precipitation that began during DJF. These conditions were associated with an overall northward and eastward shift of the entrance region of the Pacific jet stream toward northern Manchuria.

Southern Hemisphere

In the Southern Hemisphere, major surface features during MAM 1994 included abnormally warm conditions over southwestern Australia and anomalously dry conditions over virtually all of Australia and large portions of South Africa (**Fig. 3.6**). The atmospheric circulation during MAM was marked by below-normal heights throughout the Antarctic and by an anomalous zonal wave-3 pattern in the middle latitudes, with above-normal heights influencing large portions of Australia and South Africa (**Fig. 3.5, bottom**).

The pattern of above-normal heights over southwestern Australia and below-normal heights farther south reflected an enhanced anticyclonic circulation and above-normal surface pressure throughout the continent. This circulation was accompanied by a pronounced poleward shift of the mean jet stream and storm track to well south of the continent. These conditions were associated with *near-record precipitation deficits throughout Australia during the season* (see Section 4.b).

Over the southern African sector, a large area of positive height anomalies was centered to the south of the country. This feature was accompanied by an anomalous anticyclonic circulation and large rainfall deficiencies throughout South Africa. Farther east, Madagascar was hit by two additional hurricanes during March. Hurricane Litanne made landfall on 17 March with sustained winds of 56 ms^{-1}, and hurricane Nadia made landfall on 23 March with sustained winds of more than 50 ms^{-1}. *Since 1 January, most of the country had received 800-1700 mm of rain*, with the largest amounts falling on the eastern coastline in the vicinity of the hurricane/ tropical cyclone landfall locations.

c. June-August

Northern Hemisphere

In the Northern Hemisphere, important circulation features during June-August 1994 (JJA) included below-normal heights throughout the polar region and the high latitudes of the North Atlantic, and above-normal heights over western Canada, the western United States, Europe, and northeastern China/ southeastern Siberia (**Fig. 3.7, top**). Significant surface features during the season included a continuation of abnormally warm and dry conditions over western North America and above-normal precipitation over eastern North America. Abnormally warm temperatures also continued over large portions of Europe and over eastern Asia/ northern China (**Fig. 3.8**).

Over western North America, the pattern of above-normal heights during JJA brought a continuation of abnormally warm and dry conditions to the western United States, western Canada, and southern Alaska. Farther east, an amplified trough and above-normal precipitation dominated eastern North America during the season, with the mid-Atlantic and northeastern United States experiencing a third consecutive season of above-normal precipitation.

Over the North Atlantic, the overall pattern of below-normal heights at high latitudes and above-normal heights in the middle latitudes continued for the third consecutive season. In Europe, this circulation was accompanied by above-normal surface temperatures, with anomalies averaging 1-2^{o}C above normal throughout the continent in each month. This anomalous warmth was particularly acute during July and the first two weeks of August,

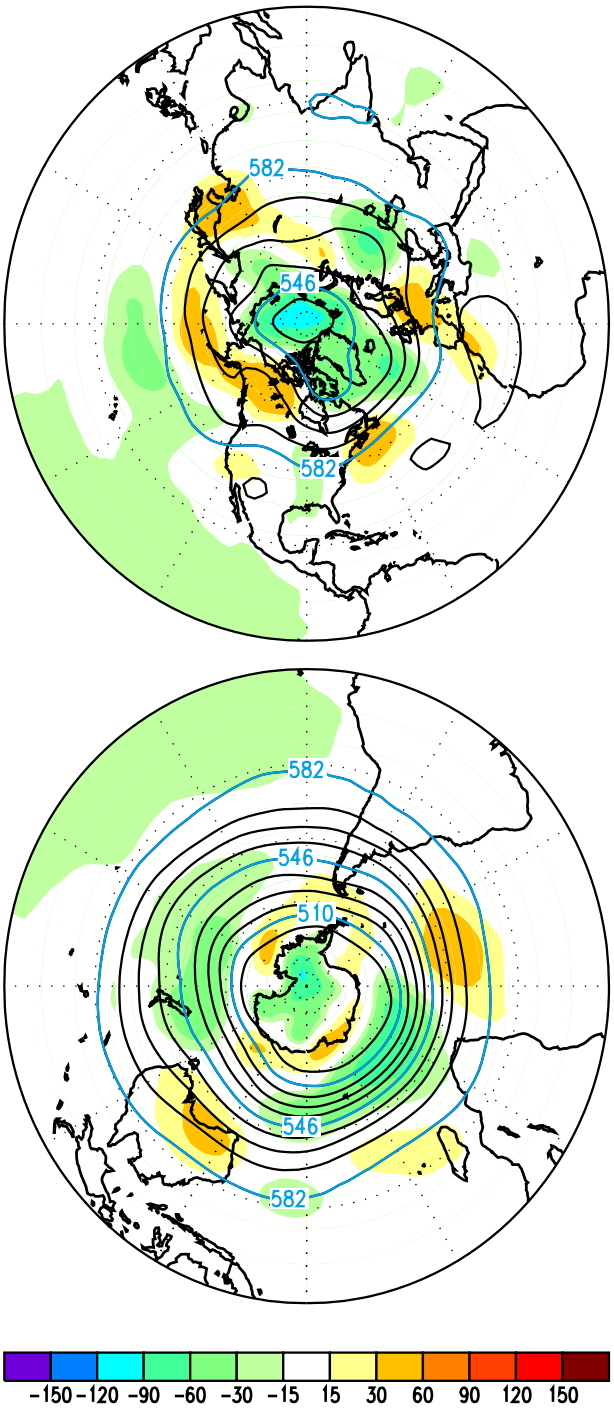

Figure 3.7 Northern Hemisphere (top) and Southern Hemisphere (bottom) 500-mb geopotential height (contours, interval is 9 dm) and anomalies (shading, in m) for June - August 1994. Anomalies are departures from the 1979-1988 base period means. (Source: CAC)

when *one of the hottest spells ever to afflict central Europe became established* (see Section 4.e). Substantially below-normal precipitation was also observed over large portions of eastern Europe and western Russia. These conditions brought an end to the pattern of above-normal precipitation which had prevailed in these regions for the past two seasons.

Farther east, negative height anomalies persisted over the Caspian Sea sector for the third consecutive season, while above-normal heights were observed over eastern Asia. Accompanying this circulation, surface temperatures averaged 1-2°C below normal in the region near the Caspian Sea, and abnormally warm conditions also covered northern China and southeastern Siberia.

Southern Hemisphere

In the Southern Hemisphere, major surface features during JJA 1994 included a continuation of abnormally warm conditions over southwestern Australia, and *the development of severe drought conditions throughout southeastern and southern Australia* (**Fig. 3.8**). The primary circulation feature during the season was a continuation of above-normal heights (**Fig. 3.7, bottom**) and above-normal surface pressure over Australia. Accompanying this circulation, the climatological longwave trough normally located near 110°E was generally weaker than normal and was displaced well west (near 80°-100°E) of normal.

These conditions were associated with a poleward shift and weakening of the storm track between the east Indian Ocean (equatorward of 40°S) and the Great Australian Bight. These factors, in combination with an overall weaker magnitude of midlatitude frontal systems, resulted in well-below-normal rainfall over large areas of southern and eastern Australia. This situation was exacerbated by a general lack of significant tropical moisture

incursions over the continent, which normally contribute substantially to rainfall in inland areas. Overall, above-normal surface temperatures (2-3°C) were observed throughout western Australia during JJA, and severe precipitation deficits, along with *severe drought conditions, were recorded throughout virtually all of southeastern and extreme southern Australia* (see section 4.b).

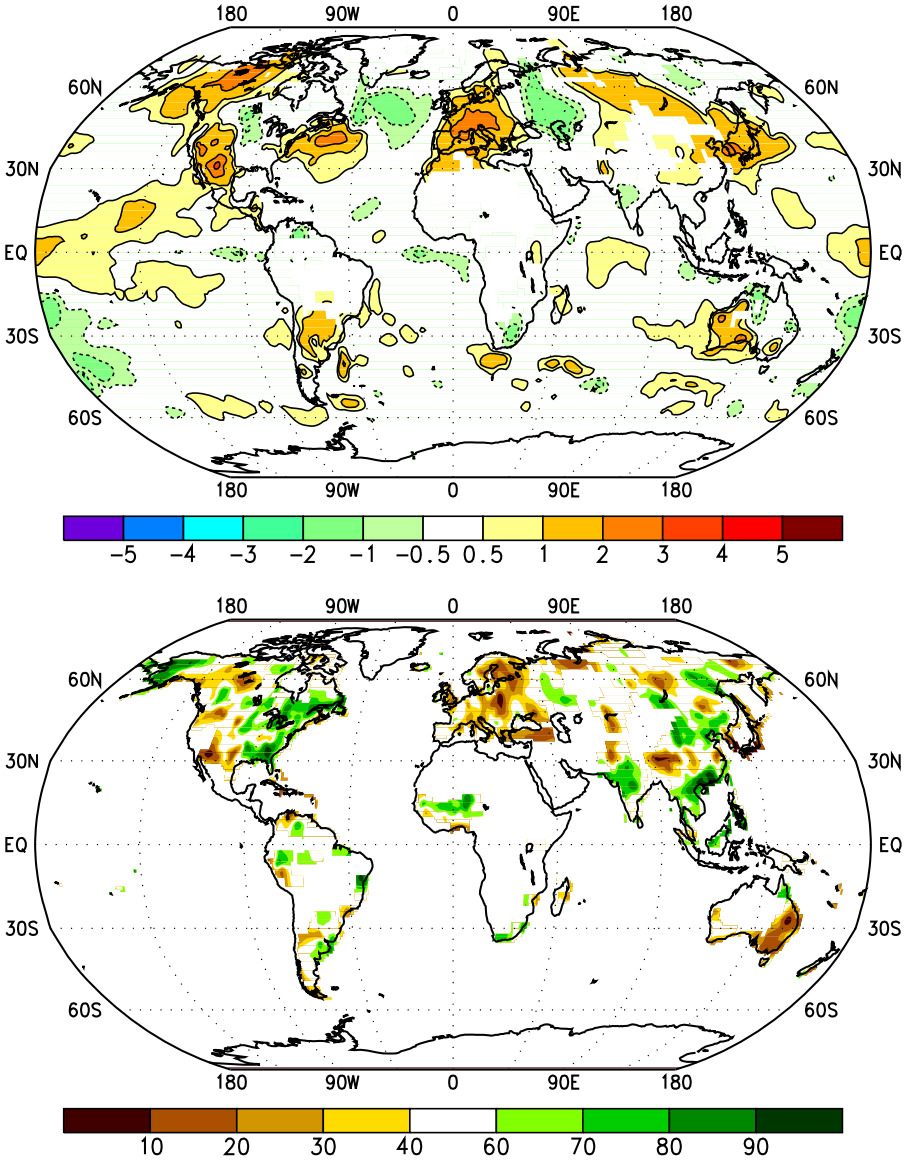

Figure 3.8 Surface temperature anomalies (°C) (top) and precipitation percentiles based on a gamma distribution fit to the 1961-1990 base period (bottom) for June - August 1994. Temperature anomalies are based on station data over land (1961-1990 base period) and sea surface temperature data (SST) over water (COADS/ICE climatology). Analysis omitted in data-sparse regions. (Source: CAC)

d. September-November

Northern Hemisphere

In the Northern Hemisphere, the primary circulation features during the September-November 1994 (SON) season included below-normal heights throughout the polar region and western North America, and above normal heights over the high latitudes of the North Pacific and eastern Canada (**Fig. 3.9, top**). Major surface features during the season included a continuation of abnormally warm conditions throughout Europe and China (**Fig. 3.10, top**). Anomalously warm conditions were also observed over much of eastern Canada during the season. In the United States, above-normal precipitation was observed over large portions of the Northwest, while drier than normal conditions covered much of the eastern part of the country (**Fig. 3.10**).

The circulation over North America was characterized by below-normal heights in the west and above-normal heights over Hudson Bay. This circulation was associated with below-normal surface temperatures throughout Alaska and the northwestern United States, and with above-normal temperatures throughout eastern Canada and the northeastern United States. Additionally, above-normal precipitation covered large portions of the west-central and northwestern United States, while much of the northeastern United States and eastern Canada experienced below-normal precipitation. *These overall circulation, temperature and precipitation patterns are opposite to those observed throughout North America during the past three seasons*.

Over the North Atlantic and Eurasia, above-normal heights were observed at high latitudes of the North Atlantic and the Caspian Sea during SON. This circulation pattern was again associated with above-normal surface temperatures (1-2°C) across much of Europe, southwestern Russia, and the Middle East. These conditions were particularly acute over central and northwestern Europe during

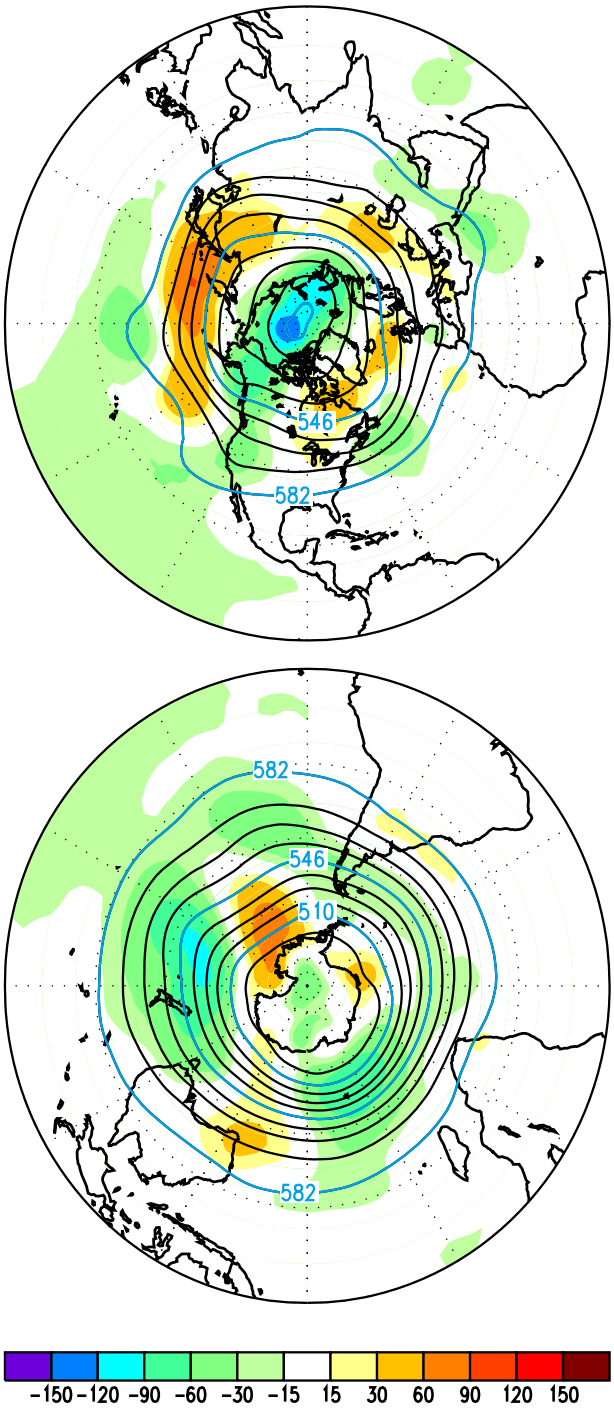

Figure 3.9 Northern Hemisphere (top) and Southern Hemisphere (bottom) 500-mb geopotential height (contours, interval is 9 dm) and anomalies (shading, in m) for September - November 1994. Anomalies are departures from the 1979-1988 base period means. (Source: CAC)

November (see section 4.e). Above-normal precipitation was also recorded throughout western Europe, Scandinavia and the eastern Mediterranean Sea during SON in conjunction with two major flood events. The first event occurred in the beginning of November, when *extreme rainfall inundated northern Italy and southern France (Mount Aiguel, France recorded 411 mm of precipitation in 60 hours*). The second event occurred during the latter half of November in the Middle East, where *many regions recorded rainfall totals in excess of 400% of their normal monthly mean*. During this event, higher elevations in Turkey also received significant snowfall and experienced blizzard conditions.

Over eastern Asia, above-normal temperatures (2-3ºC above normal) again covered

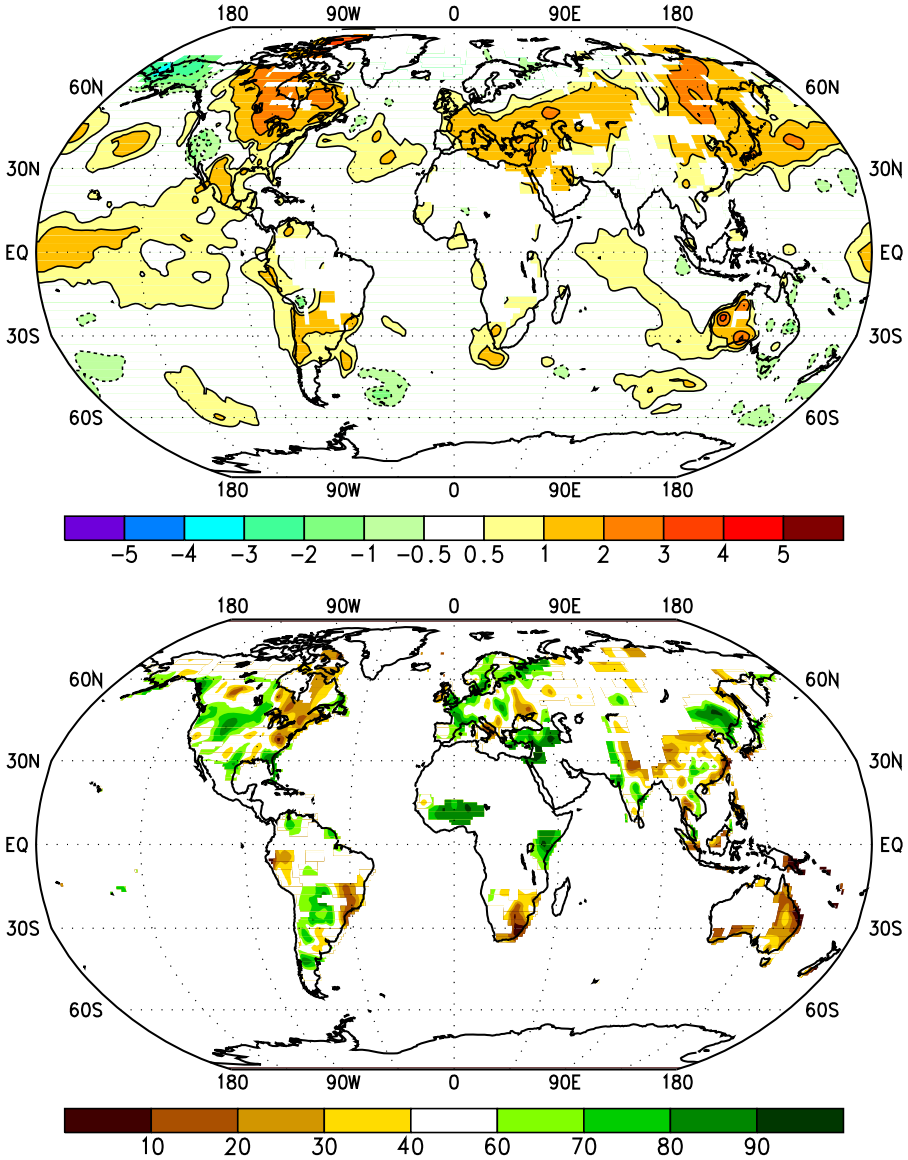

Figure 3.10 Surface temperature anomalies (ºC) (top) and precipitation percentiles based on a gamma distribution fit to the 1961-1990 base period (bottom) for September - November 1994. Temperature anomalies are based on station data over land (1961-1990 base period) and sea surface temperature data (SST) over water (COADS/ ICE climatology). Analysis omitted in data-sparse regions. (Source: CAC)

much of northeastern China and eastern Siberia during SON. During October and November, this warmth brought abnormally low areal snow cover extent to large portions of eastern Mongolia and Manchuria, with large regions recording virtually no snow cover during the period (**Fig. 3.11**). Climatologically, large portions of this region average 15-25 days of snow cover during October and November. For 1994 as a whole, abnormally warm conditions dominated this region in all seasons. This warmth was associated with an extraordinarily persistent pattern of above-normal heights at 500 mb in the vicinity of China and southeastern Siberia, along with an apparent northeastward shift of the entrance region of the Pacific jet stream.

Southern Hemisphere

In the Southern Hemisphere, the circulation during SON was marked by below-normal heights at 500 mb over large portions of the middle latitudes, and by a continuation of above-normal heights and pressure over southwestern Australia (**Fig. 3.9, bottom**).

The major surface features during the season were a continuation of abnormally warm conditions over southwestern Australia, along with *a continuation of below-normal precipitation and severe drought conditions over much of southeastern and southern Australia* (**Fig. 3.10**). Queensland and South Australia recorded precipitation totals in the lowest 10% of the historical record during the season. These conditions were associated with an anomalously strong ridge at upper levels over the southwest and with a continuation of above-normal pressure throughout the country. *These circulation, temperature, and rainfall anomalies have dominated the continent for three consecutive seasons, during which the southeastern and extreme southern regions have recorded one of their most severe droughts of the century* (see section 4.b). During November, several good rainfall episodes brought much-needed, but very short-term, relief to southwestern Queensland and to northern and central New South Wales. However, by the end of the year, severe drought had redeveloped in these regions.

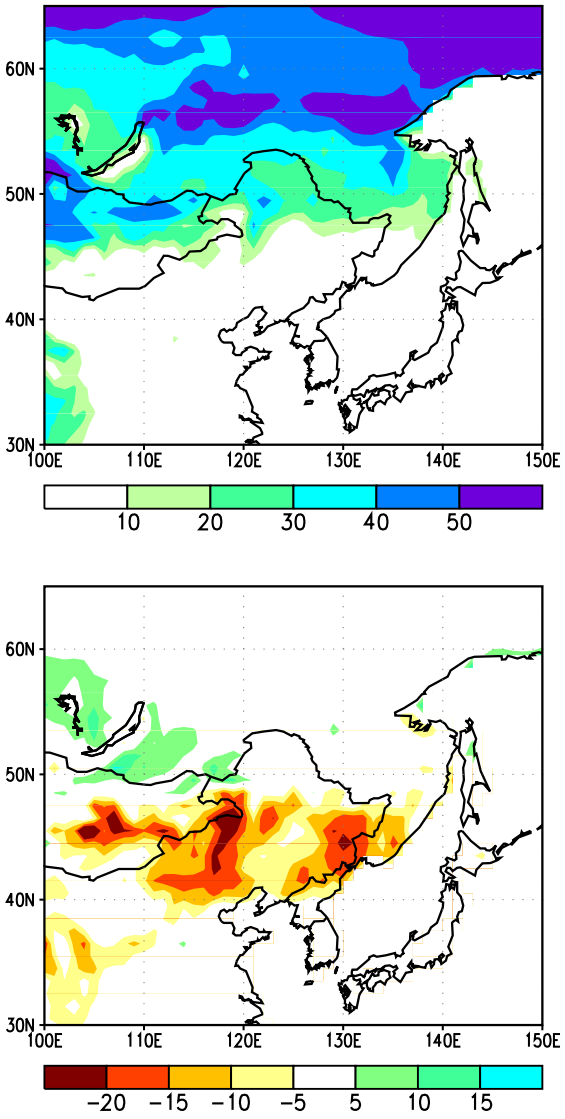

Figure 3.11 Snow cover (top) and anomaly days (bottom) for eastern Asia during October - November 1994, as determined by the Special Sensor Microwave/Imager (SSM/I). Anomalies are departures from the 1987-1994 base period means. (Source: CAC)

4. REGIONAL CLIMATE SUMMARIES

a. Southern Africa

In southern Africa the rainy season typically lasts from October to April and reaches maximum strength between December and February. Most of the region receives more than 75% of its mean annual precipitation, and parts of south-central Africa record over 90% of their mean annual rainfall total during this seven-month period. Significant precipitation is unusual throughout the region after mid-May.

As a whole, southern African received near-normal rainfall during the 1993/94 rainy season, following two years of significantly below-normal rainfall (**Fig. 4.1**). Seasonal rainfall totals exceeded 750 mm across parts of southeastern Africa (**Fig. 4.2**). Above-normal rainfall was observed over much of South Africa and north-central parts of southern Africa, with more than twice the normal seasonal total falling on parts of central and western South Africa (**Fig. 4.3**). However, rainy season totals were primarily below normal from eastern South Africa northeastward and over parts of southwestern Africa, where some locations recorded under 75% of normal wet season rainfall totals.

During the early part of the wet season, abundant rains fell on central and northwestern parts of southern Africa. Much of this area received monthly totals that were among the highest 10% of the 1961-1990 historical distribution. Additionally, weekly rainfall totals averaged 25-75 mm throughout the eastern half of South Africa during the period. In contrast, below-normal rainfall was observed farther south and east, where totals during October were among the driest 10% on record.

During December, dry weather was reported in northeastern areas while moisture surpluses accumulated along the central South

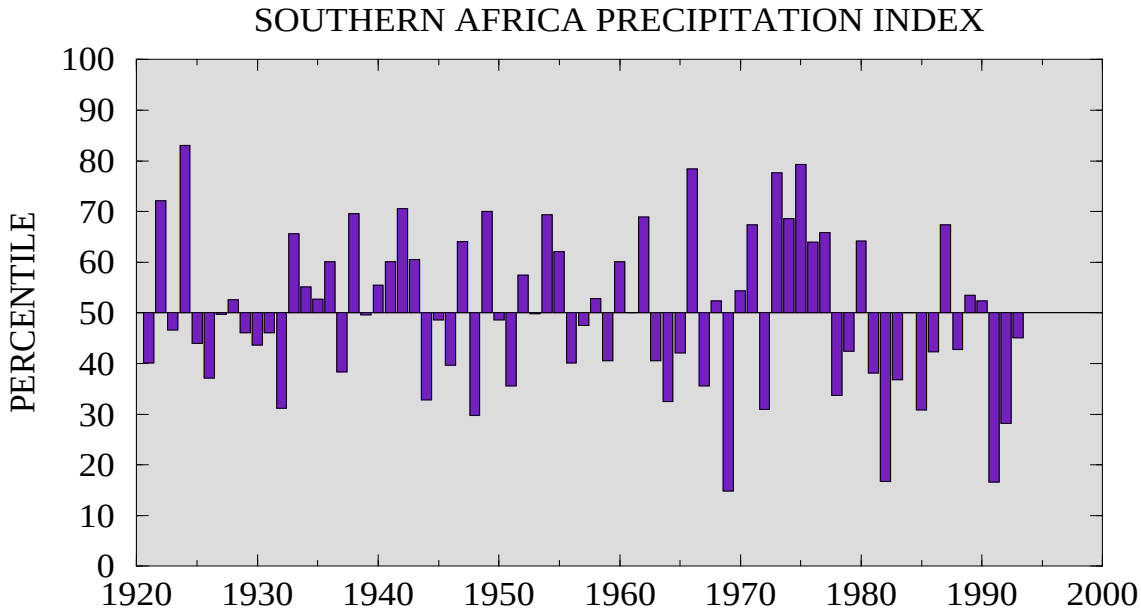

Figure 4.1 Precipitation index (average gamma percentiles of station precipitation within the region) for southern Africa for October - April. Percentiles are computed for the 1961-1990 base period. (Source: CAC)

African coast. Near to slightly above-normal precipitation totals were reported elsewhere. In January, the area of above-normal precipitation shifted westward and covered the western half of southern Africa.

During February and early March, abnormally dry conditions covered much of the northeastern quarter of the region. In contrast, surplus precipitation fell on most locations across the central, western, and southern sections of southern Africa, with many areas among the wettest 10% of mid-January-early March periods on record. The wet season came to an early end over most of southern Africa, with no significant widespread rainfall reported across much of the region during March and April.

The onset of the 1994/95 rainy season was dominated by very dry conditions in southern Africa. During October and November 1994, rainfall totals were less than 50% of normal over much of the northern and western parts of southern Africa. Elsewhere, rainfall totals were near or slightly below normal. During December, near-normal to above-normal rains covered southern and eastern areas. Elsewhere, rainfall deficits continued through the end of the year.

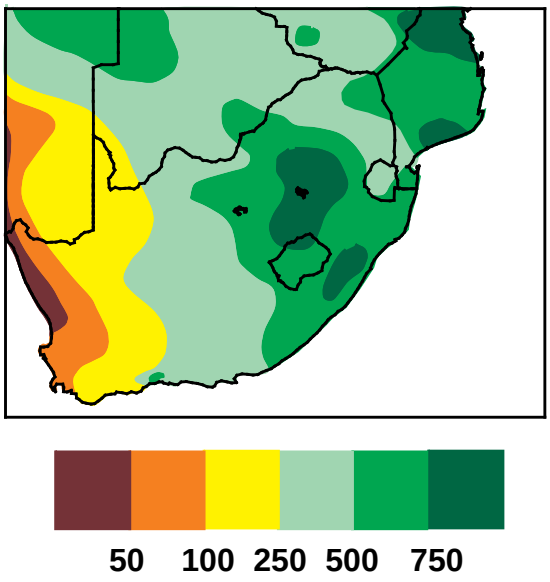

Figure 4.2 Total precipitation (mm) in southern Africa for October 1993 - April 1994. (Source: CAC)

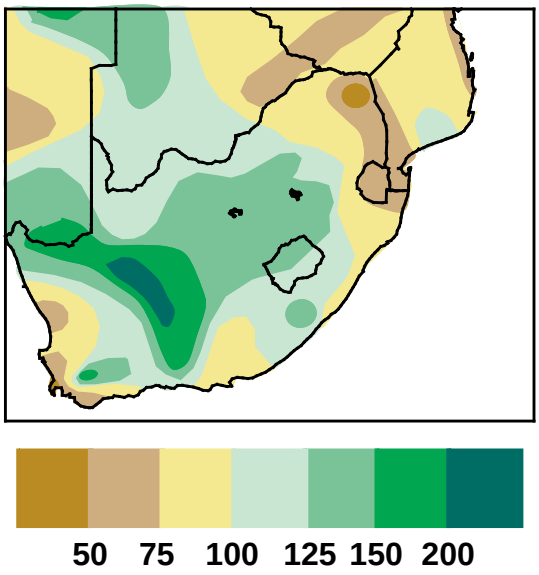

Figure 4.3 Percent of normal precipitation in southern Africa for October 1993 - April 1994, relative to the 1961-1990 base period. (Source: CAC)

b. Australia

The rainy season over northern and eastern Australia typically lasts for seven months, beginning in October and ending in April. Much of the area receives over 75% of its mean annual precipitation during this period, and parts of extreme northern Australia record more than 90% of the mean annual precipitation during this period. For the 1993/94 wet season as a whole, precipitation over northeastern Australia averaged near the 40th percentile (**Fig. 4.4**). Generally 250 - 750 mm of rain fell on the northern and eastern sections of the continent, although much larger amounts (1250 - 1900 mm) were recorded in northern Arnhem Land and the southeastern Cape York Peninsula.

The 1993/94 rainy season ended earlier than normal (March) and was followed by the development of severe precipitation deficits and extreme drought over much of Australia during the next nine months (**Fig. 4.5**). During this nine-month period, sections of eastern Australia accumulated rainfall deficits in excess of 200 mm (**Fig. 4.5, bottom**), and eastern Queensland and the northern portion of the Cape York Peninsula recorded deficits exceeding 300 mm. Farther south, southern and southwestern Australia recorded 100-200 mm deficits during the period. By the end of the year, severe drought conditions covered northeastern, east-central and southeastern Australia, and portions of the southwest (**Fig. 4.6**).

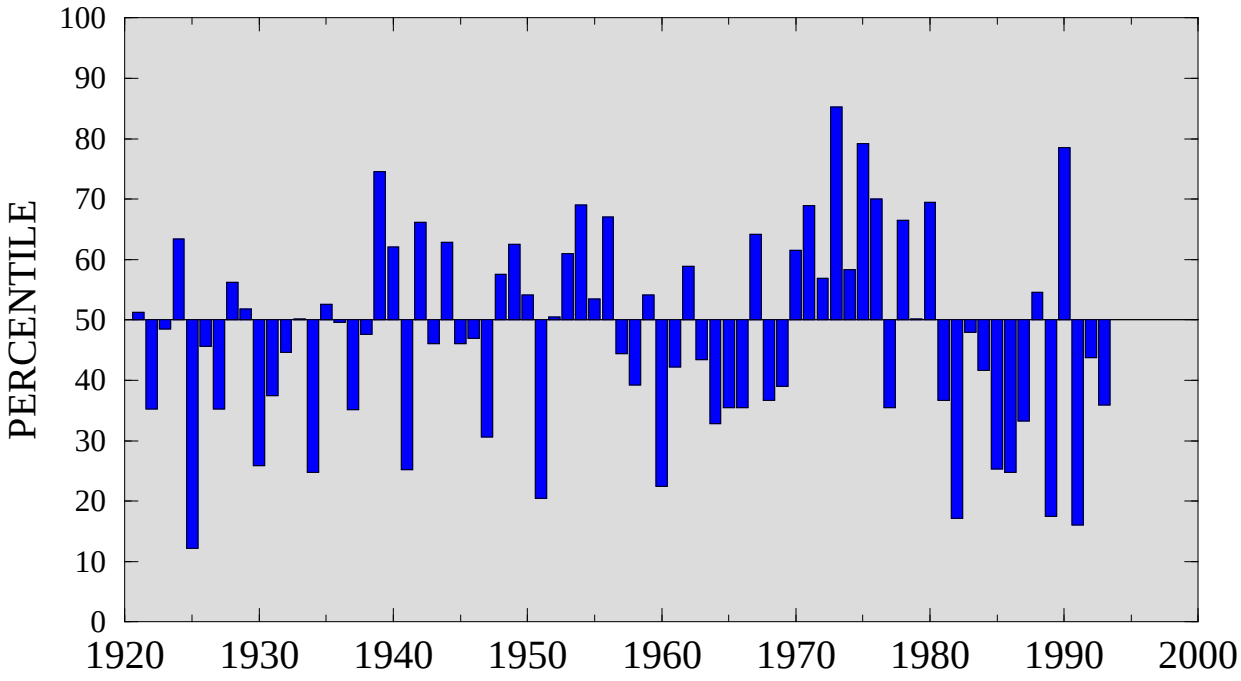

Figure 4.4 Precipitation index (average gamma percentiles of station precipitation within the region) for northeastern Australia for October - April. Percentiles are computed for the 1961-1990 base period. (Source: CAC)

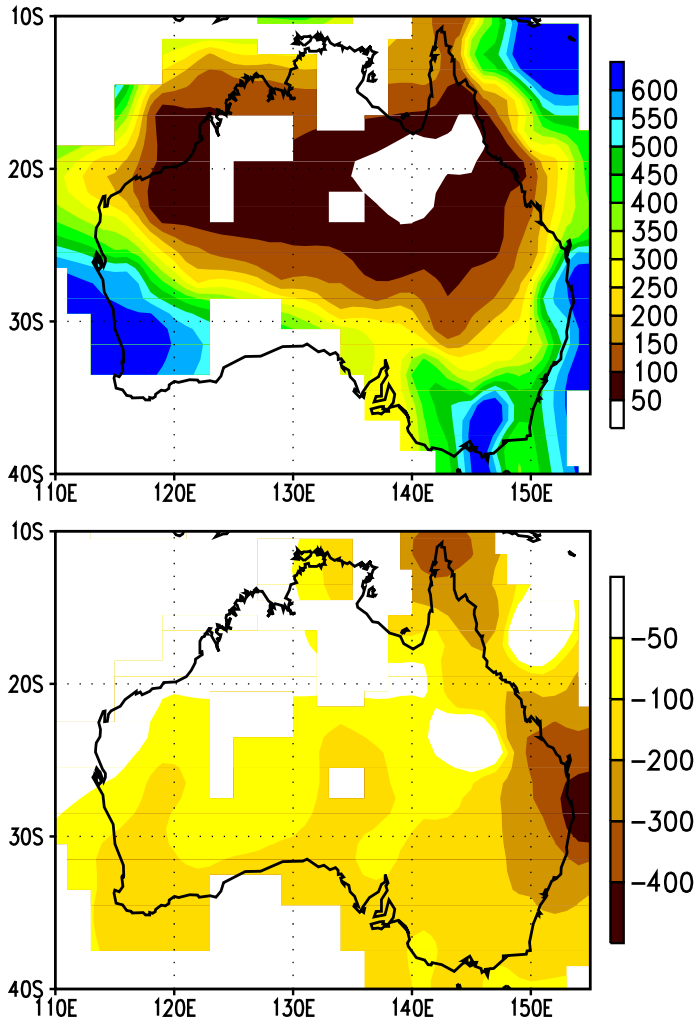

Figure 4.5 Total precipitation (mm, top) and anomalies (mm, bottom) during April - December 1994. Anomalies are departures from the 1961-1990 base period means. (Source: CAC)

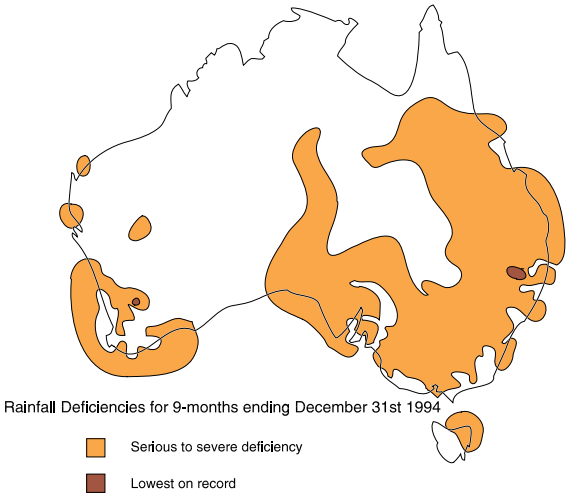

Figure 4.6 Rainfall deficiencies for April - December 1994. (Source: Australian Bureau of Meteorology)

Overall, precipitation totals during 1994 were the second lowest of the century (**Fig. 4.7a**), with the driest year being 1982. Eastern Australia also recorded its second driest year of the century during 1994 (**Fig. 4.7b**), while central/western Australia recorded its driest year of the century (**Fig. 4.7c**). These severe drought conditions were attributed to the reemergence and subsequent intensification of ENSO conditions in the tropical Pacific (see section 2), in combination with a persistent pattern of above-normal heights and pressure (**Fig. 4.8**) throughout the extratropical latitudes of the continent.

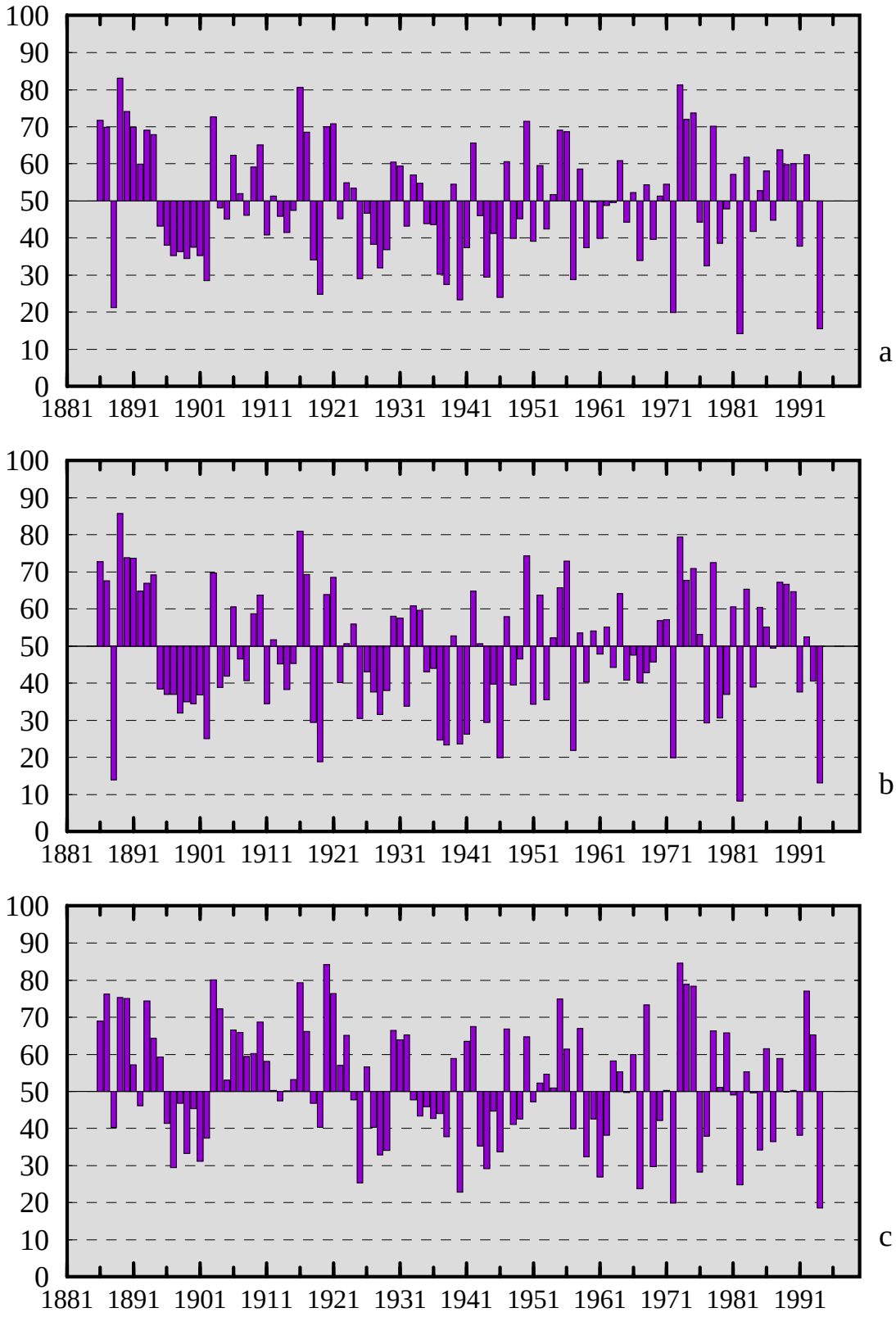

Figure 4.7 Precipitation index (average gamma percentiles of station precipitation within the region) for April - December for (a) Australia (south of 20ºS), (b) eastern Australia and (c) central/western Australia. Percentiles are computed for the 1961-1990 base period means. (Source: CAC)

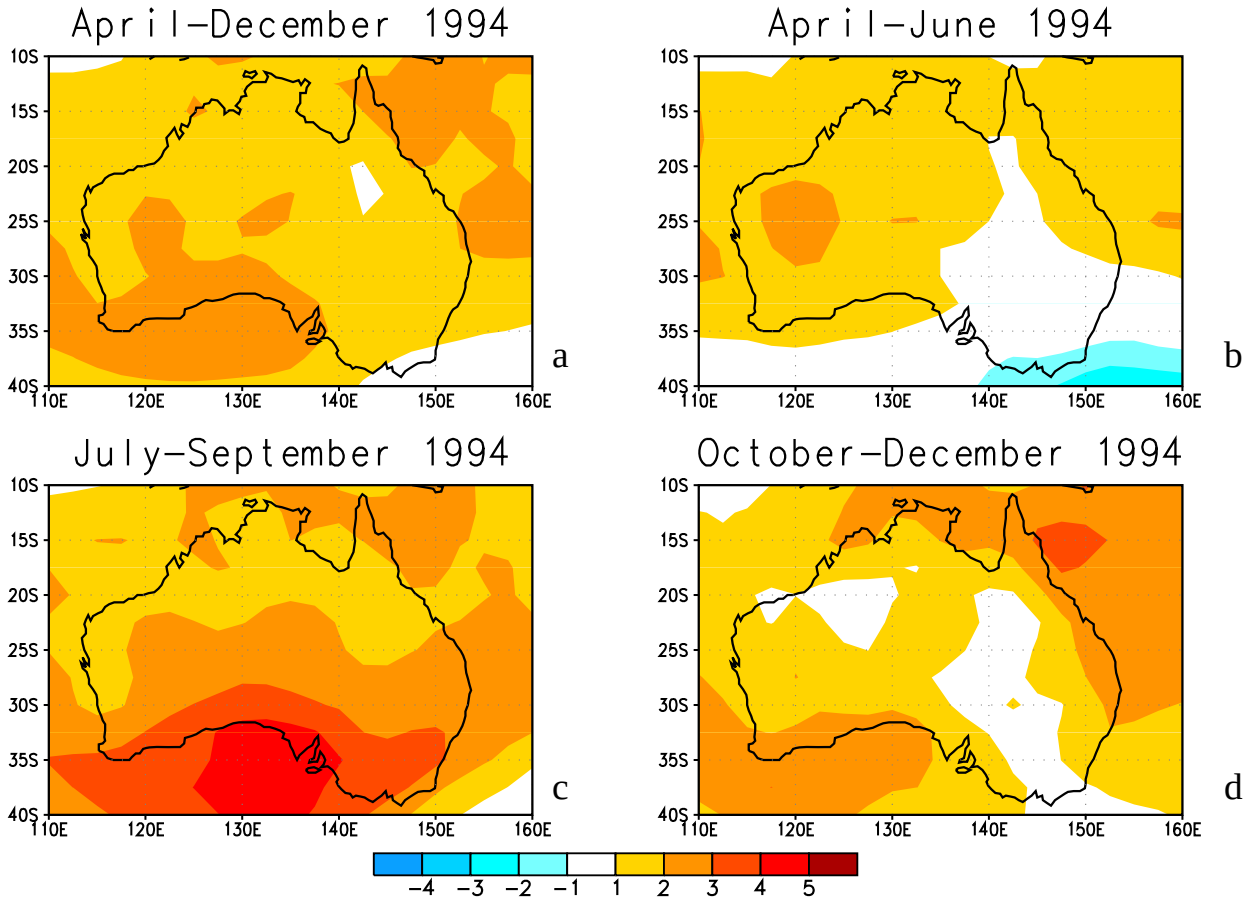

Figure 4.8 Sea level pressure anomalies over Australia for (a) April-December 1994, (b) April-June 1994, (c) July-September 1994, and (d) October-December 1994. Anomalies are departures from the 1979-1988 base period means. (Source: CAC)

During April-June, the circulation was dominated by above-normal heights in the southwest and by above-normal pressure throughout the west (**Fig. 4.8b**). These conditions reflected an enhanced anticyclonic circulation over Australia and a poleward shift of the mean jet stream and storm track to well south of the continent. Accompanying this circulation, significantly below-normal precipitation fell throughout eastern Australia and over large portions of the west (**Figs. 4.9**). For example, precipitation deficits exceeded 100 mm over extreme eastern Queensland and northeastern New South Wales, and averaged 50-100 mm over the eastern one-quarter of the continent and throughout the west (**Fig. 4.9b**). By the end of June, serious to severe precipitation deficiencies were reported over portions of southeastern Queensland and over large areas of central New South Wales, with isolated areas in these states reporting the most severe drought conditions in the historical record (**Fig. 4.10**). Farther west, serious to severe precipitation deficiencies were also reported over portions of central Western Australia at this time.

During July-September, above-normal heights and above-normal surface pressure continued throughout Australia (**Fig. 4.8c**). Pressures averaged 2-3 mb above normal over most of the continent, and 3-5 mb above normal in the extreme south. Accompanying this

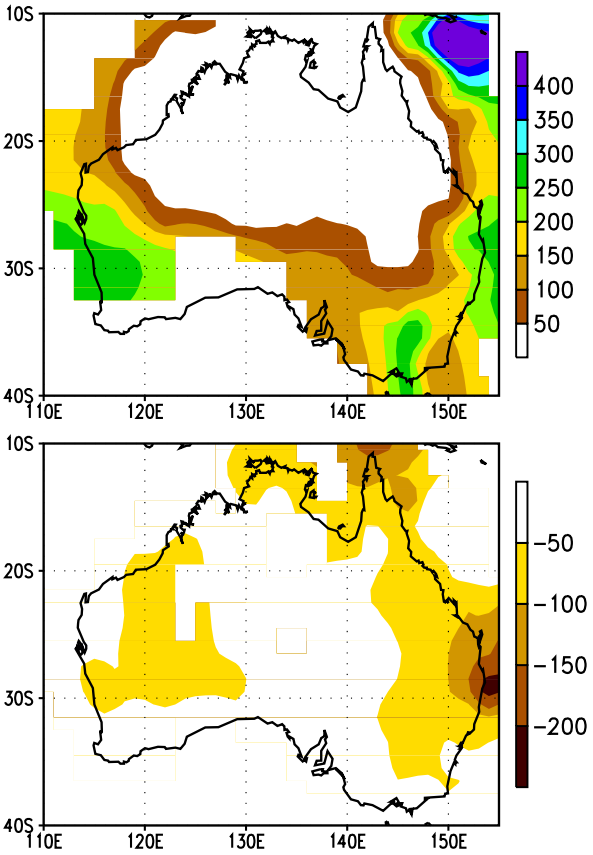

Figure 4.9 Total precipitation (mm, top) and anomalies (mm, bottom) during April - June 1994. Anomalies are departures from the 1961-1990 base period means. (Source: CAC)

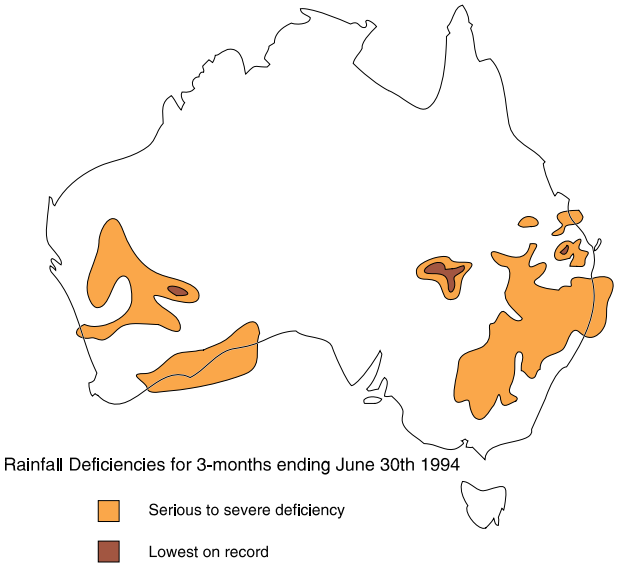

Figure 4.10 Rainfall deficiencies for April - June 1994. (Source: Australian Bureau of Meteorology)

circulation, the climatological long-wave trough normally located near 110°E tended to be weaker than normal and was displaced well west of normal (near 80°-100°E). These conditions were associated with a poleward shift and weakening of the storm track between the east Indian Ocean (equatorward of 40°S) and the Great Australian Bight. These factors, combined with an overall weaker magnitude of midlatitude frontal systems, resulted in well below-normal rainfall (**Fig. 4.11**) and a continuation of drought conditions over large areas of southern and eastern Australia. This situation was exacerbated by a general lack of significant tropical moisture incursions over the continent, which normally contribute considerable rainfall in inland areas. The entire eastern and southern portions of the continent recorded 50-100 mm precipitation deficits during July-September. These conditions were particularly acute during August, when the entire eastern half of Australia recorded one of their driest Augusts on record.

During October-December substantially below-normal rainfall was confined to the northeast (**Fig. 4.12**), and near-normal precipitation totals were observed over much of the southeast and south. During November, several good rainfall episodes brought much-needed, but very short-term, relief to southwestern Queensland and northern/central New South Wales. However, by the end of the year, severe drought had again redeveloped in these regions. In the northeast, the pattern of significantly below-normal rainfall during September-December indicated a weak onset to the 1994/95 wet season. Additionally, with the northern and eastern parts of the continent in the midst of their primary growing season as the year ended, the ongoing drought threatened to severely impact agricultural and hydrological interests in these areas.

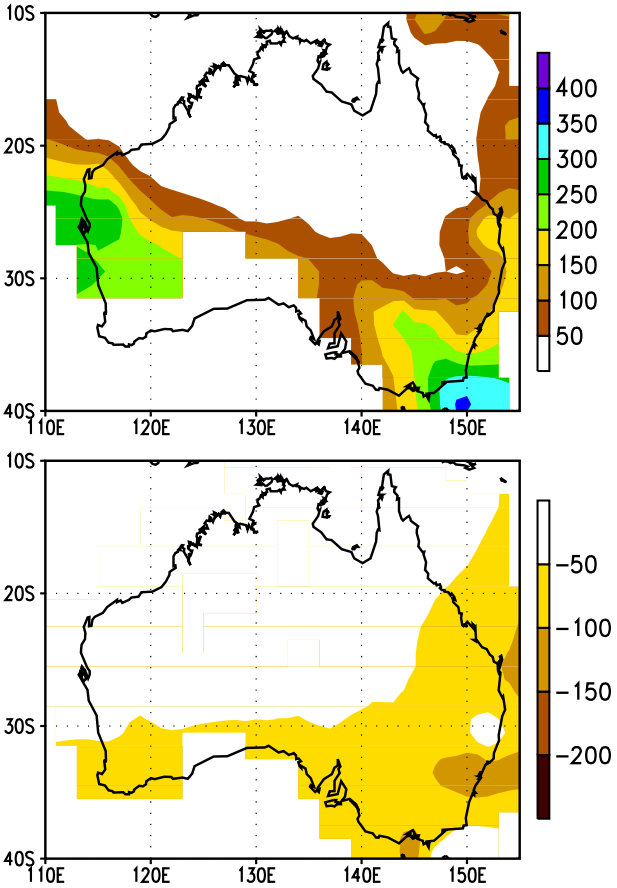

Figure 4.11 Total precipitation (mm, top) and anomalies (mm, bottom) during July - September 1994. Anomalies are departures from the 1961-1990 base period means. (Source: CAC)

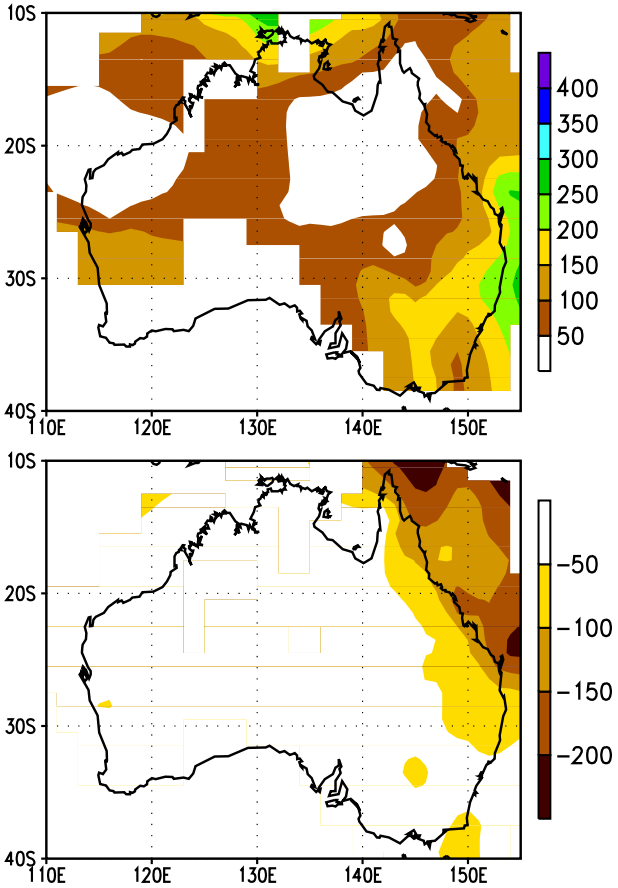

Figure 4.12 Total precipitation (mm, top) and anomalies (mm, bottom) during October - December 1994. Anomalies are departures from the 1961-1990 base period means. (Source: CAC)

c. Indian Summer Monsoon

Precipitation totals for India during the 1994 Indian monsoon season (June - September) averaged near the 60th percentile (**Fig. 4.13**). These totals were larger than has been observed during each of the past five monsoon seasons and were the second largest values recorded in the past 11 years. Precipitation amounts greater than 1000 mm were recorded throughout central India during May - September, with upwards of 3000 mm observed along the west coast (**Fig. 4.14**). During the 1994 season, most of central and western India, and central and southern Pakistan, received at least 125% of normal rainfall totals (**Fig. 4.15**). Exceptionally wet weather dominated the southern two-thirds of Pakistan and western India, where totals more than double typical seasonal amounts were observed. Several flood episodes also affected the monsoon region this year, and by the end of the season nearly 1,000 lives were lost across India and Pakistan due to flooding. Below-normal rainfall was observed only in north-central, extreme northeastern, and southern parts of India during the season (**Fig. 4.15**).

Selected notable features during the monsoon season are as follows:

Heavy rains inundated areas from West Bengal eastward across Bangladesh and extreme eastern India from April to mid-May. During this period, more than 300 people were killed and more than half a million homes were destroyed in association with torrential rains, and with the movement of Cyclone 02b through southeastern Bangladesh and portions of the Indian subcontinent. The latter half of May brought a decrease in storminess to the region.

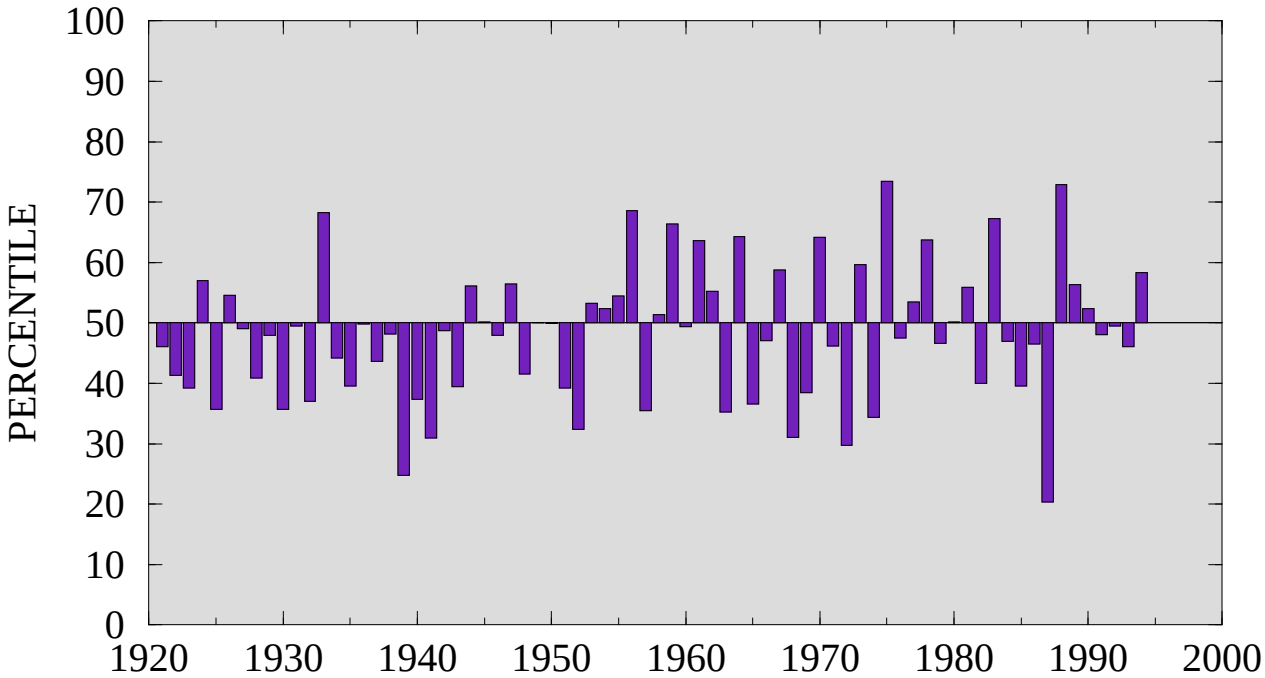

Figure 4.13 Precipitation index (average gamma percentiles of station precipitation within the region) for India for June - September. Percentiles are computed for the 1961-1990 base period. (Source: CAC)

Meanwhile, an exceptional heat wave developed from mid-May to mid-June across central and northern India and Pakistan. During this period temperatures in Delhi reached a 50-year high of 46°C, while temperatures in parts of southern Pakistan reached 50°C. This extreme heat claimed over 400 lives in India and an additional 100 lives in Pakistan.

During June and July above-normal rainfall covered western India and Pakistan. These rains helped to recharge reservoirs and improved crop prospects in most areas. Meanwhile, heavy rains across the northern and eastern fringes of India during the first week of July took 60 lives, flooded more than 100 villages, and damaged 52 highways.

Precipitation began to ease across Pakistan and western India in early August, although periodic heavy rains caused localized flooding until the end of the monsoon season in mid-September. In mid-August, flooding across the northern tier of Bangladesh took nearly four dozen lives, marooned 300,000 people, and swamped 10,000 homes.

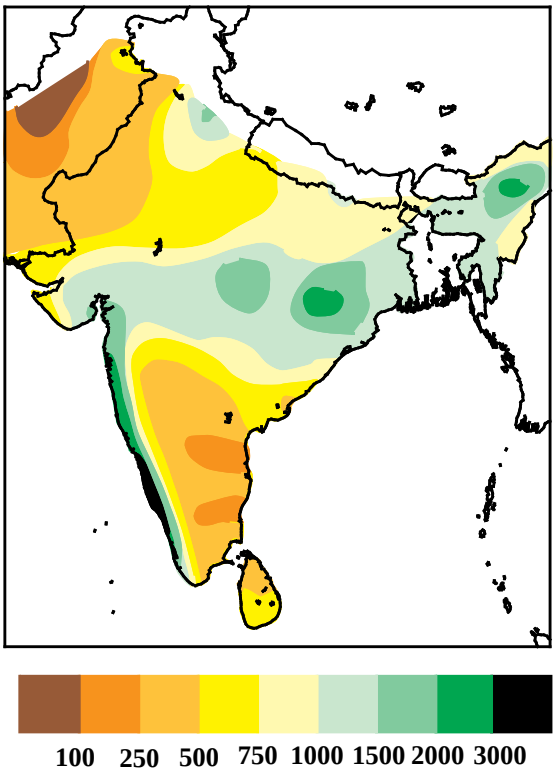

Figure 4.14 Total precipitation (mm) in India for June - September 1994. (Source: CAC)

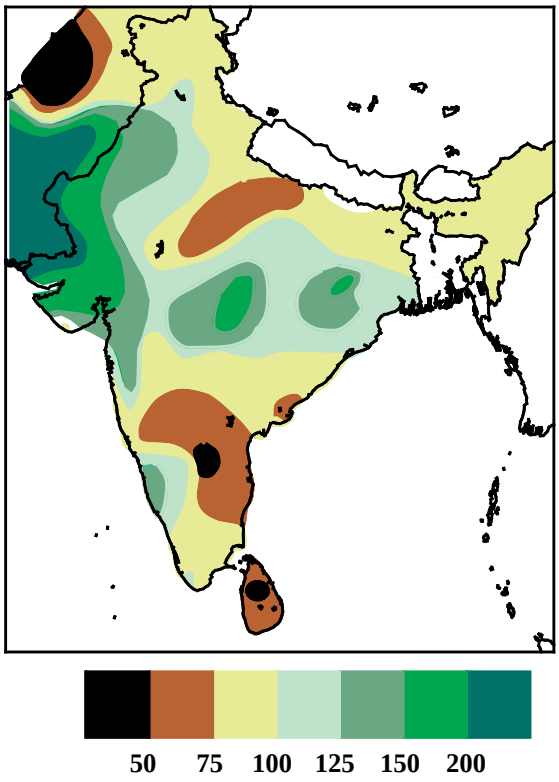

Figure 4.15 Percent of normal precipitation in India for June - September 1994, relative to the 1961-1990 base period. (Source: CAC)

d. African Sahel

During the 1994 rainy season (May - September) rainfall totals in the Sahel were among the largest recorded in the past 30 years and were more than 120% of normal in many areas. In the western Sahel, 1994 precipitation ranked in the 60th percentile relative to the 1951-1980 base period (**Fig. 4.16, top**) and was the wettest year since 1967. However, relative to the 1961-1990 base period, precipitation ranked in the 70th percentile (**Fig. 4.16, bottom**) and was comparable in magnitude to the 1988 and 1989 seasons. Thus, changing the base period results in an apparent weakening of the prolonged 25-30 year drought. [We present both time series in this assessment in order to provide continuity with previous assessments and to demonstrate the effects of changing base periods on the interpretation of time series which contain substantial interdecadal variability. All other time series in this assessment are now based on normals for the 1961-1990 base period.]

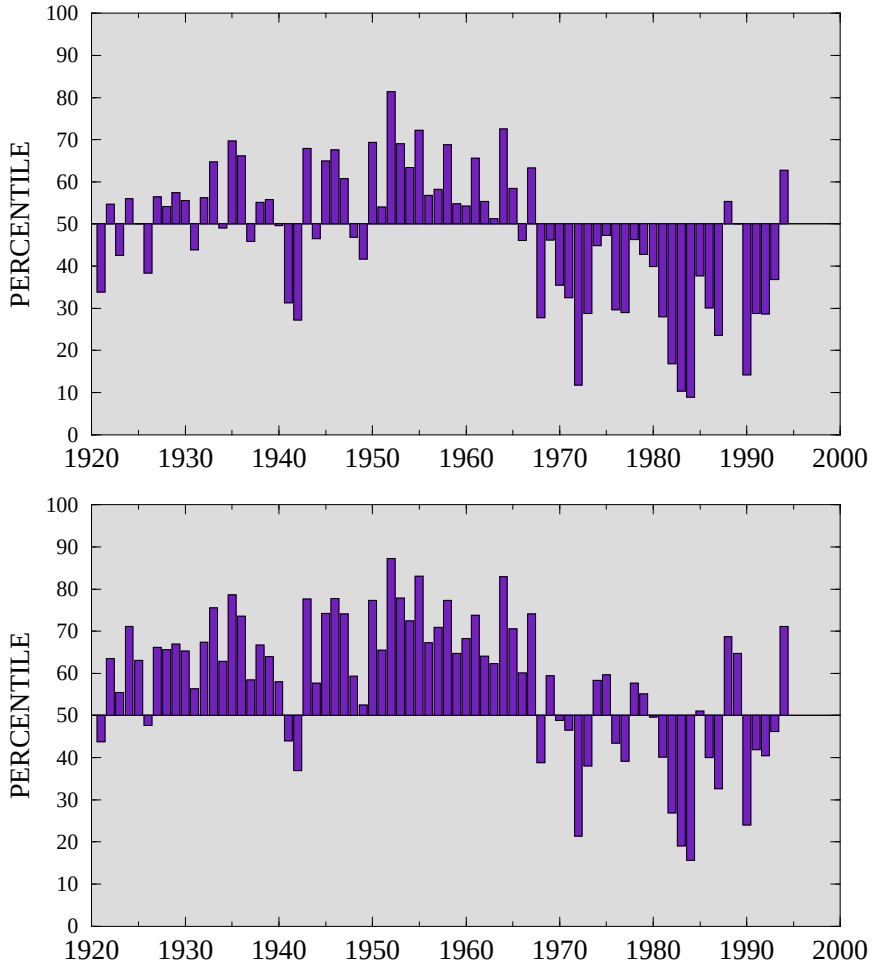

Figure 4.16 Precipitation index (average gamma percentiles of station precipitation within the region) for the western Sahel for June - September based on normals for 1951-1980 (top) and for 1961-1990 (bottom). (Source: CAC)

Above-normal precipitation during 1994 was most prominent over the western half of the Sahel, and over parts of the Sudan and Ethiopia (**Fig. 4.17**). Additionally, over 1,000 mm of precipitation was recorded on the Ethiopian highlands and in large areas from 11°N southward to the Equator (**Fig. 4.18**). In most areas, these totals were sufficient to meet agricultural and hydrological needs. However, drought conditions continued during 1994 in countries south of the western Sahel along the Gulf of Guinea coast, where generally less than 80% of normal seasonal rains fell (**Fig. 4.17**).

The onset of precipitation in May varied across the Sahel. Well above-normal totals covered most of the western Sahel and parts of the Sudan. Near-normal to below-normal totals were measured in most areas south of 10°N, and little to no rain fell on the extreme northwestern part of the region.

During June near-normal to above-normal rainfall covered much of the Sahel, with most areas south of 12°N recording more than 200 mm of rain. This rainfall alleviated immediate famine concerns through much of northeastern Africa.

In July and August, significant rains

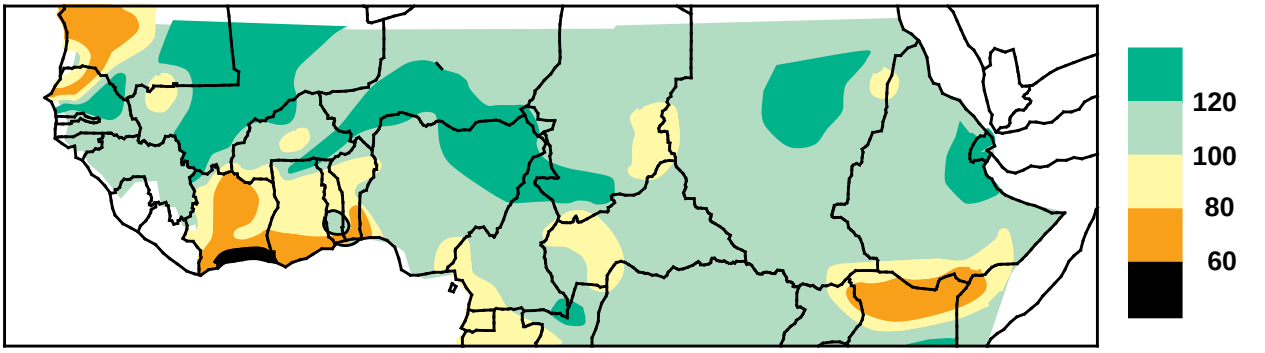

Figure 4.17 Percent of normal precipitation in the African Sahel for May - September 1994, relative to the 1961-1990 base period. (Source: CAC)

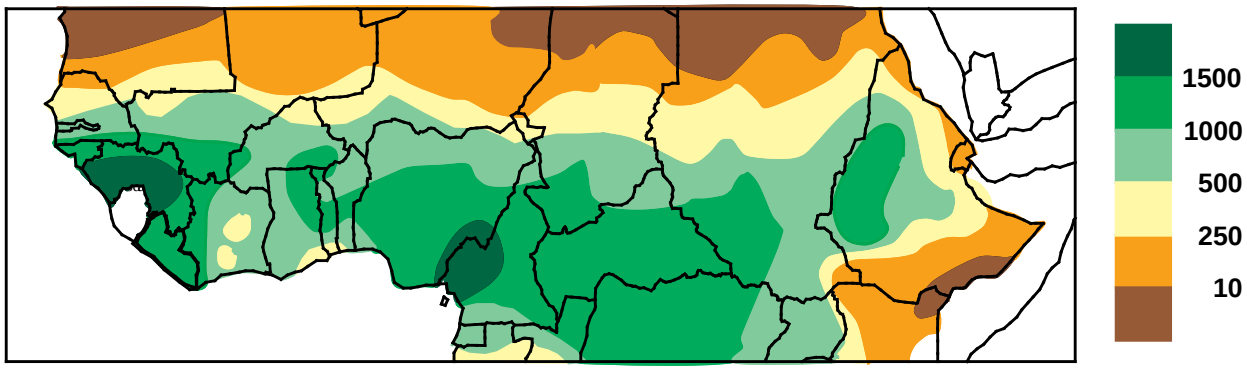

Figure 4.18 Total precipitation (mm) in the African Sahel for May - September 1994 (Source: CAC)

reached exceptionally far north (past 20°N) in central parts of the depicted region, and heavy rains (100-400 mm) drenched most areas of the central and southern Sahel. In contrast, significantly below-normal totals were again observed south of the western Sahel.

In September, abnormally heavy late-season rains of 10-100 mm were reported over most of the Sahel, except in extreme western areas. Exceptionally heavy rains (100 - 400 mm) fell on the central and southern Sahel. Convective complexes continued to track unusually far north into typically dry areas of Mali and Niger during the month, with sporadic localized floods continuing to plague portions of Niger. Rainfall totals across the western Sahel during August and September were similar to totals recorded during the 1950s and early 1960s, with the amounts ranking near the 75th percentile (**Fig. 4.19**). In contrast, below-normal precipitation again covered areas south of the western Sahel along the Gulf of Guinea coast. Drier conditions finally arrived in the Sahel in October. However, occasional heavy rains persisted unseasonably far north, with new October rainfall records established in southeastern Mauritania, and destructive flooding reported in the Sudan.

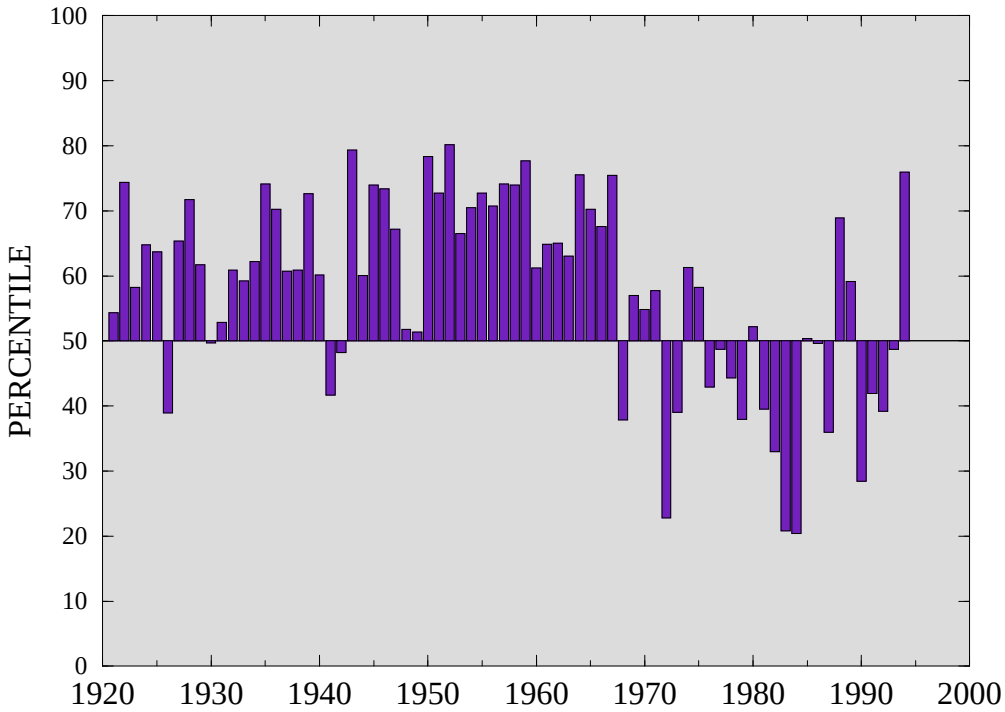

Figure 4.19 Precipitation index (average gamma percentiles of station precipitation within the region) for the western Sahel for August - September normalized by the 1961-1990 base period. (Source: CAC)

e. European Heat Wave

Europe recorded above-normal temperatures during all months of 1994, except February and October. In many places, the year ranked as the third warmest on record (after 1989 and 1990), and in some parts of southern and central Europe, it was the warmest since the beginning of observations more than 200 years ago. For example, in Vienna, Austria (**Fig. 4.20**) mean annual temperatures during 1994 were more than 2°C above normal, exceeding the previous largest anomaly of 1.8°C set in 1992 and setting a new all-time record dating back to 1775.

The extreme warmth was particularly pronounced over Europe during the second half of the year (July-December), when temperatures averaged 1.5-2°C above normal throughout central Europe (**Fig. 4.21, bottom**), and more than 1°C above normal over most of the remainder of the continent, including much of Scandinavia. In central Europe, these anomalies exceeded the 98th percentile (**Fig. 4.21, top**), while they generally exceeded the 90th percentile throughout the rest of Europe.

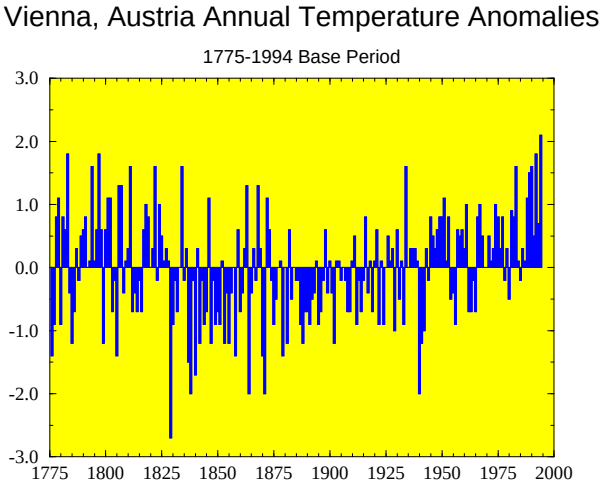

Figure 4.20 Annual temperature anomalies (°C) for Vienna, Austria. Anomalies are departures from the 1775-1994 base period means. (Data supplied by the Deutscher Wetterdienst, Hamburg, Germany.)

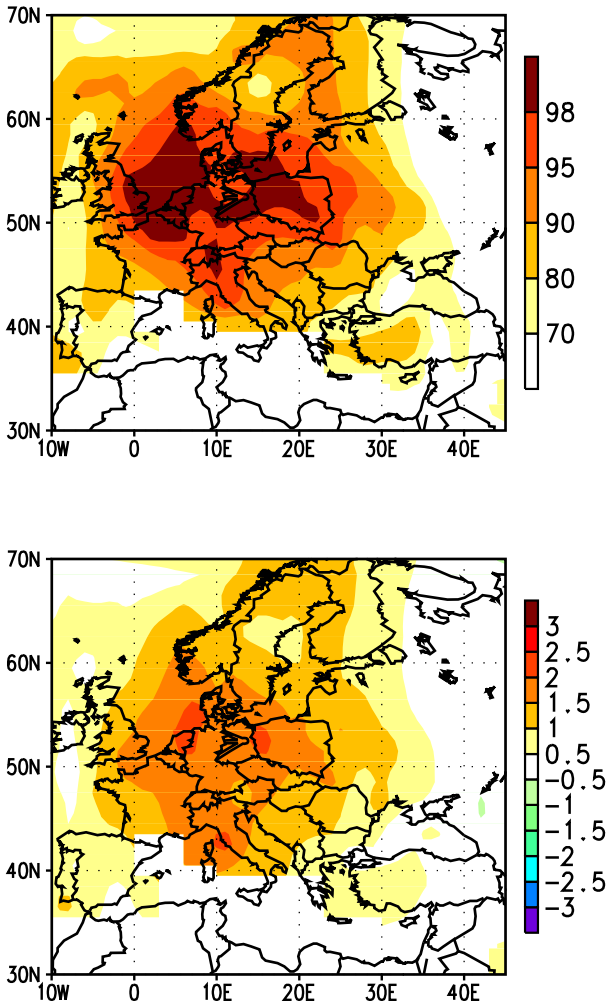

Figure 4.21 Temperature percentiles (top) and anomalies (°C) (bottom) for July - December 1994. Anomalies are departures from the 1961-1990 base period means. (Source: CAC)

Between July and December, two particularly extreme warm periods were observed. From late June through early August, one of the hottest spells ever to afflict central Europe developed (**Figs. 4.22a-d**) in association with the establishment of a major blocking anticyclone throughout the region (**Fig. 4.23**). During this period, the largest temperature anomalies (3-6°C above normal) were observed in Germany, where new all-time record maxima were set at several locations. At Hamburg, Germany a time series of July temperature anomalies beginning in 1850 (**Fig. 4.24**) indicates that July 1994 was the warmest

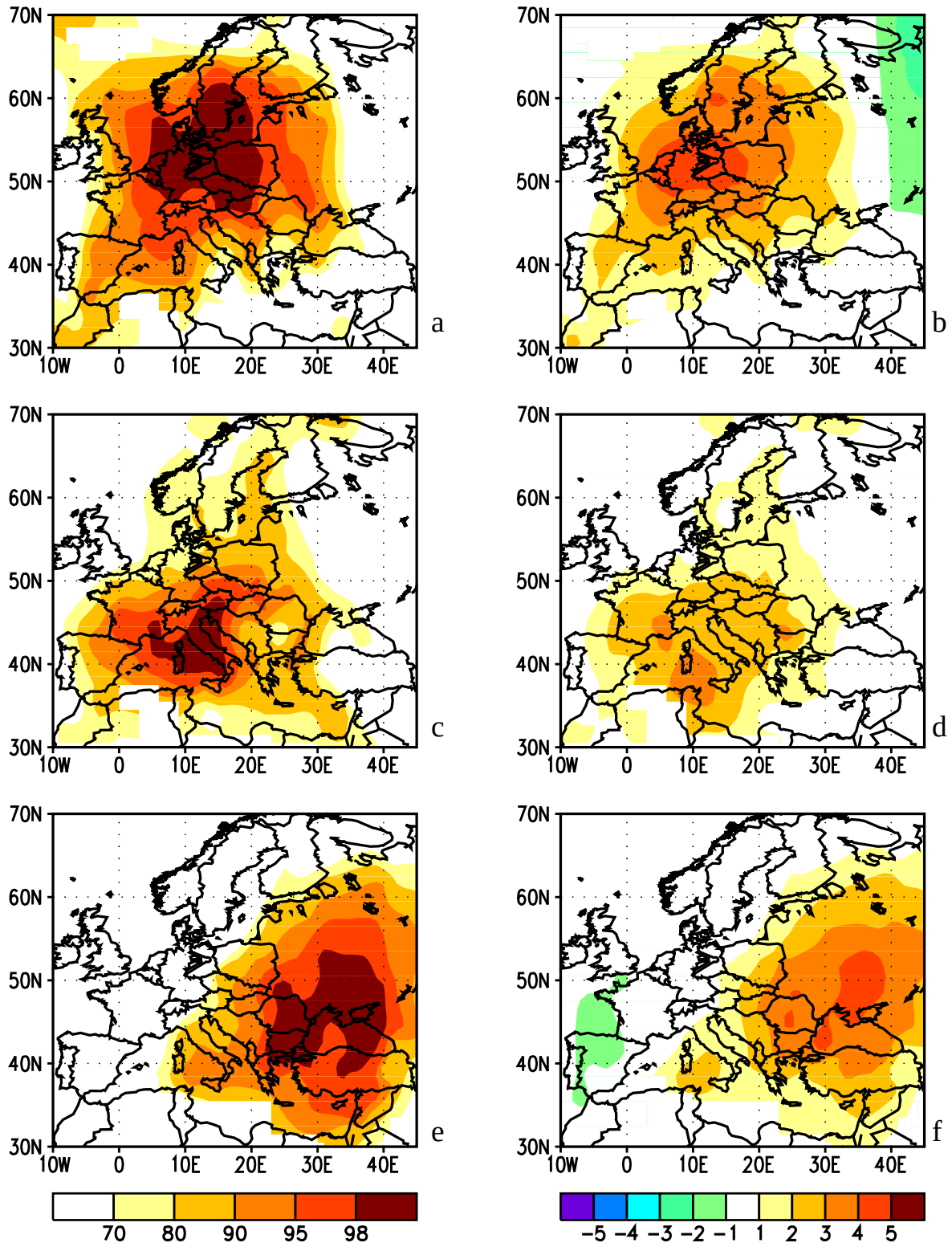

Figure 4.22 Temperature percentiles (a, c, e) and anomalies (°C) (b, d, f) for July (a, b), August (c, d) and September (e, f) 1994. Anomalies are departures from the 1961-1990 base period means. (Source: CAC)

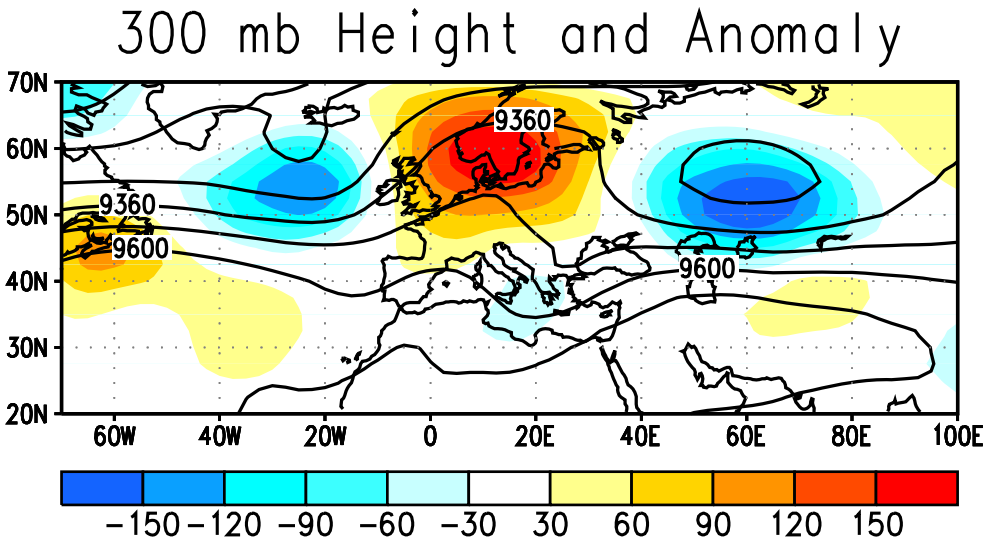

Figure 4.23 300-mb height (m) and anomaly (m) for July 1994. Anomalies are departures from the 1979-1988 base period means. (Source: CAC)

on record, exceeding the previous record anomaly of +3.0°C by more than 2.2°C. A sample of extreme daily temperatures reported during the period were: Murcia, Spain (46.1°C) on 4 July; Lycksele, Sweden (36.7°C) on 7 July; Budapest, Hungary (36.3°C) on 30 July; Berlin, Germany (38.1°C) on 1 August; Virton, Belgium (38.9°C) on 3 August; Volkel, Netherlands (36.1°C) on 4 August; and Paris, France (36.1°C) on 4 August.

During September (**Figs. 4.22e, f**), much of western and central Europe reported near-normal conditions, as the area of near-record warmth shifted well eastward into eastern Europe and southwestern Russia. In October (**Figs. 4.25a, b**), the area of above-normal temperatures shifted farther southeastward and became centered over the eastern Mediterranean Sea. Farther north, much of Europe recorded near-normal temperatures during the month, while extreme northern Europe and western Scandinavia observed below-normal temperatures (1-2°C below normal).

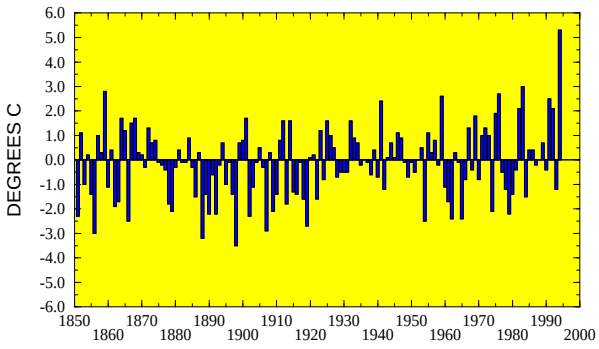

Figure 4.24 July temperature anomalies for Hamburg, Germany. Anomalies are departures from the 1961-1990 base period means. (Data supplied by the Deutscher Wetterdienst, Hamburg, Germany.)

Record or near-record warmth then returned to western Europe in November and December (**Figs. 4.25c-f**). These conditions were associated with a large-amplitude and persistent wave pattern at jet stream level throughout the North Atlantic and European sectors (**Fig. 4.26**). The key features of this pattern included below-normal heights over the high latitudes of the North Atlantic, above-normal heights throughout Europe and southern Scandinavia, and below-normal heights extending northward from the eastern Mediterranean Sea to Siberia. This circulation reflected above-normal pressure throughout Europe, and abnormally strong southwesterly

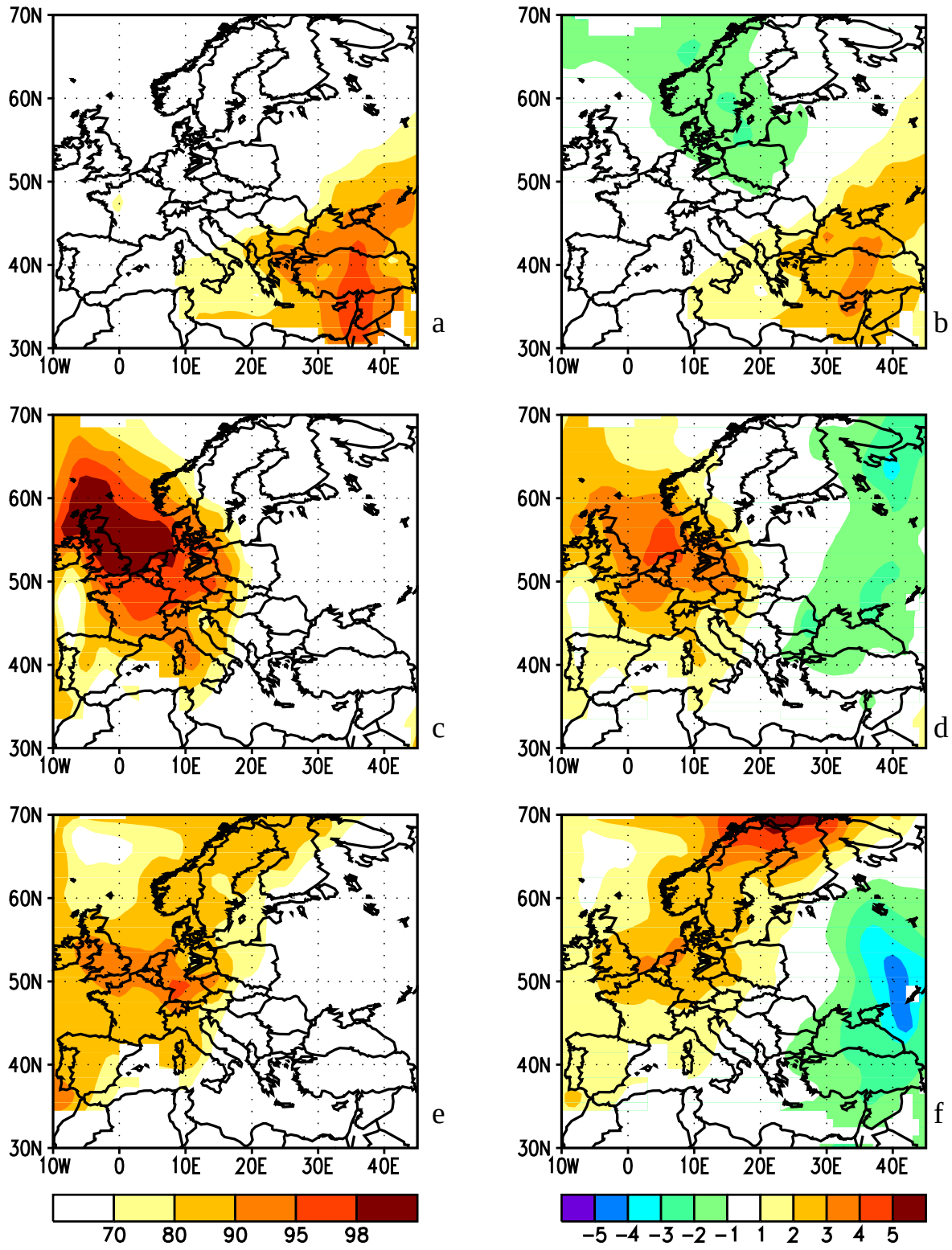

Figure 4.25 Temperature percentiles (a, c, e) and anomalies (°C) (b, d, f) for October (a, b), November (c, d) and December (e, f) 1994. Anomalies are departures from the 1961-1990 base period means. (Source: CAC)

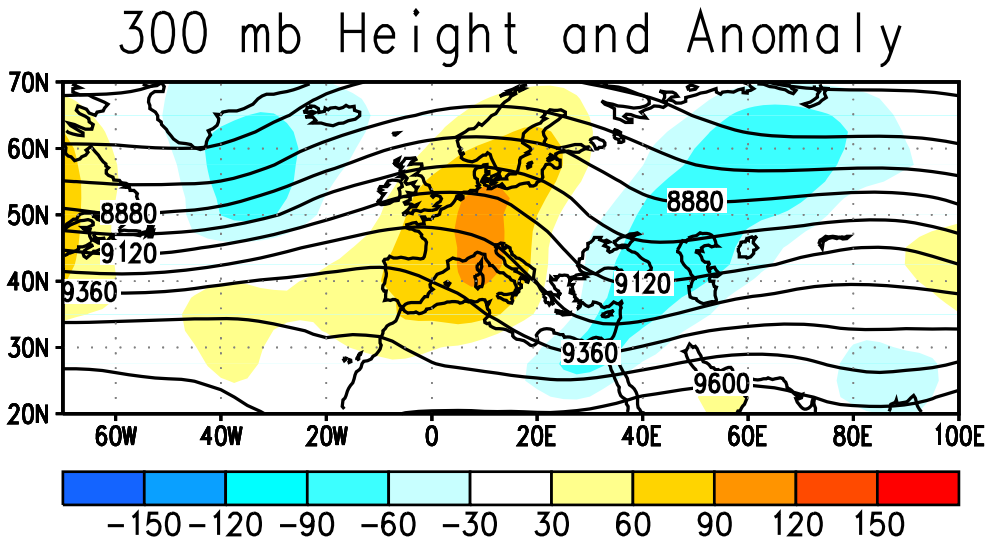

Figure 4.26 300-mb height (m) and anomaly (m) for November-December 1994. Anomalies are departures from the 1979-1988 base period means. (Source: CAC)

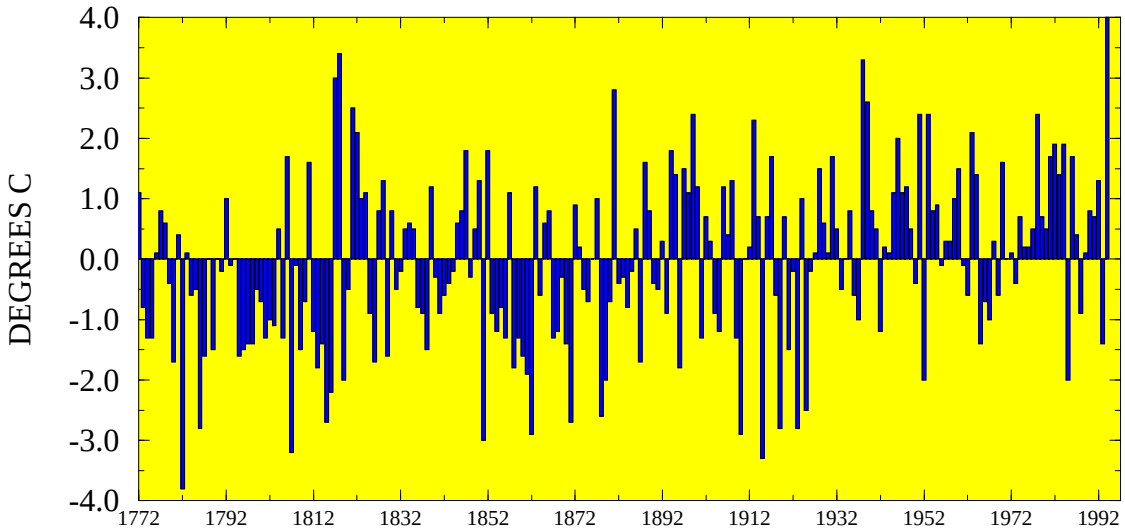

Figure 4.27 November temperature anomalies (°C) for central England. Anomalies are departures from the 1772-1994 base period means. (Data provided by the Hadley Centre for Climate Prediction and Research, UK.)

flow throughout the western portion of the continent. Accompanying this circulation, surface temperatures averaged 3-5°C above normal over large portions of Great Britain and northwestern Europe. In central England, November 1994 was the warmest November in the 336-year record, by more than 0.5°C, and it exceeded the November 1993 temperature by more than 5°C (**Fig. 4.27**, which only shows the more reliable data since 1772). During December, temperatures throughout western Europe averaged 2-3°C above normal and remained above the 80th percentile (**Fig. 4.25e, f**).

f. United States Highlights

1) Temperature and Precipitation

According to preliminary estimates, the mean annual surface temperature over the contiguous United States during 1994 was 0.48°C above the long-term mean (**Fig. 4.28**). Thus, 1994 ranked as the 16th warmest year on record since 1895. More than 25% of the nation recorded annual temperatures in the upper 10th percentile during the year, while none of the country recorded significantly colder-than-normal conditions. The warmth was found mainly in the West, which averaged in the upper one-third of the 100-year historical record. In contrast, near-normal temperatures covered much of the country east of the Mississippi River. Above-normal temperatures have dominated the United States during the past 9 years (**Fig. 4.28**), although temperatures during 1993 averaged much below normal.

On a monthly basis, above-normal temperatures dominated large parts of the country during March, June, and December, while unusually cold conditions were observed in February (**Fig. 4.29**). Remarkably, no regions experienced significantly below-normal temperatures during March, April, June, October, and December. October was unusual in that virtually none of the contiguous United States experienced either much-above or much-below temperatures.

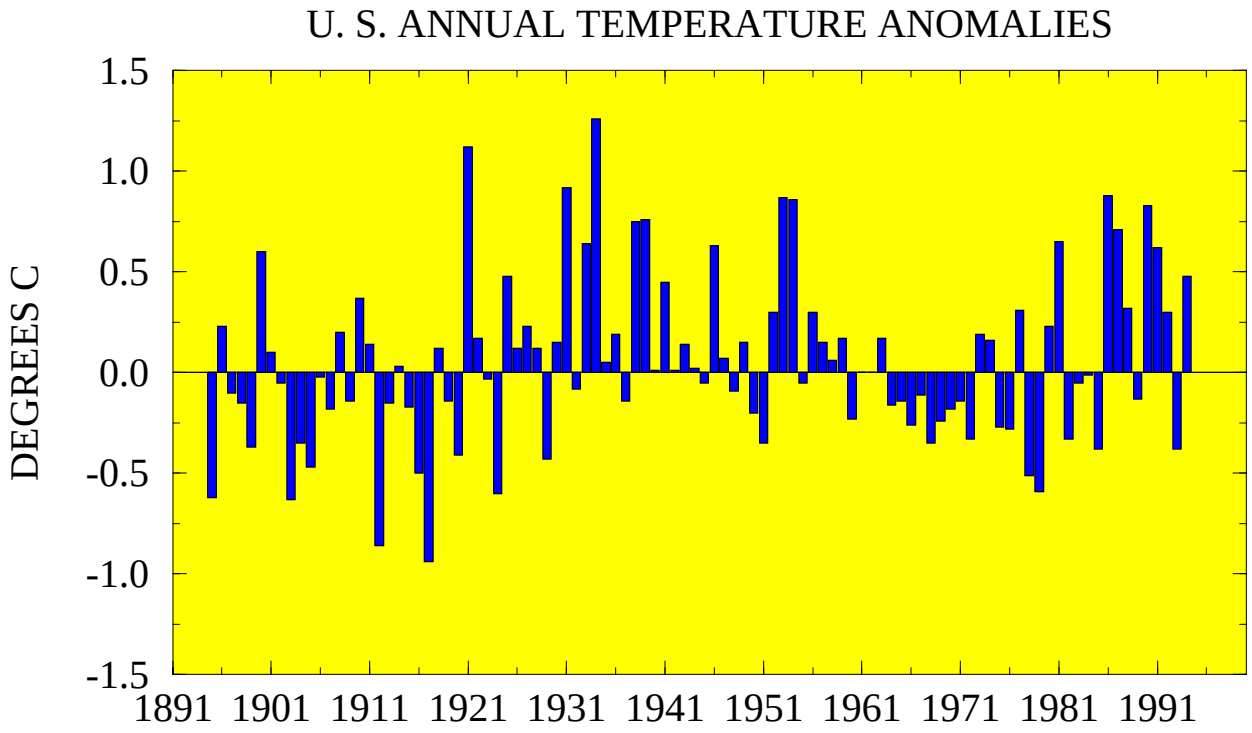

Figure 4.28 Annual surface temperature anomalies (°C) for the contiguous United States. Anomalies are departures from the 1961-1990 base period means. (Data provided by the National Climate Data Center.)

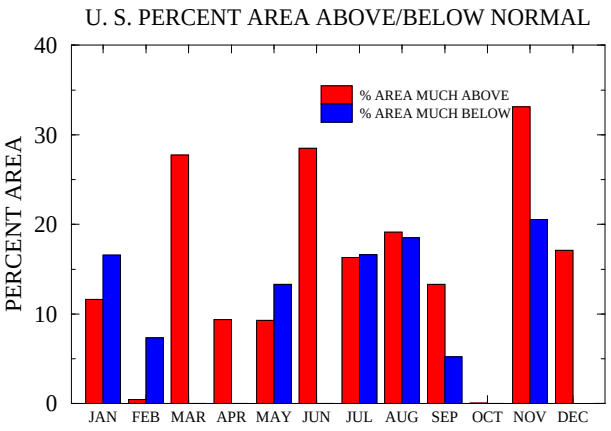

Figure 4.29 Percent area of the contiguous United States experiencing monthly mean temperatures in the upper and lower tenth percentile. (Data provided by the National Climate Data Center.)

Two major flood events dominated the precipitation anomalies during 1994. The first event occurred in July, when tropical storm Alberto crossed the Florida Panhandle. Maximum sustained winds peaked at 29 ms^{-1} at the time of landfall on July 3. The storm caused torrential rainfall throughout the eastern Gulf coast region, with the largest totals exceeding 700 mm at Americus, Georgia. Record flooding was observed along portions of several large river systems in Georgia, Alabama, and Florida (**Fig. 4.30**) during the storm, and damages were estimated at $750 million, including at least $100 million in agricultural losses.

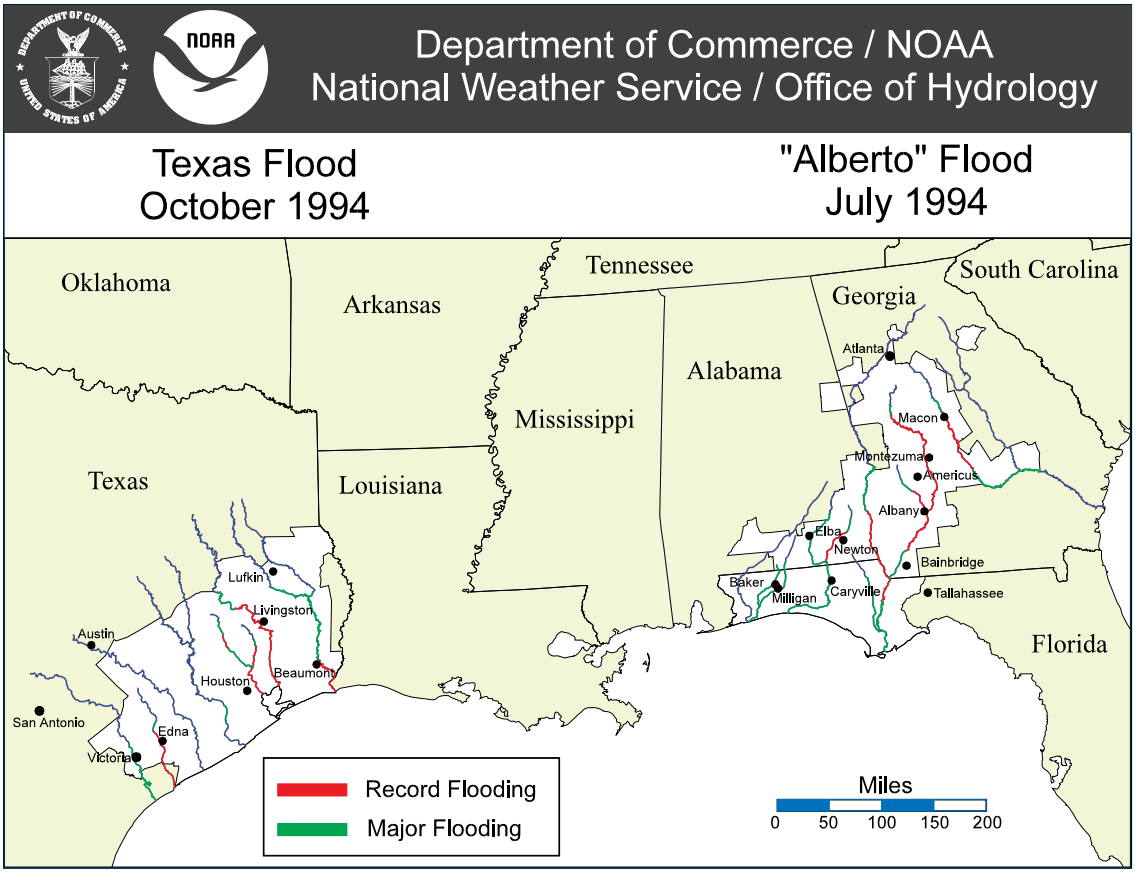

Figure 4.30 Major U. S. hydrologic events of 1994, showing: 1) the July 1994 flooding in the Southeast resulting from Tropical Storm "Alberto" and its remnants, and 2) the October 1994 flooding in Texas. Counties declared Federal disaster areas are colored white. (Source: Office of Hydrology)

The second event occurred in southeastern Texas during mid-October, in association with sustained tropical rainfall focused along a stationary frontal zone. Local totals exceeded 750 mm, and much of southeastern Texas recorded more than 150 mm during this period. Record flooding occurred along six major rivers and their tributaries (**Fig. 4.30**), and damages were estimated in the hundreds of millions of dollars.

In the western United States, the 1993-94 wet season brought below-normal precipitation (less than 50% of normal) to large portions of Washington, Oregon, California and Nevada (**Fig. 4.31, left**). Intermittent severe-to-extreme drought conditions have persisted over large parts of the Pacific Northwest and California during the past decade.

During the onset of the 1994-95 wet season (Oct - Dec), precipitation averaged above normal over much of Washington, Oregon, Nevada, and California (**Fig. 4.31, right**) and was substantially larger than observed during the past several years. Additionally, heavy snow fell over large portions of western Washington, Oregon, and northern California during October-December 1994, resulting in a much above-normal snowpack water content throughout these regions. This precipitation helped to significantly alleviate drought conditions over large parts of the West.

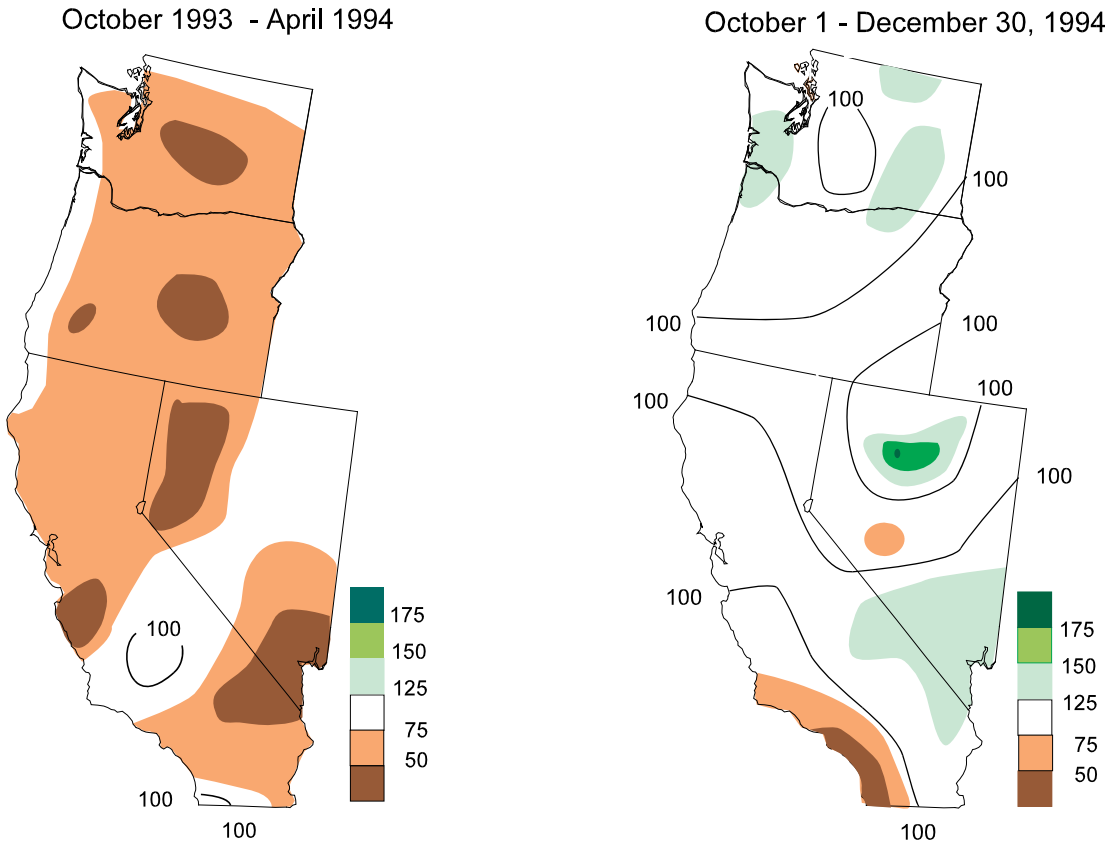

Figure 4.31 Percent of normal precipitation for October1993 - April 1994 (left) and for October - December 1994, relative to the 1961-1990 base period. (Source: CAC).

2) Tornado Activity

According to preliminary data from the National Severe Storms Forecast Center of the National Weather Service, 1073 tornadoes were observed across the contiguous United States during 1994 (**Fig. 4.32**). This compares with the 1953-1993 average of 791 tornadoes per year and represents a decrease of more than 200 tornadoes from the peak year of 1992. It should be noted that the preliminary tornado count is usually higher than the final count, and that tornado observations have generally improved with time.

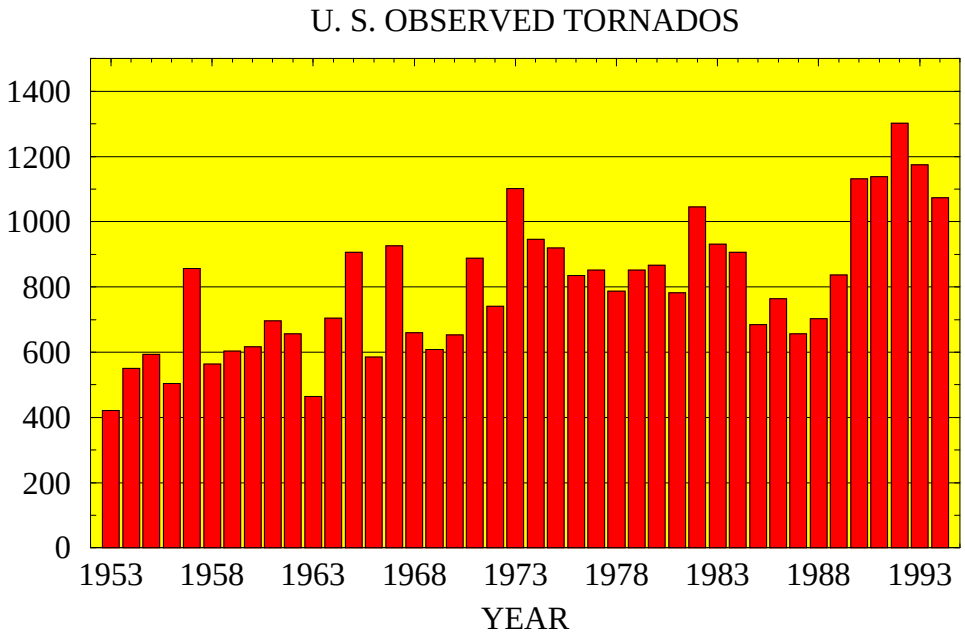

Figure 4.32 Annual number of observed tornadoes in the United States (1953-1994). (Data provided by the National Climate Data Center.)

3) 1994 Atlantic Hurricane Season

Below-normal hurricane activity dominated the 1994 Atlantic hurricane season (June - November), and the net tropical cyclone activity was only 37% of the average of the last 45 years. Three systems, all tropical storms (Alberto, Beryl, and Gordon), affected the southeastern United States coast during the season. There were three hurricanes (maximum sustained wind greater than 30 ms^{-1}) during the season, although none were of major intensity (winds greater than 49 ms^{-1}), and a total of seven named storms (hurricanes and tropical storms combined). Normally, six hurricanes (two of major intensity) and 10 tropical storms are observed during the season.

A suppression of hurricane activity has been observed during each of the past four years. Only two hurricanes have formed equatorward of 25°N, instead of the expected 14 hurricanes during this time. This lack of hurricane activity is linked to a persistent pattern of above-normal pressure throughout the tropical and subtropical Atlantic (**Fig. 2.2**), to prolonged warm episode conditions in the tropical Pacific (section 2a), and to enhanced upper-level westerlies over the Caribbean basin throughout the period (W. Gray, personal communication).

Tracks of the seven named storms during 1994 (**Fig. 4.33**) are color-coded to delineate the periods when each storm was a hurricane, tropical storm and tropical depression. Brief characteristics of these storms, numbered as shown in **Fig. 4.33**, are:

1. **Tropical Storm Alberto** (30 June- 7 July): Formed west of Cuba and made landfall in the Florida Panhandle. Alberto stalled over west-central Georgia and was notorious for its tremendous flooding in Georgia, Florida, and Alabama.

2. **Tropical Storm Beryl** (14-19 August): Formed in the northern Gulf of Mexico and also made landfall in the Florida Panhandle. Beryl caused considerably less flooding than Alberto, although tornadoes caused significant damage in South Carolina and Virginia.

3. **Hurricane Chris** (16-23 August): First hurricane of the season (weak) formed in the low-latitudes of the central Atlantic. The fringes of Chris caused heavy rains in Bermuda.

4. **Tropical Storm Debby** (9-11 September): Formed from an African wave near the central Antilles. Debby dissipated as it moved westward into the eastern Caribbean. The storm caused fatalities and extensive damage in St. Lucia and Martinique.

5. **Tropical Storm Ernesto** (21-26 September): Formed in the eastern Atlantic. It moved northward in response to an upper-level trough and dissipated west of the Cape Verde Islands.

6. **Hurricane Florence** (4-9 November): Formed in the central Atlantic and was the first November hurricane since 1986. Florence reached category 2 intensity and was the season's most intense hurricane. No major land masses were affected by the hurricane.

7. **Gordon** (10-20 November): First named storm in the Caribbean and second hurricane during November. Gordon followed an erratic path over Nicaragua, the western Caribbean Sea, Jamaica, Cuba, the Bahamas, Florida, and the southwestern North Atlantic. Gordon's torrential rains produced disastrous flooding and mud slides, which were particularly deadly in Haiti. Estimates of the death toll ranged up to 2000 in that country. In Florida, seven deaths were attributed to Gordon, with significant agricultural damage.

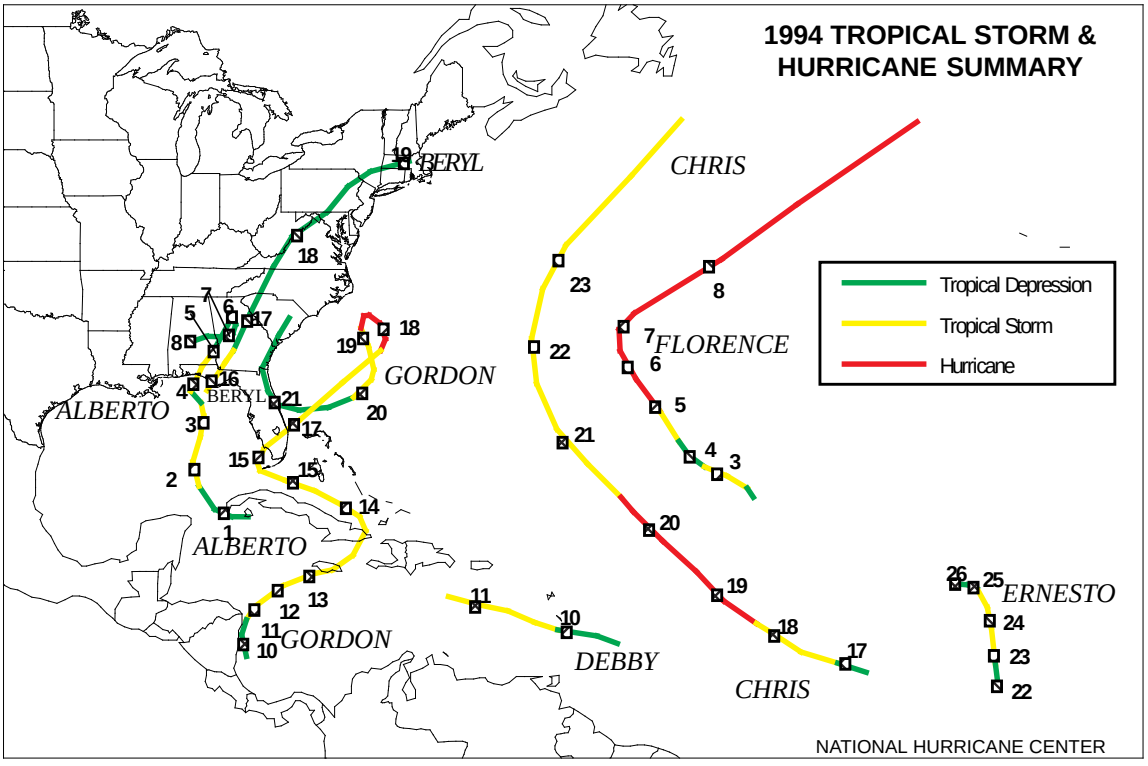

Figure 4.33 Tracks of Atlantic named storms for 1994. Red lines indicate periods of hurricane intensity, yellow lines show periods of tropical storm intensity, and green lines show periods of tropical depression intensity. Numbers pertain to day of month. (Source: National Hurricane Center)

5. CLIMATE IMPACTS (Figs. 5.1 and 5.2)

Eastern and Central North America (1)

Temperatures averaged considerably below normal across eastern and central North America from late December 1993 through January 1994. Two severe cold outbreaks in January covered most of the region, establishing at least 18 new all-time record low temperatures through the Ohio Valley and central Appalachians. Most of Ontario and the Canadian Maritime Provinces experienced their coldest January since 1920, and southern Quebec endured its coldest January ever. Montreal's mean January temperature of -16.6°C was the lowest since 1871. An unprecedented heating demand from the mid-Atlantic states through lower New England forced utilities to impose voltage reductions and controlled localized outages for several days.

In late January, a severe ice storm affected Pennsylvania, Maryland, and Virginia. The storm caused major air travel delays in the northeastern United States and southeastern Canada. Toronto/Pearson International was completely shut down for the first time in its 57 year history due to icy runways. To the west, moderating temperatures and rain caused rapid snowmelt and ice jams, resulting in river flooding across parts of West Virginia, Ohio, and Indiana.

In early and mid-February, two separate storm systems brought up to 30 cm of snow to the north-central states, and 25-70 cm of snow to New York and New Jersey. To the south, freezing rain caused numerous power outages from Texas to Georgia and northeastward to Delaware. After a brief respite in late February, another powerful East Coast storm brought heavy precipitation and strong winds to much of the eastern and southern United States and southeastern Canada. During this event thunderstorms brought up to 225 mm of rain to parts of the east-central Gulf Coast, while 10 to 20 cm of snow covered a large area from the western Carolinas northeastward to Boston, with up to 75 cm of snow falling in central New York.

Western United States (2)

Widespread below-normal precipitation was observed in the West during most of the 1993-94 wet season (October-April), with totals among the driest 10% of the 1961-1990 distribution observed in parts of northeastern California, northwestern Nevada, eastern Oregon, central Idaho, and western Montana. In addition, an upper-level ridge during much of the season kept temperatures abnormally high, further reducing the region's snowpack.

From mid-June through early August, temperatures averaged 1-3°C above normal in the West. This heat, in combination with below-normal precipitation during the wet season, resulted in moderate to severe drought throughout the region by the end of August. These conditions created an unusually severe wildfire season across the region. According to the National Interagency Fire Center, nearly 10,120 km^2 were consumed by wildfires in the United States by mid-July 1994, which was 31% more than the 1989-1993 average for the January to mid-July period.

Beginning in late October a series of storms battered the West and southwestern Canada, bringing heavy precipitation to many areas. Precipitation was particularly heavy over coastal sections of the Far West and along the windward slopes of the Cascades and Sierra Nevada where 250 to 400 mm were reported. Much of this precipitation fell as snow across the higher elevations, establishing new November snowfall records at Alta, UT (480 cm), Prince Rupert/Terrace, B. C. (182.5 cm), and Salt Lake City, UT (80 cm).

Southeastern United States (3)

In late March and early April a slow-moving cold front brought heavy rains from the lower Mississippi Valley northeastward to the mid-Atlantic states. Up to 355 mm of precipitation fell in central and southern Tennes-

see, forcing small rivers out of their banks. The front also spawned more than two dozen tornadoes that claimed 43 lives in northern sections of Alabama and Georgia, the western Carolinas, and southern Tennessee. During one event in Piedmont, AL nineteen individuals lost their lives and 90 others were injured when a tornado demolished a church during Palm Sunday services.

In late April through mid-May, severe weather and heavy rains inundated much of Texas. Several tornadoes in late April prompted the Federal Government to declare the entire state a disaster area, while in mid-May heavy rains (up to 330 mm) from a slow-moving upper-air disturbance inundated most of central and southern Texas.

During late June, numerous thunderstorms brought almost 250 mm of rain to northern Georgia and western South Carolina. Shortly thereafter, Tropical Storm Alberto moved over the Florida Panhandle and then stalled in central Georgia while slowly dissipating.

In mid-October, a strong low-level flow of moist, tropical air into and over a weak stationary front brought a return of exceptionally heavy rains (storm totals of 200 to 750 mm) across southeastern Texas. This event produced record or near-record flood levels to several rivers, including the San Jacinto River near Houston, where floating debris ruptured several petroleum pipelines and ignited over 1.2 million gallons of gasoline and fuel oil.

Subtropical eastern North Pacific (4)

The persistence of abnormally warm waters across much of the subtropical North Pacific east of the date line contributed to the development of intense hurricanes in the region. For example, in July Hurricanes Emilia and Gilma, each with sustained winds of 72 ms^{-1}, passed well south of Hawaii. Both systems shattered records for the most intense storms ever observed in the central Pacific. On August 9, a typical eastern Pacific depression tracked westward and eventually became Hurricane John. Two weeks later, John intensified into the strongest storm ever recorded in the central Pacific but fortunately never affected any inhabited areas with its estimated sustained winds of 76 ms^{-1}. John crossed the date line on August 28 and then weakened to a tropical depression on September 3. The storm subsequently regained strength and was again upgraded to hurricane status. John finally became an extratropical disturbance one month after its formation.

Central South America (5)

In late May, unusually mild conditions developed across Paraguay, Uruguay, northern Argentina, and southern Brazil, with weekly temperature departures approaching +6°C at some locations. The abnormally warm weather persisted through the first half of June, with weekly departures reaching +9°C at many locations during mid-month. However, in late June and early July, a brief cold outbreak brought freezing temperatures as far north as Brazil's northern Parana state, damaging part of Brazil's coffee crop.

During August, unusually dry weather developed across much of southern Brazil, Paraguay, and northeastern Argentina. By mid-September, 100 to 150 mm of rain brought some relief to parts of southern Brazil, southeastern Paraguay, and adjacent areas of Argentina. However, unseasonably hot weather (>40°C) in late September aggravated dry conditions in some locations. The hot and dry weather spread throughout central South America during the first half of October, but widespread moderate to heavy rains during the second half of the month ended the dry spell. However, above-normal temperatures persisted through the end of the year, with only brief respites during November and December.

Europe (6)

Winter

Surplus precipitation fell on much of central Europe during the 1993-94 winter, with very large totals recorded in northwestern sections of the Iberian Peninsula and parts of the Alps. Additionally, bitterly cold air dominated Europe in late January, with several winter Olympic events in Norway nearly postponed because of extreme cold. Farther south, a bitterly cold Arctic outbreak penetrated to southern Italy and the Balkans in late January. During the event, subfreezing temperatures dominated the Continent, and readings plummeted to -50°C in northern Russia, -28°C in Romania, and -12°C in Italy. Nearly two dozen lives were lost and travel was disrupted by heavy snows from the British Isles eastward to Russia and the Ukraine, and from the Baltic Sea southward to Turkey. In addition, heavy snows downed power lines in southern France, leaving tens of thousands without electricity, while blizzard conditions isolated hundreds of villages in Turkey.

Summer

From late May through August, below-normal precipitation was observed across large sections of Europe. By the end of July, two-month moisture shortages of 40-75 mm accumulated in many areas, while deficits of 100-140 mm were observed from southwestern France eastward into northern Romania and across north-central Europe and western Russia. Accompanying this dry spell, extreme warmth dominated Europe throughout the period. After a brief respite in mid-June, a major heat wave developed across most of Europe by the end of the month. In Spain, the prolonged dryness and high temperatures engendered wildfires which charred nearly 1500 square kilometers and claimed 21 lives.

A major change in the upper-air storm track in mid-August steered several strong storms across southern Scandinavia and the Baltics, alleviating the region's dryness. However, on 28 September, more than 900 lives were lost when the ferry boat MS Estonia sank in high seas (waves as high as 22 meters) during a powerful storm in the Baltic Sea.

Middle East and Southwestern Asia (7)

A series of winter storms moved across the region in middle to late November, forcing the closure of some Egyptian harbors and delaying convoys in the Suez Canal. Blizzards isolated villages in eastern Turkey during the period, while torrential rains in Iran claimed at least ten lives, destroyed more than 10,000 homes, and caused more than $170 million in damages. Weekly temperatures averaged as much as 9°C below normal in parts of Turkey and 7°C below normal in Iran.

In early December snow covered much of Jordan and parts of eastern Turkey. The accompanying cold conditions persisted into mid-December but began to abate as 1995 approached. However, a late December snow storm in eastern Turkey contributed to an airplane crash that claimed 54 lives.

Madagascar (8)

Five tropical systems made landfall on Madagascar during the first three months of the year. Cyclones Daisy (mid-January) and Geralda (early February) traversed the southern and central portions of the island. The latter cyclone claimed more than 200 lives as 400 mm of rain and winds exceeding 60 ms^{-1} lashed the island and destroyed numerous buildings and damaged crops. National officials described Geralda as the “Cyclone of the Century,” because of its extreme devastation in Toamasina (95% of the city was reportedly damaged).

In mid-February Tropical Cyclone Julita grazed extreme southwestern Madagascar but did little damage. In mid-March, Hurricane Litanne inundated the southeastern coast of Madagascar with sustained winds of 56 ms^{-1} and 100-250 mm of rain. One week later, Cyclone Nadia, with sustained winds greater than 50 ms^{-1}, claimed a dozen lives and

dumped up to 250 mm of rain on the northern tip of the island. After crossing the Mozambique Channel, Nadia continued westward into northern Mozambique, where it claimed more than 240 lives, left thousands injured and rendered almost 1.5 million people homeless.

Sahel and East-Central Africa (9)

Widespread heavy rains soaked much of the Sahel from late July through mid-October. Flooding along the Niger River left more than 130,000 homeless in Niger alone. By August, well above-normal precipitation also covered the Sudan and Ethiopia. Additional flooding in Sudan during late September and early October forced thousands of individuals from their homes. Heavy November rains inundated Kenya, Somalia, and Djibouti, and the resultant flooding claimed more than 100 lives and forced thousands to flee their homes.

Southeastern Asia (10)

In early June, Tropical Storm Russ dumped heavy rains on southeastern China and northern Vietnam. Flooding claimed over three dozen lives, stranded at least 120,000 individuals, and inflicted more than $115 million in damages. In mid-June, additional heavy rains (250 to 525 mm during June 5 - 18) caused the worst flooding in decades across portions of Guangxi and Guangdong provinces, claiming hundreds of lives and leaving tens of thousands homeless.

Relentless rains continued throughout July in association with an active western Pacific tropical storm season. In late August, Typhoon Fred slowly moved into east-central China, bringing 100-225 mm of rain, wind gusts exceeding 57 ms^{-1}, and a large storm surge. Fred's landfall near Wenzhou coincided with an unusually high astronomical tide, resulting in coastal floods that reportedly took over 1,000 lives. Total economic losses from Fred reached $1.2 billion.

Bangladesh (11)

In early May, powerful Tropical Cyclone 02B, with estimated winds of 69 ms^{-1}, slammed into southeastern Bangladesh and brought several hundred millimeters of rain to much of Bangladesh, extreme eastern India and western Burma. The storm claimed more than 250 lives in Bangladesh alone and left nearly half a million people homeless. However, advanced warnings, cyclone shelters, and the absence of a large tidal surge kept casualties to a minimum compared to the devastating 1991 cyclone that took over 135,000 lives.

Australia (12)

Severe precipitation deficits and extreme drought covered much of Australia from March-December, with overall precipitation totals the second lowest of the century. During July-September drought conditions resulted in an early start to the fire season over Queensland and New South Wales, and by late August, fires were already affecting many parts of New South Wales. In the second half of September, several major fire outbreaks occurred along the coast and in the mountain ranges north of Sydney. On 27 September, at least 200 fires extended from the Atherton Tableland in North Queensland to the south coast districts of Queensland. In the subsequent three days, these fires caused millions of dollars in damage to crops, forests, and pastures.

Indonesia (13)

Sporadic but severe flooding affected much of Indonesia from January through early April as an active monsoon brought heavy precipitation to Sumatra, Java, southern Borneo, and Celebes. Press reports indicated that flooding in January may have been the worst in a decade. However, little or no rain fell from June through mid-October over Indonesia, thereby creating large moisture deficits. The 1994-95 rainy season failed to start until late October in Java and southern Sumatra, but ample and widespread rains during November and early December eased the long-term moisture deficits throughout the region.

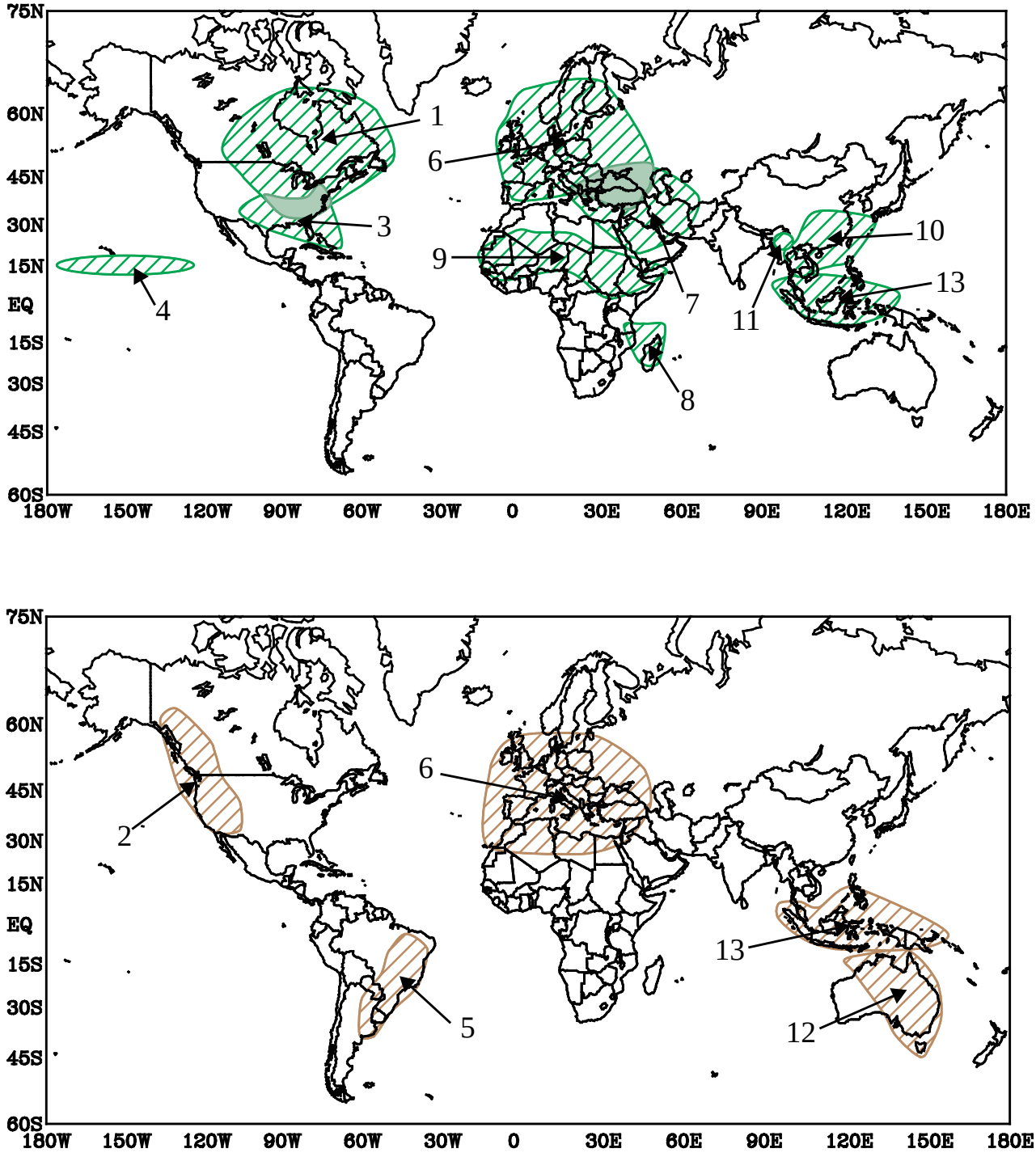

Figure 5.1 Significant above-normal precipitation anomalies (top) and below-normal precipitation anomalies (bottom) during 1994. The numbers are keyed to the descriptive paragraphs. (Source: CAC)

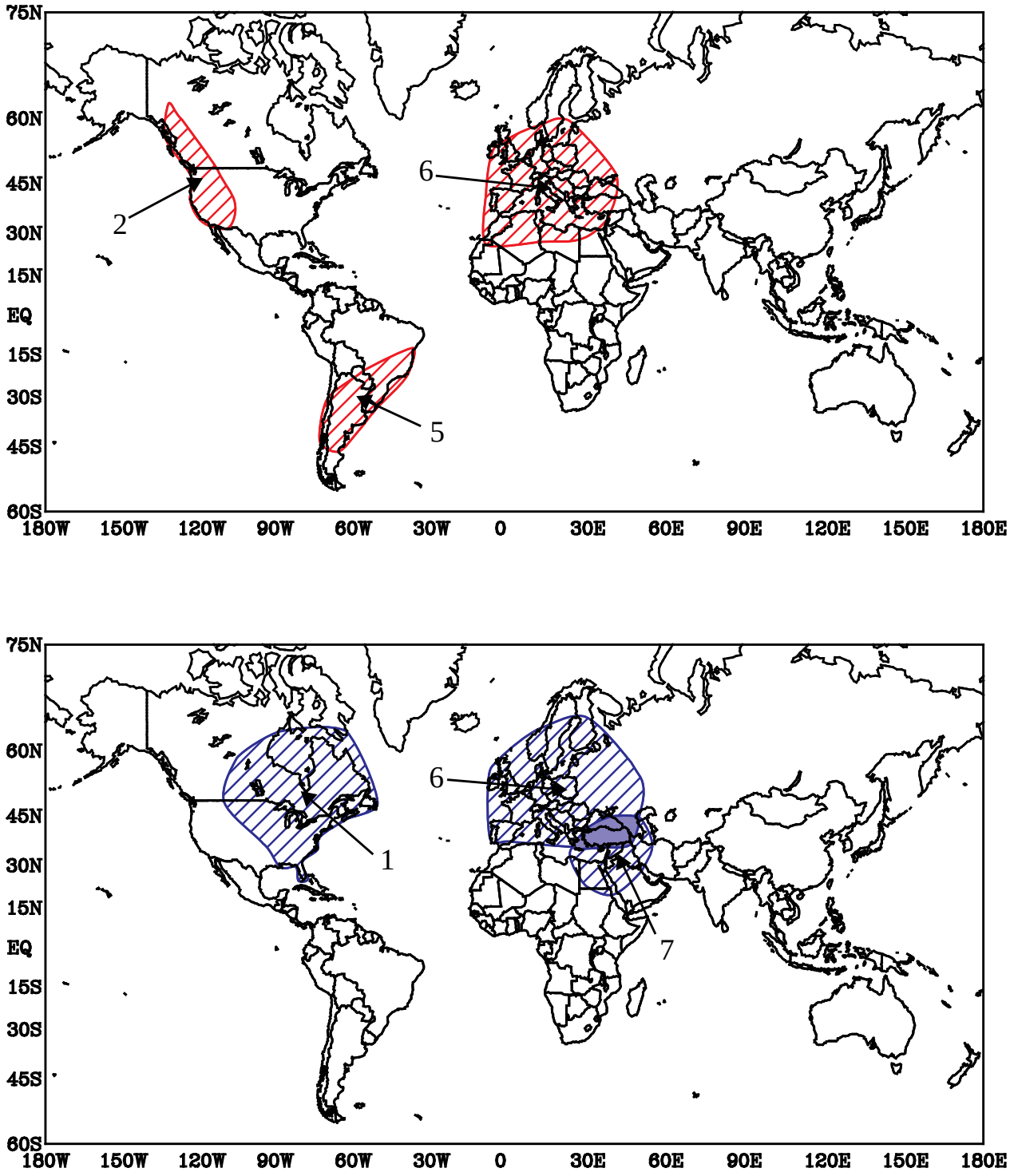

Figure 5.2 Significant above-normal temperature anomalies (top) and below-normal temperature anomalies (bottom) during 1994. The numbers are keyed to the descriptive paragraphs. (Source: CAC)

REFERENCES

Climate Analysis Center, 1992: Third Annual Climate Assessment: 1991. M. S. Halpert and C. F. Ropelewski editors. Dept. of Commerce, NOAA/NWS/ NMC, Climate Analysis Center [U. S. Printing Office: 1992, 74 pp.

Dlugokencky, E. J., K. A. Masarie, P. M. Lang, P. P. Tans, L. P. Steele and E. G. Nisbet, 1994: A dramatic decrease in the growth rate of atmospheric methane in the Northern Hemisphere during 1992. *Geophys. Res. Let.*, **21**, 45-48.

Ellis, H. T., and R. F. Pueschel, 1971: Solar radiation: Absence of air pollution trends at Mauna Loa. *Science*, **172**, 845-846.

Hansen, J., J. Fung, A. Lacis, D. Rind, S. Lebedeff, R. Ruedy, G. Russell and P. Stone, 1988: Global climate changes as forecast by Goddard Institute for Space Studies three-dimensional model. *J. Geoph. Res.*, **93**, 9341-9364.

Hansen, J., A. Lacis, R. Ruedy and M. Sato, 1992: Potential climate impact of Mount Pinatubo eruption. *Geoph. Res. Lett.*, **19**, 215-218.

Keeling, C. D., R. B. Bacastow, and T. P. Whorf, 1982: Measurements of the concentration of carbon dioxide at Mauna Loa Observatory, Hawaii. *Carbon Dioxide Review: 1982*. W. C. Clark, Editor. Oxford University Press, New York, 377-385.

Leetmaa, A., and M. Ji, 1989: Operational hindcasting of the tropical Pacific. *Dyn. Atmos. and Oceans,* **13**, 465-490.

Madden, R.A., and P. R. Julian, 1994: Observations of the 40-50 day tropical oscillation --a review. *Mon. Wea. Rev.*, 122, 814-837.

Reynolds, R. W., 1988: A real-time global sea surface temperature analysis. *J. Climate*, **1**, 75-86.

Reynolds, R. W. and T. M. Smith, 1995: A high resolution global sea surface temperature climatology. Accepted for publication by *J. Climate*.

Robinson, David A., 1993: Monitoring Northern Hemisphere Snow Cover, *Proc. of Snow Watch '92,* Niagara-on-the-Lake, Ontario, April 1992.

Salstein, D.A., D.M. Kann, A.J. Miller and R.D. Rosen, 1993: The Sub-bureau for Atmospheric Angular Momentum of the International Earth Rotation Service: A meteorological data center with geodetic applications. *Bull. Amer. Meteorol. Soc.*, 74, 67-80.

Spencer, R. W., J. R. Christy and N. C. Grody, 1990: Global atmospheric temperature monitoring with satellite microwave measurements: Method and results 1979-84. *J. Climate*, **3**, 1111-1128.

Thorning, K. W., P. P. Tans and W. D. Komhyr, 1989: Atmospheric carbon dioxide at Mauna Loa Observatory 2. Analysis of the NOAA/GMCC data, 1974-1985. *J. Geophys. Res.*, **94**, 8549-8565.